


5-2018

VASCULAR INJURY IN Col3a1+/- MICE MODEL OF VASCULAR EHLER-DANLOS SYNDROME

Ping ZHOU MS

Follow this and additional works at: https://digitalcommons.library.tmc.edu/utgsbs_dissertations

 Part of the [Genetics Commons](#), [Molecular Genetics Commons](#), and the [Other Genetics and Genomics Commons](#)

Recommended Citation

ZHOU, Ping MS, "VASCULAR INJURY IN Col3a1+/- MICE MODEL OF VASCULAR EHLER-DANLOS SYNDROME" (2018).
UT GSBS Dissertations and Theses (Open Access). 844.
https://digitalcommons.library.tmc.edu/utgsbs_dissertations/844

This Dissertation (PhD) is brought to you for free and open access by the Graduate School of Biomedical Sciences at DigitalCommons@TMC. It has been accepted for inclusion in UT GSBS Dissertations and Theses (Open Access) by an authorized administrator of DigitalCommons@TMC. For more information, please contact laurel.sanders@library.tmc.edu.

**VASCULAR INJURY IN *Col3a1*^{+/-} MICE MODEL OF VASCULAR
EHLER-DANLOS SYNDROME**

by

Ping Zhou, M.S.

APPROVED:

Dianna M. Milewicz, M.D., Ph.D., Advisor

Min Sup Song, Ph.D.

Ann Killary, Ph.D.

Yang Xia, M.D., Ph.D.

Yong-Jian Geng, M.D.

APPROVED:

Dean, The University of Texas MD Anderson Cancer Center UTHealth Graduate School of
Biomedical Sciences

VASCULAR INJURY IN *Col3a1*^{+/-} MICE
MODEL OF VASCULAR-EHLER DANLOS SYNDROME

A DISSERTATION

Presented to the Faculty of

The University of Texas

MD Anderson Cancer Center UTHealth

Graduate School of Biomedical Sciences

in Partial Fulfillment

of the Requirements

for the Degree of

Doctor of Philosophy

by

Ping Zhou, M.S.
Houston, Texas

May 2018

Acknowledgments

First and foremost, thanks to my advisor Dr. Dianna Milewicz who supervised and trained me to be a scientist. During the past 4 years, you spent a huge amount of time encouraging me to be a mature scientist. Your passion for science and your hard work to solve real clinical problems set a role model for me. Thank you!

I would like to thank you, my Advisory Committee members: Ann Killary, Yang Xia, Yong-Jian Geng and Min Sup Song. Thank you to you all to serve on my committee and for your time and your feedback.

Unending thanks to the Program Director, Dr. Ann Killary -- you always know your students so well. You don't just memorize our names, you know us personally. You are always there to help us no matter what.

Special thanks to Callie, you are such an amazing friend and lab mate. Your encouragement and friendship played a huge role in the last stage of my study. You are my role model in managing your work and the relationship with those around you.

Many thanks to Limin Gong and Dongchuan Guo for all the times you encouraged me in my PhD journey. Thanks, too, to Jiyuan Chen and Xueyan Duan who were always there for me when I asked for help, even in the numerous late evenings. Zhen, you are such a great surgeon and an amazing friend and lab mate. Thanks for helping me whenever I needed it. Shanzhi and Shuangtao, you made my time in the lab fun. Tommy Reese, you were amazing the way you helped me get my work done by sacrificing your precious weekends. Words can't express how much I appreciate your support.

Thank you Callie, Anna, Tamara and Mimi for supporting me when I was writing this thesis. Thank you for your kind help, support, and, above all, love.

My friends Ren Zhao, Alexa, Jamie Wright, Melisa Walker, Amelie, Ellen H and Stephanie Wallace, your trust in me as a friend and the support from our friendship helped me survive and become a strong and confident woman, which is so important now and in my future.

Many thanks to my friends (too many to list) from the greater Houston area -- you all made me feel like I was at home during my 5- year stay in Houston. You were with me as I changed from an innocent girl

to a wife and then to a mother. You are all amazing in balancing your work and life, in contributing to the community, and in devoting your time to help others.

Last but not least, I would like to thank my parents who are always there to encourage me and help me go through any challenge, and my siblings, all of whom work so hard to contribute to our big family. Many thanks to Jun's family -- you embraced me and gave me a second home. And thanks to my husband Jun, your love and support every single day makes me a happier person. With your support and appreciation, I can be more efficient in getting my work done and in living a more balanced life, which I never had before. I am so grateful to be loved by so many people.

Thank you!

Abstract

Vascular type of Ehlers-Danlos Syndrome (vEDS) is an inherited cardiovascular disease affecting the middle to large sized arteries, with an incidence rate of 1/5000. vEDS patients also show a significant phenotype of easily bruised skin, indicating aberrant wound healing and injury repair ability. Over 70% of the patients carry a glycine mutation located in their *COL3A1* gene, which encodes the propeptide of type III collagen. Mutations in glycine residues lead to a disruption in the assembly and maturation of type III collagen. The goal and significance of the current study was to investigate the potential role of *COL3A1* haploinsufficiency in the development of vEDS and develop new potential therapies for vEDS patients.

Carotid ligation was applied to the *Col3a1*^{+/-} mouse as an injury model, and the results confirm that *Col3a1*^{+/-} mice have aberrant arterial injury repair. Arteries from the injured *Col3a1*^{+/-} mice showed increased cell proliferation, inflammation, and neovessel formation. *In vitro*, fibroblasts explanted from *Col3a1*^{+/-} mice have persistent myofibroblast status after treatment with TGF-β1, which validates the *in vivo* findings.

Finally, two treatments were tested on *Col3a1*^{+/-} mice after carotid ligation: bone marrow transplantation and celiprolol. Transplantation of *Col3a1*^{+/+} bone marrow to *Col3a1*^{+/-} mice corrects the post-injury phenotypes, suggesting that bone marrow derived fibrocytes can be differentiated into myofibroblasts and produce sufficient type III collagen for successful wound healing. Celiprolol treatment on the *Col3a1*^{+/-} mice also corrects the wound healing impairment by decreasing inflammation and cell proliferation. Therefore, this study validates a novel paradigm for vEDS that decreased supply of mature type III collagen fibrils affects fibroblasts in arterial wound healing and also provides evidence for bone marrow transplantation and celiprolol as potential new therapeutic approaches to the treatment of vEDS patients.

Table of Contents

1	Introduction.....	1
1.1	What is vEDS?.....	2
1.2	Diagnosis of vEDS.....	4
1.3	Current therapeutic approaches and management to vEDS.....	4
1.4	Vascular Structure and Aorta.....	5
1.5	Structure of collagen and their function.....	7
1.6	Mutation of <i>COL3A1</i> gene leading to deficiency of type III collagen.....	7
1.7	Increased Carotid wall stress in vEDS.....	10
1.8	vEDS and <i>Col3a1</i> mice.....	11
1.9	Myfibroblasts and wound healing.....	13
1.10	TGF- β signaling pathway and differentiation of fibroblasts.....	14
1.11	Neovascularization in arterial diseases.....	14
1.12	Previous studies in our lab on the <i>Col3a1</i> mice.....	15
2	Bone Marrow Transplantation Rescues the Phenotypes in <i>Col3a1</i> ^{+/-} Mice.....	17
2.1	Introduction.....	18
2.2	Hypothesis.....	21
2.3	Methods.....	22
2.3.1	Carotid Ligation Injury.....	22
2.3.2	Histology studies.....	23
2.3.3	Immunohistological (IHC) staining.....	24

2.3.4	Bone marrow transplant	25
2.4	Results	28
2.4.1	Increased neointimal formation after carotid arterial ligation in <i>Col3a1</i> ^{+/-} mice at POD2128	
2.4.2	Increased myofibroblast proliferation in the <i>Col3a1</i> ^{+/-} mice after carotid ligation.....	29
2.4.3	Increased inflammation in <i>Col3a1</i> ^{+/-} mice after carotid ligation	31
2.4.4	Persistent neovascularization in the media of injured <i>Col3a1</i> ^{+/-} arteries at POD21	33
2.4.5	Bone marrow from the <i>Col3a1</i> ^{+/+} mice rescues the ability of injury repair in <i>Col3a1</i> ^{+/-} mice	35
2.4.6	Reverse Bone Marrow Transplantation worsens the phenotypes shown in the <i>Col3a1</i> ^{+/-} mice	41
2.5	Discussion	55
3	Celiprolol Trial on <i>Col3a1</i>^{+/-} Mice to Modulate the Thrombus Resolution	58
3.1	Introduction	59
3.1.1	β-adrenergic receptors (β-ARs) and wound healing	59
3.1.2	Drug: celiprolol.....	61
3.2	Methods	64
3.2.1	Measurement of basic blood pressure for <i>Col3a1</i> mice.....	64
3.2.2	Carotid artery ligation and sample harvesting	64
3.2.3	Histological Analysis: Morphology	65
3.2.4	Immunohistochemical (IHC) staining.....	66
3.3	Results	67

3.3.1	No difference in basal systolic or diastolic blood pressure of <i>Col3a1</i> ^{+/+} and <i>Col3a1</i> ^{+/-} mice	67
3.3.2	Decreased neointimal layer formation in <i>Col3a1</i> ^{+/-} mice carotid arteries after celiprolol treatment	69
3.3.3	Altered cell proliferation and inflammation in the neointimal layer after celiprolol treatment	70
3.3.4	No difference in the formation of new vessels in the medial layer after celiprolol treatment at both POD14 and POD21	73
3.4	Discussion.....	75
4	Dysregulated Myofibroblasts from <i>Col3a1</i>^{+/-} Mice Contribute to the Abnormal Injury Repair	78
4.1	Introduction.....	79
4.1.1	Myofibroblasts in wound healing	79
4.1.2	Role of TGF-β in differentiation of fibroblasts and arterial injury	80
4.1.3	Focal adhesions (FAs) and focal adhesion kinase (FAK) in the differentiation of fibroblasts	82
4.1.4	MRTFA and fibroblasts differentiation	82
4.1.5	Studies with fibroblasts from <i>Col3a1</i> ^{+/-} mice and unpublished data on mice embryonic fibroblasts (MEF) and fibroblasts from vEDS patients.....	84
4.2	Methods.....	87
4.2.1	Fibroblast explant from mouse lung tissues.....	87
4.2.2	Isolation of Vascular SMCs from <i>Col3a1</i> ^{+/+} and <i>Col3a1</i> ^{+/-} mice.....	87
4.2.3	Isolation of RNA and q-PCR	88

4.2.4	Protein preparation and Western blotting	89
.....		90
4.2.5	Cell proliferation assay	90
4.2.6	TGF-β1 administration to fibroblasts and immunofluorescent staining (IF)	91
4.3	Results	93
4.3.1	Both the <i>Col3a1</i> ^{+/+} and <i>Col3a1</i> ^{+/-} fibroblasts respond to stimulation by TGF-β1	93
4.3.2	More formation of stress fibers in <i>Col3a1</i> ^{+/-} cells at basal level but not after TGF-β1 stimulation.....	95
4.3.3	Significantly increased activity of focal adhesion signaling in the <i>Col3a1</i> ^{+/+} cells after TGF-β1 stimulation for 72 hours	95
4.3.4	No activation of pFAK in <i>in vitro</i> tissue culture of <i>Col3a1</i> ^{+/-} fibroblasts.....	96
4.3.5	Increased translocation of MRTFA into the nucleus of <i>Col3a1</i> ^{+/-} myofibroblasts	98
4.3.6	Increased differentiation of <i>Col3a1</i> ^{+/-} SMCs after stimulation with TGF-β1	101
4.3.7	Altered focal adhesion by vinculin staining and increased differentiation of <i>Col3a1</i> ^{+/-} SMCs	102
4.3.8	Altered production of collagen and their receptors <i>Col3a1</i> ^{+/-} SMCs.....	104
4.3.9	Decreased cell proliferation and increased viability of <i>Col3a1</i> ^{+/-} SMCs.....	104
4.4	Discussion	106
5	Discussion	109
5.1	Discussion of the project	110
5.2	Future direction	113

5.2.1	<i>In vitro</i> studies on <i>Col3a1</i> ^{+/+} and <i>Col3a1</i> ^{+/-} fibroblasts to test their metabolism and cell interaction	113
5.2.2	Investigating the role of specific bone marrow derived cell types in <i>Col3a1</i> ^{+/-} mouse model	113
5.2.3	Specialized cell therapy for vEDS.	114
5.2.4	Effects of celiprolol on cells explanted from <i>Col3a1</i> mouse.	114

List of Figures

Figure 1.1 Distribution of 132 vascular complications	3
Figure 1.2 Schematic comparison of medial architecture in a muscular artery (left) and an elastic artery (right).	6
Figure 1.3 Fibroblast assembly of collagen fibrils	8
Figure 1.4 Fibrillar procollagens and fibril assembly	10
Figure 1.5 Comparison of the diameters of collagen fibrils in the adventitia of aorta of wild-type and mutant mice	12
Figure 2.1 Three over-lapping phases for wound healing	20
Figure 2.2 Slower neointima remodeling in the <i>Col3a1</i> ^{+/-} mice	28
Figure 2.3 Increased cell proliferation within the <i>Col3a1</i> ^{+/-} arteries	30
Figure 2.4 Increased inflammation within the <i>Col3a1</i> ^{+/-} arteries	32
Figure 2.5 Increased medial neovessel formation in <i>Col3a1</i> ^{+/-} arteries	34
Figure 2.6 Flow chart for Forward BMT	36
Figure 2.7 Confirmation of F-BMT	37
Figure 2.8 Similar ability in neointimal remodeling after F-BMT	38
Figure 2.9 Decreased cell proliferation in <i>Col3a1</i> ^{+/-} arteries after F-BMT	39
Figure 2.10 Decreased neointimal inflammation in <i>Col3a1</i> ^{+/-} arteries after F-BMT	40
Figure 2.11 Decreased neovessel formation in the <i>Col3a1</i> ^{+/-} arteries after F-BMT	42
Figure 2.12 Flow chart for Reverse Bone Marrow Transplant (BMT) – R-BMT	44
Figure 2.13 Confirmation of R-BMT	45
Figure 2.14 Similar ability in neointimal remodeling after R-BMT	46
Figure 2.15 No significant difference in cell proliferation after R-BMT	47
Figure 2.16 No significant difference in neointimal inflammation after R-BMT	48
Figure 2.17 No significant in neovessel formation arteries after R-BMT	50

Figure 2.18 H&E staining indicating changes in the neointima remodeling-----	51
Figure 2.19 Comparison of cell proliferation in the neointima for all groups -----	52
Figure 2.20 Comparison of inflammation in the neointimal layer for all groups-----	53
Figure 2.21 Comparison of medial neovessel formation for all groups -----	54
Figure 3.1 Schematic representation of interaction of the β 2-AR -----	60
Figure 3.2 Flow chart of celiprolol trial-----	63
Figure 3.3 Comparison of the systolic blood pressure after celiprolol administration -----	68
Figure 3.4 Remodeling of neointimal by H&E staining after celiprolol administration -----	69
Figure 3.5 Decreased cell proliferation in <i>Col3a1</i> ^{+/-} arteries after celiprolol administration -----	71
Figure 3.6 Decreased neointima inflammation in <i>Col3a1</i> ^{+/-} arteries after celiprolol administration -----	72
Figure 3.7 No significant difference in neovessel formation after celiprolol administration -----	74
Figure 4.1 Summary of TGF- β signaling in hypertrophic scarring -----	81
Figure 4.2 Schematic of the proposed regulatory pathways involved in myofibroblast differentiation. ---	83
Figure 4.3 Increased α -SMA expression by <i>Col3</i> ^{+/-} and <i>Col3</i> ^{-/-} cells compared to <i>Col3</i> ^{+/+} cells -----	86
Figure 4.4 Expression level of contractile proteins-----	92
Figure 4.5 Expression of collagens(a) and two collagen receptors(b) -----	94
Figure 4.6 Abnormal actin polymerization in <i>Col3a1</i> ^{+/-} myofibroblasts -----	95
Figure 4.7 Altered focal adhesions in both <i>Col3a1</i> ^{+/+} and <i>Col3a1</i> ^{+/-} cells -----	98
Figure 4.8 Increased translocation of MRTFA into the nucleus of <i>Col3a1</i> ^{+/-} myofibroblasts-----	100
Figure 4.9 Increased expression of contractile proteins in <i>Col3a1</i> ^{+/-} myofibroblasts-----	101
Figure 4.10 Altered focal adhesion signaling in <i>Col3a1</i> ^{+/-} SMCs-----	102
Figure 4.11 Expression of collagens and collagen receptors at RNA level in SMCs-----	103
Figure 4.12 Decreased cell proliferation while increased viability of <i>Col3a1</i> ^{+/-} SMCs -----	104

List of tables

Table 1 Media and buffer used in this project	88
Table 2 Information of antibodies used in this study.....	90

List of Abbreviations

BMD bone marrow derived

BMT bone marrow transplant

β -AR β -adrenergic receptors

2D/3D two-dimensional/three-dimensional

α -SMA smooth muscle α -actin

ACTA2/Acta2 smooth muscle α -actin gene (human/mouse)

COL1A1/Col1a1 type I collagen, $\alpha 1$ subunit gene (human/mouse)

COL1A2/Col1a2 type I collagen, $\alpha 2$ subunit gene (human/mouse)

COL3A1/Col3a1 type III collagen, $\alpha 1$ subunit gene (human/mouse)

DAB 3,3'-diaminobenzidine

EC endothelial cells (ECs)

ECM extracellular matrix

FA focal adhesion

FAK focal adhesion kinase

FBS fetal bovine serum

GAPDH/Gapdh glyceraldehyde-3-phosphate dehydrogenase gene (human/mouse)

H&E hematoxylin and eosin stain

HI haploinsufficiency

HIER heat-induced epitope retrieval

ITGA1/A2/B1 integrin $\alpha 1/\alpha 2/\beta 1$ subunit genes

LCA/RCA left/right common carotid artery

MRTF-A myocardin-related transcription factor-A

MRTF-B myocardin-related transcription factor-B

NSAIDs nonsteroidal anti-inflammatory drugs

PDGF platelet-derived growth factor
pH3 phosphorylated histone H3
pN/Ccollagen partially-cleaved procollagen
POD post-operative day
pRb phosphorylated retinoblastoma protein
ROI region of interest
SMCs smooth muscle cells
TGF- β 1 transforming growth factor- β 1
TGFB1 TGF- β 1 gene
TGFBRI/2 TGF- β 1 receptors 1 and 2 genes
vEDS vascular Ehlers-Danlos syndrome
VEGF vascular endothelial growth factor

1 Introduction

1.1 What is vEDS?

Vascular type of Ehlers-Danlos Syndrome (EDS) is prominent by thin, translucent and easily bruised skin; rupture of uterine, dissection of arterial or intestinal tissues and obvious facial appearance. These defects affect connective tissues like skin and joints, causing abnormalities in uterus, colon and other hollow organs¹. vEDS is mostly resulted from the mutations in *COL3A1* gene. Propeptide of type III collagen is encoded by *COL3A1* gene. vEDS patients develop aneurysms and dissection of arteries throughout the body (**Figure 1.1**). Most patients with this syndrome develop when they are relatively young, their medium to large sized arteries are usually accompanied with spontaneous arterial complications. vEDS patients bruise easily and have spontaneous ecchymosis, which leads to chronic skin discoloration from hemosiderin deposition most commonly on the shins and knees. In addition, they also suffer from obstetric and gynecologic complications, including cervical insufficiency, vaginal tears and lacerations. Gastrointestinal complications occur in up to 25% of patients, and the majority of these are spontaneous rupture of the sigmoid colon². The median life expectancy of vEDS patients is 40-50 years. Death is likely due to the secondary to complications associated with vascular and hollow organ rupture³.

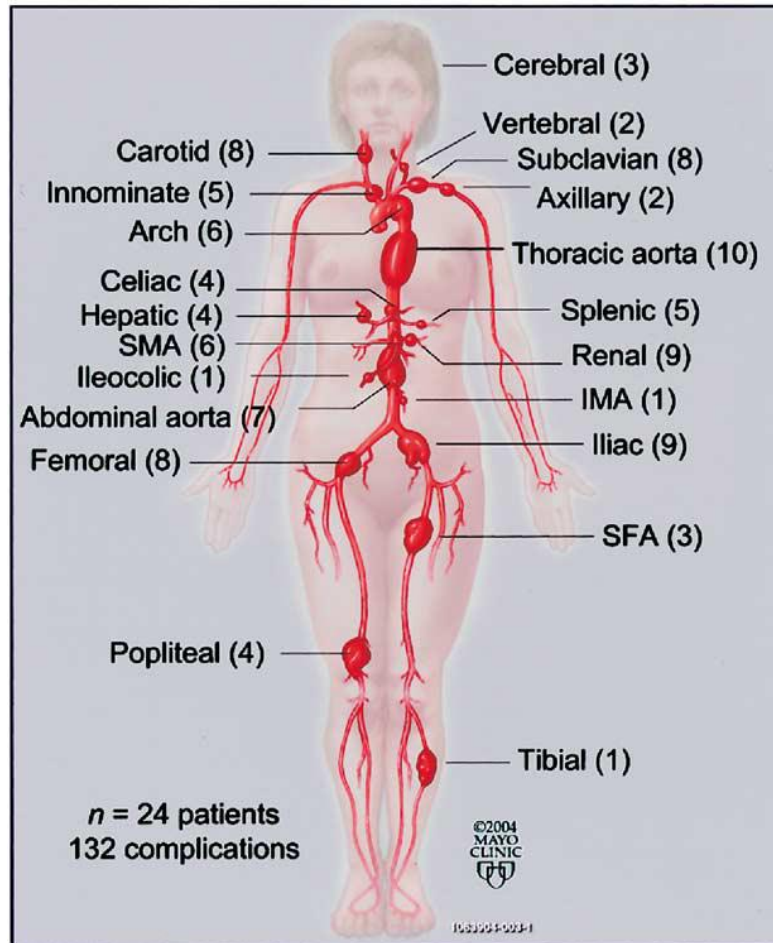


Figure 1.1 Distribution of 132 vascular complications

Reprinted with permission from Elsevier [The spectrum, management and clinical outcome of Ehlers-Danlos syndrome type IV: a 30-year experience. Oderich GS, Panneton JM, Bower TC, et al. *Journal of Vascular Surgery*. 2005].

1.2 Diagnosis of vEDS

It is difficult to diagnose vEDS because many of the traits that vEDS patients have are subtle and nonspecific. Easy bruising is the most frequent manifestation and is present in childhood³. Other phenotypes such as premature rupture of the arteries, membranes of different hollow organs, or recurrent joint dislocation or subluxation. vEDS patients also have distinct facial features, like prominent and wide-open eyes, pinched nose, small and thin lips as well as lobeless ears. Early clinical diagnosis is extraordinarily difficult without a diagnosis of familiar affection or major complication found in vascular or intestinal tissues⁴.

1.3 Current therapeutic approaches and management to vEDS

vEDS is a rare genetic connective tissue disorder with life threatening complications that include arterial dissection and ruptures, and intestinal and uterine ruptures, currently, there have been no therapeutics with FDA-approval for vEDS patients in the United States, and physicians face the challenge of establishing an effective preventative treatment plan for their patients⁵. One problem with assessing treatment of vEDS patients is that the disease is relatively rare. Very few centers around the world have significant experience in treating and managing these patients. In addition, given the extreme fragility of the tissues, outcomes for interventions tend to be very poor, as even relatively simple diagnostic procedures have a high rate of catastrophic complications. To possibly create a milder treatment, Pierre Boutouyrie et al proposed a clinical trial for the drug, celiprolol, a cardio-selective β blocker (β -blocker) with β_2 agonist vasodilatory properties⁶. Because beta-blockers have historically been used for arterial diseases, it was surmised that celiprolol could also help alleviate vEDS patients' arterial dissection or rupture. Surgical repair may decrease mortality caused by bowel rupture, arterial rupture, or uterus rupture. However, even if the tissues are friable, repair procedure is very difficult, vascular surgeons must pay special attention to these patients given their complicated vascular phenotypes and the complexities involved in repairing their tissues.

1.4 Vascular Structure and Aorta

In vertebrate mammals, the arterial system is a network of extensive and dynamic vessels that transport blood and deliver essential nutrients and oxygen to other parts of the entire body. Large arteries are important for proper cardiac function because they serve as important reservoirs. These large arteries enable the arterial tree to withstand great changes blood volume when there is barely pressure change⁷. Although blood vessels are different in size, function and anatomy, they share similar basic elements to form functional structure. Both arterial and muscular vessels are basically formed by three different layers, the intima, the media, and the adventitia in comparison to the central lumen. There is a thin layer with the lumen side of the intima which are lined by endothelial cells (ECs). ECs play a major role in development of vasculatures as well as recruitment of smooth muscle cells (SMCs) to the vascular wall upon arterial injury. The media is mainly composed of specialized vascular SMCs (vSMCs) and elastin. Under a variety of circumstances, SMCs serve both to contracture and to produce components of extracellular matrix (ECM). ECM mainly provide structures to resist forces generated by fluid flow and other mechanical strength to arteries. The elastin is arranged in fenestrated sheets, and the collagen fibers, SMCs and ECM float among the sheets. The adventitial layer is mainly composed of fibroblasts which also produce adventitia components such as connective tissues. The larger aortic and vascular arteries also contain the vasa vasorum which supply nutrients to the vessel walls themselves (**Figure 1.2**).

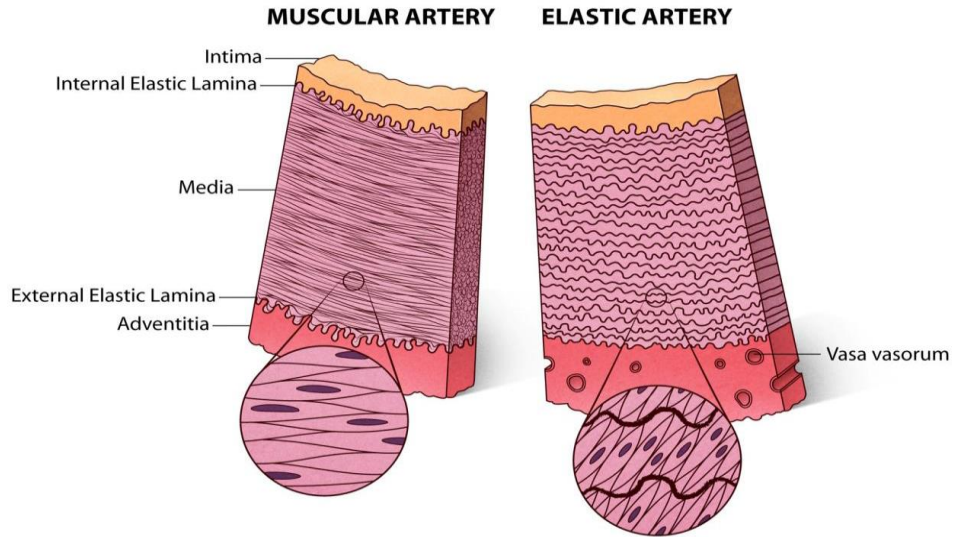


Figure 1.2 Schematic architecture of a representative medial in a muscular artery (left) and an elastic artery (right).

The media of a muscular artery is bordered by the internal and external elastic laminae and contains overlapping and concentrically-oriented smooth muscle cells. The media of an elastic artery instead contains many elastic laminae alternating with muscular layers of smooth muscle cells that each span the full thickness. The adventitia in a larger elastic artery also contains small blood vessels (vasa vasorum) that nourish the outer layers of the wall. [Arteries, Smooth Muscle Cells, and Genetic Causes of Thoracic Aortic Aneurysms. Chapter 12: Inflammatory Diseases of the Blood Vessels, 2nd ed. Reid AJ and Milewicz DM1].

Quoted text and figure reprinted with minimal modification and permission from John Wiley and Sons [Arteries, Smooth Muscle Cells, and Genetic Causes of 12 Thoracic Aortic Aneurysms. Chapter 12: Inflammatory Diseases of the Blood Vessels, 2nd ed. Reid AJ and Milewicz DM1].

1.5 Structure of collagen and their function

Fibroblasts are the major cell type which synthesize and secrete collagens. Among the 17 collagen types, types I, III, IV, V and VI have the highest amount distributed in different tissues. Collagens I, III, and V are assembled into fibrillary structure, with types I and III collagens playing a major role in withstanding strength to the vessel wall. The fibrils are then formed according a self-assembly principle. A protein monomer with the correct structure may aggregate with itself following a precise manner⁸. The procollagens, also known as precursors, are first synthesized and then enzymatically cleaved to form the corresponding collagens (**Figure 1.3**). Difference in the distribution of collagens I and III also occur in different vascular vessel regions. In the ascending aorta's media and adventitia, collagens I and III are common while in the descending and medial layer, they are different distribution of type I and III collagens⁷.

We will focus on type III collagen because only mutations in *COL3A1* gene are widely studied as a potential factor to cause vEDS. The type III procollagen molecule is assembled from three identical pro $\alpha 1$ (III) chains. The N-pro-peptide domain contains specific structure which is part of the cleavage site. The enzymes function at the site to remove propeptide. The C-propeptides of the procollagen are entirely globular. After forming the triple helix structure, they are secreted to the extracellular area where they undergo post translational modification and assembly to form mature collagen fibrils (**Figure 1.4**) (Heritable diseases of collagen).

1.6 Mutation of *COL3A1* gene leading to deficiency of type III collagen

Causative mutations are mainly identified in vEDS patients in the *COL3A1* gene which locates at position 31 of chromosome 2 (2q31)⁴ and encodes pro-type III collagen. Its transcription produces the pro- αI chain of type III collagen. Three αI chains are strictly assembled into a triple helix. To successfully assemble a triple helix, a glycine residue is required the formation of a structure of (Gly-X-Y) n repeats. The glycine residue locates at every third amino-acid of the polypeptide chain. This motif ensures the three

α I chains forming a triple-helical structure (**Figure 1.4**), while residues X and Y adjacent the glycine residue locating outside on the surface, all the other residues are buried within the protein⁹. Also, this motif provides the stability of the collagen fibrils by increasing hydrogen bonding. The C-propeptide domain of the procollagen is critical in initiating the process of trimerization. There are two major events involved in trimerization: specific chain recognition and formation of a stable nucleus¹⁰. After folding into homotrimers, the collagen will be transported outside of the cells and into the extracellular matrix (ECM), where it is processed enzymatically with different enzymes mainly metalloproteinases which belong to the ADAMTS2 (a dis-integrin and a metalloproteinase with thrombospondin repeats)¹¹. After the formation of procollagen, the final step for the biosynthesis and assembling of collagens is the stabilization of the supramolecular which is initiated by lysyl oxidases¹². These super cross-links produce long, thin fibrils that comprise the intercellular space. Individuals with *COL3A1* gene mutations have severe defects in the

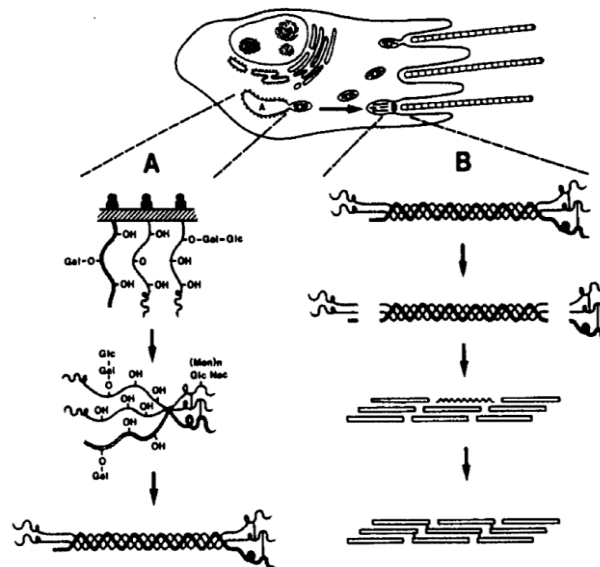


Figure 1.3 Fibroblast assembly of collagen fibrils

Panel A shows intracellular post-translational modifications of pro- α -chains, association of C-propeptide domains, and folding into triple-helical conformation. Gal denotes galactose, Glc glucose, GlcNac N-acetylglucosamine, and (Man)_n mannose residues. Panel B shows enzymatic cleavage of procollagen to collagen, self-assembly of collagen monomers into fibrils, and cross-linking of fibrils. Reproduced with permission from [Heritable diseases of collagen. Prockop DJ, Kivirikko K. New England Journal of Medicine. 1984], Copyright Massachusetts Medical Society.

overall structure of the type III pro- α I chain. Single nucleotide substitutions for the glycine residues are the most common mutations which have been found within the *COL3A1* gene. Gly substitution destabilizes

the structure of the triple helix. This results in decreased functional type III collagen. As of now, over 700 COL3A1 gene mutations have been identified, another mutation is the splicing skipping mutation. Both types of mutations lead to equal production of abnormal and normal procollagen peptides, but because collagen III is a homotrimer formed by three identical procollagen peptides, such mutations lead to production of a seven-to-one ratio of abnormal to normal collagen molecules, thus a minimal (MIN) amount (10%-15%) of normal collagen is produced.

Some other mutations such as splicing at the level of transcription, deletion of the gene, and null mutation have also been observed. Exon skip mutations result in an exon splicing error, which leads to a frame shift mutation during the translation process. This results in premature degradation of the mutant messenger RNA. This causes expression of a single gene thus termed haploinsufficiency (HI) which result in only 50% of the normal amount of type III procollagen¹³. Clinically, people with haploinsufficient COL3A1 mutations have a milder phenotype and an extended life expectancy as well as a later age at the time of their first complication.

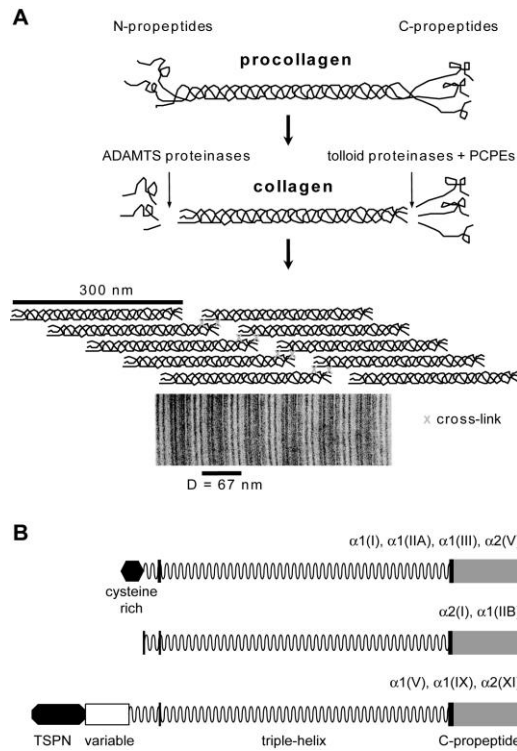


Figure 1.4 Fibrillar procollagens and fibril assembly

A. N- and C-terminal processing leads to spontaneous assembly of collagen fibrils, which are subsequently stabilized by the formation of covalent-cross-links. **B** Domain structures of fibrillar procollagen chains. Reproduced with permission from [Heritable diseases of collagen. Prockop DJ, Kivirikko K. New England Journal of Medicine. 1984], Copyright Massachusetts Medical Society.

1.7 Increased Carotid wall stress in vEDS

Studies from Boutouyrie et al¹⁴, used a biomechanical method to detect if there are changes in arterial wall mechanics that might predispose to dissection and rupture. In vEDS patients, there were 43% and 39% higher in intimal medial ratio (IMT) and either internal diameter or midwall diameter compared to that in control subjects. The feature seen in the arterial wall of vEDS patients may result from the reduction of collagen I fibers.

1.8 vEDS and *Col3a1* mice

The haploinsufficient *Col3a1* mouse was generated by Liu et al. for study of the function of collagen III in fibrillogenesis of collagen I and in development of cardiovascular system. The first exon as well as the promoter of the *Col3a1* gene was replaced with a PGK-neo cassette (a eukaryotic promoter (PGK) with the expression of neomycin resistant gene in mammalian cells)¹⁵. The *Col3a1*^{-/-} mouse was generated from intercrosses of heterozygous mice¹⁵. About only 10% of the *Col3a1*^{-/-} animals survive to adulthood, while the rest of *Col3a1*^{-/-} animals die with 3 days after birth. The most common reasons leading to the death of *Col3a1*^{-/-} mice is the rupture of vasculatures and colons, which are very similar to complications in vEDS patients. Liu et al also performed ultrastructural analysis on tissues harvested from *Col3a1*^{-/-} mice which revealed that type III collagen plays a critical role in normal type I collagen fibrillogenesis, in the development of cardiovascular as well as the function and development of other organs¹⁶.

To find out other structural defects in *Col3a1*^{+/-} mice, they also carried out a detailed analysis with electron microscopy for aorta and heart, (**Figure 1.4**) showing that the collagen fibrils were absent or significantly decreased in the media of the *Col3a1*^{+/-} aorta. At the same time, they also found that the fibril number in *Col3a1*^{+/-} aorta decreased to even less than one third of that in *Col3a1*^{+/+} aorta while mean diameter was significantly increased in *Col3a1*^{+/-} mice (**Figure 1.5**). In addition to the vascular system, other tissues, such as the skin and lung of *Col3a1*^{+/-} mice were also microscopically analyzed. It was found

that the collagen I fibrils in the *Col3a1*^{+/-} skin were both highly variable in diameter and disorganized in

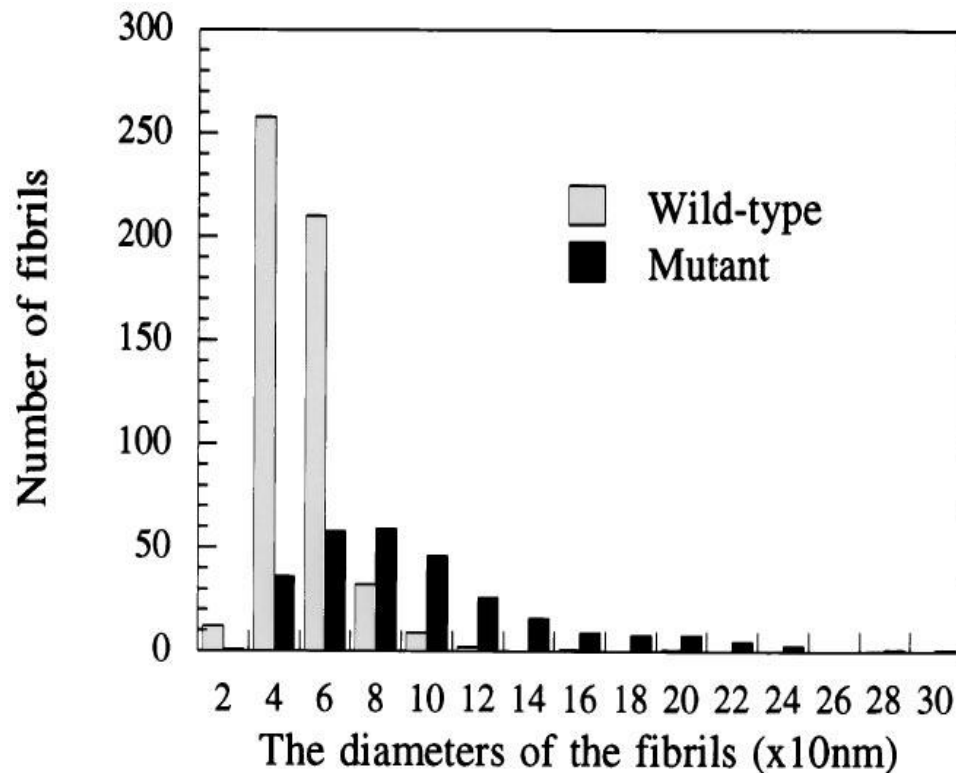


Figure 1.5 Comparison of the diameters of collagen fibrils in the adventitia of aorta of wild-type and mutant mice

A 2 mm 32 mm area in the adventitia of either wild-type or mutant aorta was randomly chosen, and all the fibrils in this area were measured for their diameters and counted. Reproduced with permission from [Heritable diseases of collagen. Prockop DJ, Kivirikko K. New England Journal of Medicine. 1984], Copyright Massachusetts Medical Society.

structure. Their results suggested that type III collagen was important in regulating the formation and assembly of type I collagen fibrils, specifically the diameter. They concluded that the phenotypes shown by the *Col3a1*^{-/-} resembled to the clinical complications of vEDS patients.

Cooper et al expanded Liu's study and demonstrated that the *Col3a1*^{+/-} could be used as a model for vEDS¹⁷. They found that the collagen content the heterozygotes was reduced in the abdominal aorta, and functional studies revealed diminished aortic wall strength in *Col3a1*^{+/-} mice. There were also reduced strength and increased wall compliance in the heterozygotes via pressure test. However, the mice did not show life-threatening clinical signs nor did they develop gross vascular lesions which were similar to those happen to vEDS patients. Overall, they suggested to generate a new mouse model with a single glycine substitution which represent the severity of mutation for vEDS patients. However, few studies focus on the mechanisms by which deficiency of type III collagen can cause vascular disease. Reid et al (unpublished data) induced artificial injury of the left carotid artery by permanent ligation in both *Col3a1*^{+/-} heterozygous and *Col3a1*^{+/+} mice. By comparing the histological changes in the ligated *Col3a1*^{+/-} and *Col3a1*^{+/+} arteries, they found delayed thrombus resolution and increased formation of neo-vessels in the medial layer of the artery in the *Col3a1*^{+/-} mice after both 14 and 21 days of carotid artery ligation.

1.9 Myofibroblasts and wound healing

Numerous reports have investigated that cells derived from bone marrow (BMDs) or mesenchymal originated cells such as fibroblasts, are important for remodeling after arterial injury^{18,19}. During tissue repair, fibrin clot formed at the injury site to further recruit inflammatory cells. The fibrin is soon followed by various migrating cells that modulate the fibrin matrix, resulting in a collagenous scar²⁰. These activated fibroblasts produce critical components of ECM for the wound area. Then, the fibroblasts become myofibroblasts and gain the ability to contract and generate contractile forces during repair. After all the initial steps of wound repair, myofibroblasts disappear with the process of cell apoptosis. When myofibroblasts persistent into differentiated myofibroblasts instead of dying, there will be extra ECM components deposited, which are usually found in hypertrophic scar, as well as fibrotic processes in the kidneys, heart, and lungs²¹.

1.10 TGF- β signaling pathway and differentiation of fibroblasts

TGF- β 1 is a cytokine secreted by platelets and fibroblasts and macrophages. In the classical TGF- β signaling, three isoforms in TGF- β family of ligands are bound to receptor T β RI and T β RII. T β RII is constitutively phosphorylated and further phosphorylates T β RI upon binding of the ligand. After that, the intracellular SMAD signaling pathway will be activated by the receptor-ligand-complex through Smad-2, Smad-3 and co-Smad4. SMAD proteins will then be translocated to the nucleus where they regulate expression of a number of genes²². However, the differentiation of myofibroblasts from fibroblasts, characterized by increased expression of SMA is first activated by TGF- β signaling and followed by FAK signaling pathway as results shown by Thannickal et al²³. In this study, they demonstrated that both TGF- β 1 and FAK signals were required for a stable status of the myofibroblasts. TGF- β 1-induced myofibroblast differentiation would be inhibited in non-adherent cells even if TGF β -Smad2 phosphorylation signaling was active. Tyrosine phosphorylation of FAK induced by TGF- β 1 which including Tyr-397 was also delayed in relative to early TGF- β 1-Smad signaling. Blockage of FAK or induction of FAK mutation could inhibit expression of α -SMA, formation of stress fibers and cell proliferation induced by TGF- β 1.

1.11 Neovascularization in arterial diseases

Rapid revascularization is essential in restoring organ function after injury, ischemia, or in regenerating organs. An angiogenic switch often initiates the revascularization process, and this starts the process of recruiting endothelial cells that assemble into neovessels^{24,25}. However, because tissue injury often prevents pre-existing endothelial cells (ECs) from performing their original function, exogenous vascular progenitors might facilitate the restoration of re-vascularization. Adult bone marrow (BM) provides different tissue specialized stem cells and other progenitor cells. There is a small cell population known as epithelial progenitor cells (EPCs). These EPCs can circulate and contribute to the neovascularization processes that promote rapid organ revascularization.

The concept of fibrocyte was first described by Richard et al. in 1994 as circulating monocyte-derived cells, capable of expressing fibrotic phenotypes²⁶. Monocytes derived fibrocytes show both macrophages features and the tissue remodeling properties²⁷. They uniquely co-express the haematopoietic stem cell markers, CD45 and CD34. Fibrocytes also produce extracellular matrix (ECM) proteins. They adopt a spindle shape and are present in wound exudates. Fibroblasts have remarkable plasticity in *in vitro* studies, demonstrating their ability to be reprogrammed into haematopoietic appearance-wise, fibrocytes also appear to be an intermediate between fibroblasts and macrophages. This phenotypical overlap could be because fibrocytes are an intermediate population in the conversion of fibroblasts into macrophages, and vice versa²⁷. In injured tissues or inflammatory locations, fibrocytes can be induced into fibroblasts by inflammatory factors to execute the function of ECM producing cells and function in injury repair or wound healing²⁷. In fact, it may be more appropriate to call them “fibrophages” or “macroblasts.” Additionally, in injured tissues or locations of inflammation, fibrocytes can be induced to transform into fibroblasts when in the presence of inflammatory factors. These new fibroblasts can then execute the same functions of ECM-producing cells in injury repairing or wound healing. Studies from Desmoulière et al proposed that fibrocytes derived from circulating precursor cells in the blood could be induced to differentiate into fully functioning myofibroblasts; they express collagen and α -SMA, induce contractile proteins, and contribute to thrombus resolution. More and more studies discover that the BM not only originates hematopoietic cells for skin function, but dermal fibroblasts and myofibroblasts. Study from Carrie Fathke et al. shows that bone marrow is significant more important to normal skin function and healing cutaneous wounds than that had previously been recognized. In fact, of all dermal fibroblasts, 15-20% were derived from the BM. This population of BM-derived dermal cells was more versatile than its normal counterpart.

1.12 Previous studies in our lab on the *Col3a1* mice

Prior *in vivo* studies by Dr. Amy Reid on the *Col3a1* mice using an artificial arterial injury model at the left carotid artery found that: 1) There is increased inflammatory response in the *Col3a1*^{+/-} artery

compared with that in the *Col3a1*^{+/+} artery; 2) There are persistent proliferative myofibroblasts in the *Col3a1*^{+/-} artery compared with that in the *Col3a1*^{+/+} artery; 3) There is increased new vessel formed in the medial layer in the *Col3a1*^{+/-} artery compared with that in the *Col3a1*^{+/+} artery. *In vitro* cellular studies using 3D fibrinogen gel experiments, by comparing the dermal fibroblasts from vEDS patients and normal control, demonstrating a dysfunctional matrix remodeling by myofibroblasts in vEDS patients.

Based on the prior findings, we hypothesize that fibroblasts from the bone marrow of *Col3a1*^{+/+} mice can rescue the post-injury phenotypes in the *Col3a1*^{+/-} mice and administration of celiprolol will be able to alleviate post-injury phenotypes in *Col3a1*^{+/-} mice. My dissertation research focused on the following: 1. Confirm that haploinsufficiency in *Col3a1* leads to aberrant wound healing after vascular injury of *Col3a1*^{+/-} mice; 2. Determine if bone marrow transplant rescues the aberrant arterial injury repair of *Col3a1*^{+/-} mice; 3. Assess if celiprolol treatment on the *Col3a1* mice improves aberrant injury repair in this model; 4. Understand the role of myofibroblasts in injury repair by *in vitro* cellular study using cells explanted from *Col3a1* mice.

2 Bone Marrow Transplantation Rescues the Phenotypes in *Col3a1*^{+/-} Mice

2.1 Introduction

Vascular Ehlers-Danlos Syndrome (vEDS) patients have aberrant healing of their skin, such as easy bruising, abnormal cutaneous scar appearance, and hypertrophic and fibrotic keloids^{28,29}. The cutaneous wound healing process repopulates and remodels the structural matrix of the tissue following injuries²⁰. There are three overlapping phases of the wound healing procedure (**Figure 2.1**): the inflammatory phase from 3 to 7 days after injury, the tissue formation/proliferative phase from day 7 to day 14 followed by the phase of tissue remodeling/contraction^{20,30}.

The inflammatory phase includes the circulating inflammatory cells' recruitment, infiltration and activation at the injury site, resulting in formation of fibrin clot via chemo-attractants such as platelets as well as activated macrophages produced transforming growth factor- β 1 (TGF- β 1)²⁰. Monocytes infiltrate to the injury site in response to certain chemo-attractants, such as fragments of ECM protein, TGF- β 1 and monocyte chemoattractant protein 1 (MCP-1). After infiltration, monocytes are activated and become macrophages. Macrophages function as the sources to produce and release PDGF and VEGF. Both PDGF and VEGF participate in initiating the formation of granulation tissue²⁰. Signaling transduction by macrophages critically promotes downstream injury repair activity by local cells^{20,30,31}. The tissue formation, also referred to as the proliferative phase, begins with the recruitment of macrophages followed by activation of fibroblasts into the wound area where fibroblasts proliferate. TGF- β 1 can both promote the proliferation and differentiation of fibroblasts³¹. Myofibroblasts entails a great potency and striking capacity for synthesizing ECM proteins and cellular contractility³². It was demonstrated that formation of granulation tissues is a critical event in wound healing for vEDS patients and *Col3a1*^{+/-} mice, because conversion of fibrin clot after injury into collagenous matrix relies heavily on newly produced type I and type III collagen^{32,33}. As shown by a study in rats, along with neointimal formation after intraluminal injury, there was a similar production of type I and type III collagens which were examined by qPCR to measure the transcription of *Colla2* and *Col3a1* genes³⁴.

We have demonstrated aberrant thrombus resolution in the *Col3a1*^{+/-} mice (Amy Reid, unpublished data). However, thrombus resolution progresses are similarly to wound healing, with evidence that the fibroblast-type cells, termed fibrocytes, come from the bone marrow³⁵. It has been shown that bone marrow-derived (BMD) fibrocytes are important in wound healing^{35,36}. Abe et al. also identified a potential pathway through which blood-borne fibrocytes differentiate into myofibroblasts. It was postulated that activated T cells could interact with circulating precursor cells of fibrocytes, triggering the early differentiation of fibrocytes (toward the fibrocyte phenotype). Fibrocytes then migrate to the wound site, where these early differentiated fibrocytes could further interact with T cells, which promote fully differentiation and maturation of fibrocytes, termed as myofibroblasts with stimulation of TGF- β 1. These myofibroblasts then express α -Smooth muscle actin (α -SMA), produce collagen as well as other ECM proteins that promote contracture and wound healing³⁷. Finally, studies by Han et al. also showed a distinct neointimal lineage cells that were originated from circulating BMD cells and participated in vascular injury repair. These BMD neointimal cells also resemble stem cell-like fetal/immature vascular smooth muscle cells (SMCs) or myofibroblasts³⁸.

Neointimal SMCs proliferation occurs in vascular injuries, and most proliferative cells may come from the arterial wall³⁰. Many studies using the carotid injury model focus on resident SMCs proliferation from the arterial wall. As reviewed by Daniel et al. SMCs contributing to the neointima formation after arterial injury are primarily from the wall, and BMD progenitors rarely contribute to SMCs in neointima formation³⁹.

Fadini also reviewed that SMCs contributing to the formation of atherosclerosis are mostly from the local arterial wall⁴⁰. A study by Kawasaki using a mouse carotid artery ligation model shows that thrombus formation and resolution is a prerequisite for neointimal formation⁴¹, and thrombus resolution also ensures successful arterial injury repair⁴². Based on the current information, we speculate that immediately after arterial injury, BMD fibrocytes circulate to the injury site to resolve the thrombi, followed by cells migrating from the arterial wall for neointima formation to secure successful injury repair.

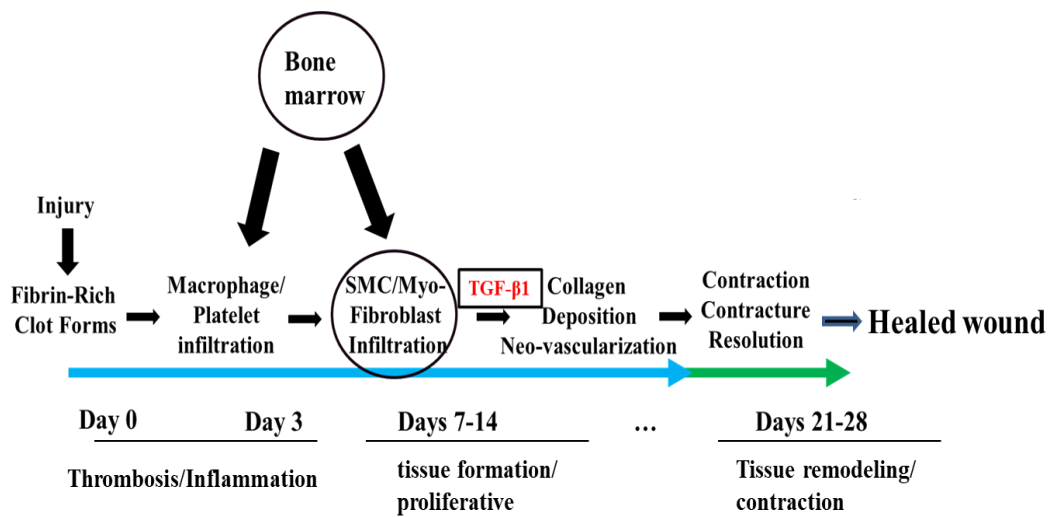


Figure 2.1 Three over-lapping phases for wound healing

Myofibroblasts are in the three over-lapping wound healing process.

2.2 Hypothesis

We hypothesize that deficiency of type III collagen results in aberrant vascular injury repair in vEDS patients since their myofibroblasts are not producing sufficient type III collagen to effectively and efficiently resolve thrombi after vascular injury. In the *Col3a1*^{+/-} carotid ligation mouse model, after induced ligation injury, arteries from *Col3a1*^{+/-} mice show a persistent inflammation and proliferative cells, presumably myofibroblasts, and increased medial neovessel formation. We hypothesize that the extended thrombus resolution seen in *Col3a1*^{+/-} arteries and the formation of neovessels in the wall, weaken that wall and predispose to arterial events like dissection. We further hypothesize that by introducing BMD fibrocytes with *Col3a1*^{+/+} genotype to *Col3a1*^{+/-} mouse, these fibrocytes could then differentiate into myofibroblasts with full expression of procollagen type III and correct the aberrant wound healing in *Col3a1*^{+/-} mice after carotid ligation. Therefore, we performed bone marrow transplant (BMT) of wildtype bone marrow into the *Col3a1*^{+/-} mice to test this hypothesis.

Specific aims:

- (1) **To replicate Dr. Amy Reid's study results in 12 to 14-week-old mice instead of 22 to 24-week-old mice.** This will confirm that the younger mice can be used for these studies.
- (2) To perform a forward and reverse bone marrow transplant to rigorously address the stated hypothesis.
 - a) Assess the response and pathological changes to vascular injury in *Col3a1*^{+/-} mice after they receive bone marrow transplants (BMT) from *Col3a1*^{+/+} mice.
 - b) Assess the response and pathological changes to vascular injury in reverse BMT, i.e., *Col3a1*^{+/+} mice after they receive a bone marrow transplant from *Col3a1*^{+/-} mice.

2.3 Methods

2.3.1 Carotid Ligation Injury

Mice used in the experiment (purchased from Jackson Laboratories, and bred in the animal facility of UT McGovern Medical School at Houston) weighed between 25-30g. The animal study protocol was approved by Animal Welfare Committee at UThealth at Houston. Mice were surgically ligated at the left common carotid artery at the age of 12-14 weeks (unless otherwise stated). This age corresponds to the mature adulthood phase in mice. The risk of fatal complications in vEDS patients increases within the age range. However, there is no significance difference in risks for either complication or survival between *Col3a1*^{+/+} and *Col3a1*^{+/-} mice.

The surgery procedure was modified from that described in Dr. Reid's study (Amy Reid unpublished data). Briefly, surgical mice were induced to anesthesia with 4% isoflurane which was maintained at 2-2.5% by a nose cone connected to the mouse. Aseptic techniques were used during the procedure and the fur at the neck area was shaved off with Nair gel and sanitized with alcohol swabsticks. Afterwards, analgesia with subcutaneous bupivacane (2.5 mg/kg) was applied immediately before making a midline incision of 3mm in length in the neck with sterilized scissors. Followed by dissecting away the left common carotid artery from the carotid sheath and vagus nerve. A ligature was made on the artery with 6-0 silk suture immediately at the bifurcation site where the internal carotid arteries separate from external carotid arteries. It was important to be gentle to avoid bleeding. The open skin area was irrigated with iodine alcohol and closed by 2 interrupted stitches with 5-0 suture which would be absorbed after about one week.

About 10% of animals experienced stroke symptoms of during the first 7 post-operative days (POD7). Mice which failed to maintain 80% of their body weight were sacrificed. About 5% of the mice died before ligation due to massive bleeding caused by the procedure of carotid artery dissection. Mice that did not show neurological phenotypes such as stroke were monitored and treated subcutaneous with ketoprofen (2-5mg/kg) twice a day for 2 days after surgery. They were weighed daily and injected mice as needed with 0.5-1ml lactated Ringer's solution based on their weight for over 10% drops. Normally mice would

survive 95% after POD7. Mice were sacrificed on 7, 14 and 21 days after surgery for the different following up experiments.

2.3.2 Histology studies

For studies and analysis of POD7 arteries (N = 6 *Col3a1*^{+/+}, 6 *Col3a1*^{+/-}), POD14 (N = 6 *Col3a1*^{+/+}, 6 *Col3a1*^{+/-}), and POD21 (N = 5 *Col3a1*^{+/+}, 5 *Col3a1*^{+/-}), mice were first sacrificed, followed by puncturing of the left ventricles with a 27-gauge needle. An incision was made on the right atria to allow the outflow of perfusate. Mice were then perfused with phosphate-buffered saline (PBS) at <20 ml/min until blanching of the liver completely. Mice were then perfused with 10ml of 10% formalin at the similar rate to fix arteries in the native geometry. Both the entire lengths of carotid arteries were harvested for multiple experiments.

Arteries were followed by fixing in 10% buffered formalin for about 24 hours. After fixation, arteries were cleaned up and the connective tissues were removed followed by processing. After processing, the arteries were left in fridge to chill up. Then the arteries were cut three times with a scalpel: one cut was immediate to the ligature to remove the suture; a second cut was at the location of the descending aorta to remove extra descending aorta; the third cut was in the mid-carotid artery. The remaining two pieces of the artery were embedded with careful attention to maintain correct orientation. The entire block with embedded artery was serial sectioned and three 5- μ m-thick sections were collected per slide all through the entire length of the arteries. Every tenth slide from the entire slides sequence was then performed with hematoxylin and eosin (H&E) staining, followed by imaging a representative section on each slide. This set of sequential images were enough for us to build up an entire arterial length along the axis of the arteries. Each carotid artery could supply approximately 60 to 80 slides. All images in this dissertation were presented at 20x, unless otherwise stated, and scale bars represent 100 μ m.

2.3.3 Immunohistological (IHC) staining

The IHC staining method was modified from Dr. Reid's study (unpublished data) and most of the methods were similar with only minor corrections. Briefly, each arterial segments as obtained above from H&E-staining provided a relative location of each segment with neointima formation. Those unstained slide neighboring each neointima positive slide was subjected to IHC probes (Mac-2, pH3 and CD31) to investigate the amount of macrophages, the number of actively proliferating cells locate within the neointima and the neovascularization in the medial layer. The first slide was probed with Mac-2, which showed the number of macrophages. The second local slide was used to measure the number of pH3-positive nuclei. The third slide was subjected to CD31 which was used to detect endothelial cells that are precursors for neovessels. Unstained sections were processed before heat-induced epitope retrieval (HIER citrate pH 6.0) followed by blocking for 1 hour at room temperature.

For detecting the local macrophages, slides with arterial sections were probed with rat anti-mouse Mac-2 primary antibodies (Cedarlane, Burlington, NC) and incubated for 1 hour at room temperature. For detection of proliferative cells, slides with arterial sections were probed with with rabbit anti-mouse pH3 primary antibodies (Millipore, Billerica, MA) followed by incubation overnight at 4°C. To examine neovessel formation in formalin-fixed paraffin-embedded tissues, slides were left overnight at 4°C with rat anti-mouse CD31 antibodies (Dianova, Hamburg, Germany). Slides with arterial sections were then washed with PBS, followed by incubation at room temperature for 1 hour with the appropriate biotinylated secondary antibodies, and then tissues were probed with peroxidase-conjugated avidin/biotin complexes (Vectastain ABC-AP Kit, Vector Laboratories, Burlingame, CA). Activity of peroxidase was detected using a 3, 3'-diaminobenzidine (DAB) chromogen (Dako, Glostrup, Denmark). Slides were counterstained with methyl green at the last step of staining.

For statistical analysis, slides were counted one by one to get the number of positive cells or vessels independently. And then, for each genotype, a mean \pm SD of positive cells was generated by averaging out

all the number from each group from the pooled neointima-positive slides, representing *Col3a1*^{+/+} or *Col3a1*^{+/-}. Significant differences were determined by the Student's *t*-test between the means (**p* < .05).

2.3.4 Bone marrow transplant

Forward BMT by generating *Col3a1/GFP* chimeric mice

The green fluorescent protein transgenic (*GFP*⁺) marker was used to track cells from the donor mouse. After BMT from *Col3a1*^{+/+} to *Col3a1*^{+/-} mouse, the fibrocytes in the *Col3a1*^{+/-} bone marrow would be replaced by the *GFP*⁺ marked fibrocytes from the *Col3a1*^{+/+} genotype. Using this procedure, we generated chimeric *Col3a1*^{+/+}/*GFP*⁺ and *Col3a1*^{+/-}/*GFP*⁺ mice. Engraftment of bone marrow was confirmed after 4-8 weeks by flow cytometry with the blood drawn from the tail vein of each animal upon sacrificing. Further confirmation was done by immunofluorescent staining with GFP antibody to detect the expression of GFP in the carotid artery section.

Forward BMT

BMT was performed in *Col3a1* mice (6-8 weeks in age). Briefly, recipient mice were irradiated with 8Gy X-ray. The first 4Gy irradiation (usually 7pm) was given 12 hours before the second 4Gy irradiation (usually 7am). Donor mice (CByJ.B6-Tg (CAG-EGFP) 10sb/J) were sacrificed humanely, the skin of the lower half was cut open, followed by spraying the animal down with 70% alcohol. The legs were removed and the skin and muscles were removed by cutting skin off. Kim wipes were used to remove the muscles by “rubbing”. Bones were transferred to a 100mm cell culture dish containing RPMI-1640 and the dish was brought to tissue culture hood. Bones were rinsed with fresh RPMI-1640 and transferred to a new dish with RPMI-1640. Femurs were separated from the tibia and fibula at the knee and the ends of the bones were cut off followed by transferring the bones to a new dish containing RPMI-1640. All the bone marrow cells were flushed out with a 27-gauge needle and syringe. This process was repeated with all bones until all the bone marrow cells were collected. Bone marrow cells were passed through a 22-gauge needle for

breaking up of all the clumps, then the large fragments in the cell suspension were removed by passing through a cell strainer (40 μ m) and bone marrow was then collected in a 50ml tube. 100-200 μ L iced PBS was added to the cells per mouse used, then the tubes were spun for 5 minutes at 500g or 1000rpm. Pellets were re-suspended in iced PBS, and then the number of cells from bone marrow was counted with a hemocytometer. Bone marrow was stored on ice until ready to inject. About 100-200 μ L of bone marrow (roughly 5-10 million cells) was injected retro-orbitally into the venous plexus of each lethally irradiated and anesthetized recipient mouse 3-5 hours after second irradiation. Recipient mice were kept in irradiated room and fed with irradiated chow as well as baytril water for 2 weeks. The 8Gy dosage control mice would often die after 10-14 days, while the 4Gy dosage control mice could survive (100% survival). Bone marrow cells repopulated in the lethally irradiated mice after a 4-8 weeks recovery.

Confirmation of chimera by flow cytometry

10 μ L of blood from the tail vein was drawn from sacrificing mice. Blood was then lysed by cell lysis buffer, (recipe: 0.155M NH₄Cl, 0.01M KHCO₃, 0.1mM Na₂.EDTA.2H₂O). Cells were then washed two times with wash buffer (1% FBS in PBS) before conjugating with APC/Cy7 anti-mouse CD45 antibody (Bio Legend Inc., CA) at 1:100 dilution, incubated at 4 degrees for 1 hour. After incubation, cells were washed for two more times followed by loading onto Gallio's Flow Cytometer (Beckman-Coulter Inc., CA) to detect the expression of GFP in the lymphocytes and analysis was achieved by using Kaluza software.

Reverse BMT

Similar to forward BMT, reverse BMT was performed in *Col3a1* mice (aging 6-8 weeks). Briefly, male recipient mice were irradiated with 8Gy X-ray. The first 4Gy irradiation (usually 7pm) was given 12 hours before the second 4Gy irradiation (usually 7am). The whole bone marrow cells were isolated from humanely sacrificed female *Col3a1*^{+/-} donor mice as described above. Bone marrow cells (5 million to each recipient mouse) were re-suspended in sterile PBS and injected retro-orbitally into the recipient *Col3a1*^{+/+} or *Col3a1*^{+/-} mice. Chimeric male *Col3a1*^{+/+} mice with the expression of type III collagen from circulating bone marrow cells of female *Col3a1*^{+/-} donor mice were generated.

Confirmation of reverse BMT

Since all donor mice are female and all recipient mice are male, we designed a method to detect the ratio of white blood cells from donor mice in recipient mice by measuring the ratio of mouse X and Y chromosome content in blood from recipient mice. The idea of this method was based on a traditional competitive RT-PCR for RNA quantification. By comparing homologous genes and sequences in mouse X and Y chromosomes, we designed a set of primers in *Zfx* and *Zfy* genes. The primer sequences on these genes were identical, forward primer: 5'- CATAGGCCTTCAGAACTCAAG and reverse primer: 5'- CTTTCGTATGAATGGAGATAACG. To further validate this result, we designed a set of primers in *Usp9x* and *Usp9y* genes and the primer sequences on these genes were identical, forward primer: 5'- AACAGAATGAGCAGTCTGAAAG and reward primer: 5'- TCCACCATCTTTTCTGACGCC.

2.4 Results

2.4.1 Increased neointimal formation after carotid arterial ligation in *Col3a1*^{+/-} mice at POD21

To compare the injury response between *Col3a1*^{+/+} and *Col3a1*^{+/-} mice, carotid ligation on the left carotid arteries was performed in *Col3a1*^{+/+} and *Col3a1*^{+/-} mice at around 12 weeks of age. Neointima formation was examined over three weeks after surgery by H & E staining. On POD7 after ligation, the *Col3a1*^{+/+} mice's tissues exhibited a thicker neointimal layer compared to their *Col3a1*^{+/-} counterparts. By POD14 and POD21, the *Col3a1*^{+/+} mice had fully completed thrombus resolution, and the neointima of their arteries had formed scars. At the same time, the *Col3a1*^{+/-} arteries were still thickening its neointimal layer. However, it has to be noted that the remodeling of neointima was slower in the arteries from *Col3a1*^{+/-} mice compared with that from *Col3a1*^{+/+} mice (**Figure 2.2**). To conclude, there was a slower neointima remodeling in the *Col3a1*^{+/-} arteries after carotid injury.

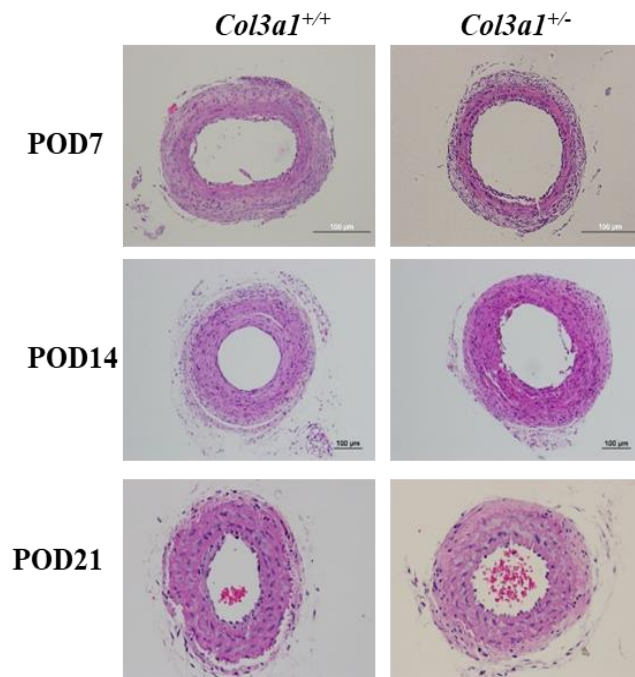


Figure 2.2 Slower neointima remodeling in the *Col3a1*^{+/-} mice

Representative cross sections of H&E-stained carotid arteries from both *Col3a1*^{+/+} and *Col3a1*^{+/-} mice after carotid ligation at POD7 (top panel), POD14 (middle panel) and POD21 (bottom panel), original magnification, 100x

2.4.2 Increased myofibroblast proliferation in the *Col3a1*^{+/-} mice after carotid ligation

We next examined if there was difference in the accumulation of cells in the neointima using IHC with an anti-pH3 antibody, to detect the cell mitosis marker pH3, which indicated the proliferative cells within the arterial lumen. At POD7, there was no difference observed in cell proliferation comparing *Col3a1*^{+/+} to *Col3a1*^{+/-} tissues (**Figure 2.3**). However, at POD14 and POD21, cell proliferation in the *Col3a1*^{+/-} tissues was significantly higher. This indicated that *Col3a1*^{+/-} mice have more neointimal hyperplasia at later time points after arterial injury.

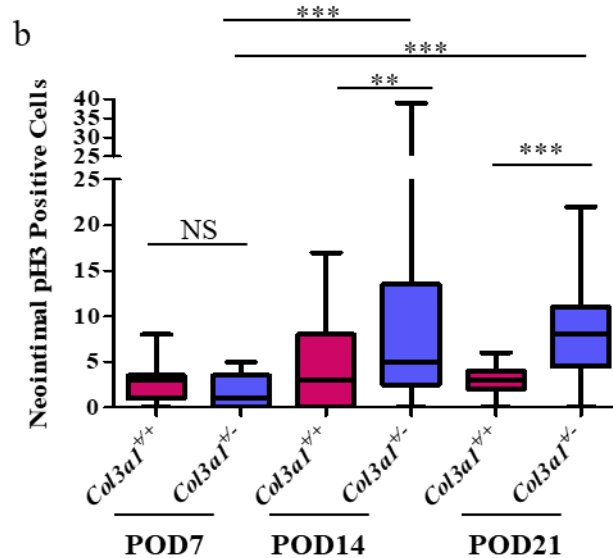
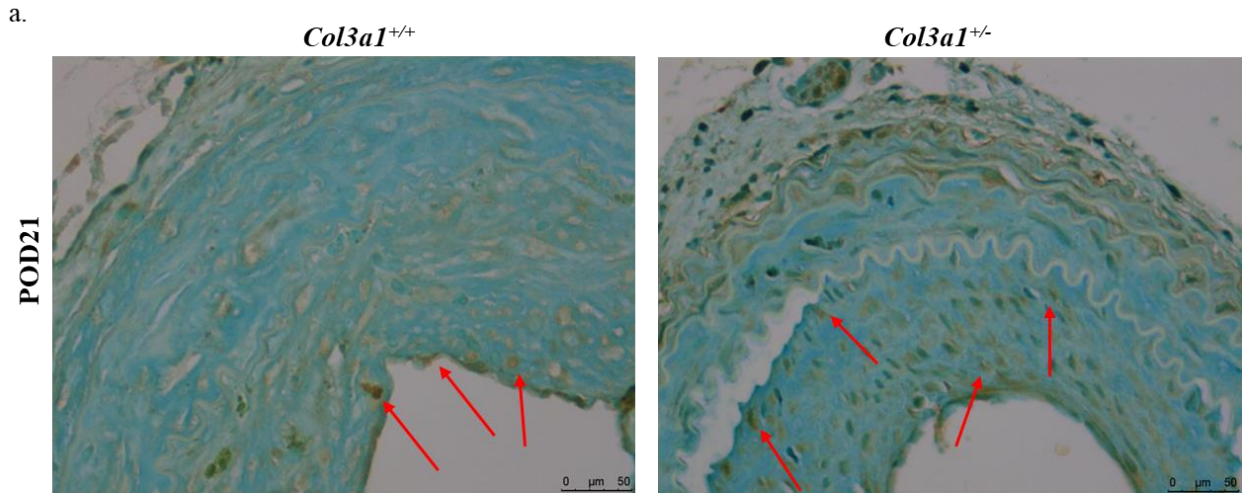


Figure 2.3 Increased cell proliferation within the *Col3a1*^{+/-} arteries

(a) Representative cross sections with anti-p-H3 staining (pH3, for proliferative cells) of carotid arteries from both *Col3a1*^{+/+} and *Col3a1*^{+/-} mice at 7, 14 and 21 days after carotid ligation. The cellular proliferation marker showed no difference between *Col3a1*^{+/+} and *Col3a1*^{+/-} arteries at 7 days after ligation but there was significant increased pH3 positive cells in the *Col3a1*^{+/-} arteries compared with that in the *Col3a1*^{+/+} arteries at both 14 and 21 days after ligation. Original magnification 400x, and scale bars: 50µm, red arrow was showing the pH3 positive cell (b) Quantitation: showed that there was increased cell proliferation in the arteries from *Col3a1*^{+/-} mice by POD14 and POD21 compared with that from the *Col3a1*^{+/+} mice. $n = 6$ per group. ** $p < 0.01$, $p^{***} < 0.001$ by Student's t -test, NS: no significance.

2.4.3 Increased inflammation in *Col3a1*^{+/-} mice after carotid ligation

In Dr. Amy Reid's unpublished data, there was increased macrophage burden in the *Col3a1*^{+/-} arteries at later time points. To determine if consistent phenotype existed in younger mice, we examined inflammation status with tissues from these mice. Arterial sections with tissues from POD7, POD14, and POD21 arteries were probed with mouse macrophage marker, Mac-2. Mac-2 positive cells in the neointima were counted in all sections. Result showed no significant difference in macrophage accumulation at POD7 (**Figure 2.4b**). However, we found a significantly increased number of macrophages in *Col3a1*^{+/-} arteries per section at POD14 and POD21 arteries. There were very few remaining inflammatory cells in the *Col3a1*^{+/+} sections by POD21. By contrast, Mac-2 positive cells are still present at high numbers in the *Col3a1*^{+/-} arteries through POD21 (**Figure 2.4b**). These results indicated the increased inflammation in the *Col3a1*^{+/-} mice after carotid injury.

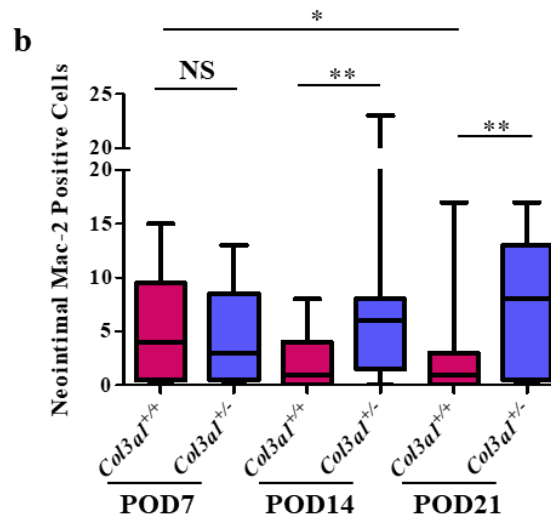
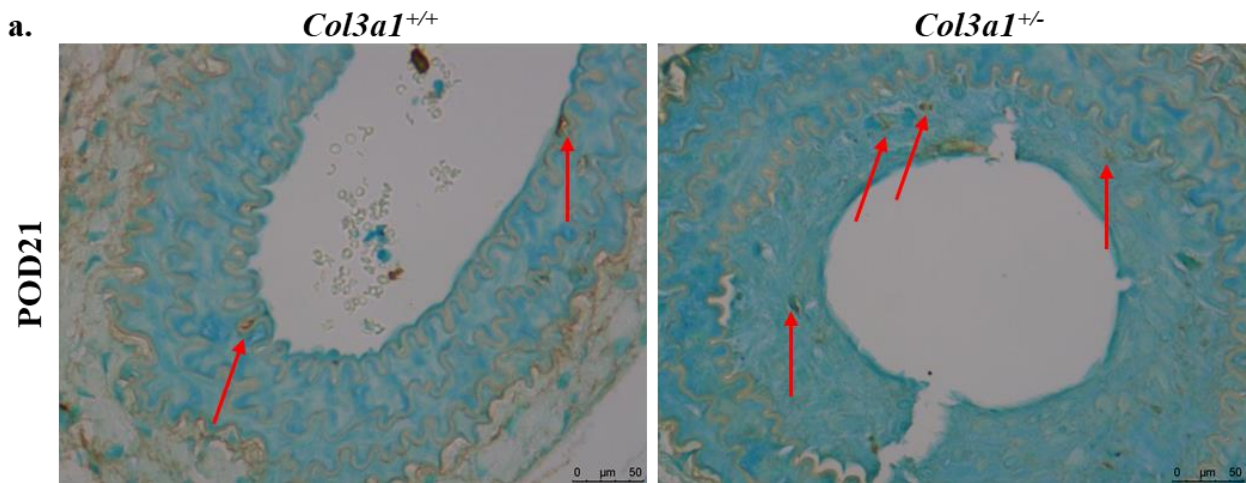


Figure 2.4 Increased inflammation within the *Col3a1*^{+/-} arteries

(a) Representative cross sections with anti-Mac-2 staining (Mac-2, for inflammatory cells) of carotid arteries from both *Col3a1*^{+/+} and *Col3a1*^{+/-} mice at 21 days after carotid ligation. The inflammatory marker showed no difference between *Col3a1*^{+/+} and *Col3a1*^{+/-} arteries at 7 days after ligation but showed an increase in Mac-2 positive cells in the *Col3a1*^{+/-} arteries at both 14 and 21 days after ligation, and there was a trend in increased Mac-2 stained cells in the *Col3a1*^{+/-} arteries from 7 days after ligation and persistent up until 14 and 21 days while a significant decrease in Mac-2 stained cells from 7 days to 21 days in the *Col3a1*^{+/+} arteries. Original magnification 400x, scale bars: 50μm, red arrow was showing the Mac-2 positive cell (b) Quantitation: showed increased inflammation in the arteries from *Col3a1*^{+/-} mice by POD14 and POD21. *n* = 6 per group. **p* < 0.05, *p*** < 0.01 by Student's *t*-test, NS: no significance.

2.4.4 Persistent neovascularization in the media of injured *Col3a1*^{+/-} arteries at POD21

Neovascularization was driven by VEGF and other cytokines secreted by platelets and macrophages. It plays an important role in venous thrombus resolution^{43,44}. Dr. Reid observed some blood-filled neovessels within the media of *Col3a1*^{+/-} arteries, while fewer or no neovessels were found in the arteries of the *Col3a1*^{+/+} mice. To determine if neovessel formation could also be observed in the younger mice, immunostaining for immature endothelial cells lined within the arterial lumen using an antibody directed against CD31 was conducted. Data showed consistently increased numbers of neovessels in the medial layer at POD14 and POD21 in the *Col3a1*^{+/-} arteries (**Figure 2.5**). We speculate that persistent inflammation in the *Col3a1*^{+/-} arteries drive continuous secretion of VEGF and further drive the formation of neovessels in the arterial wall which predispose the fragility of arterial wall in the *Col3a1*^{+/-} mice.

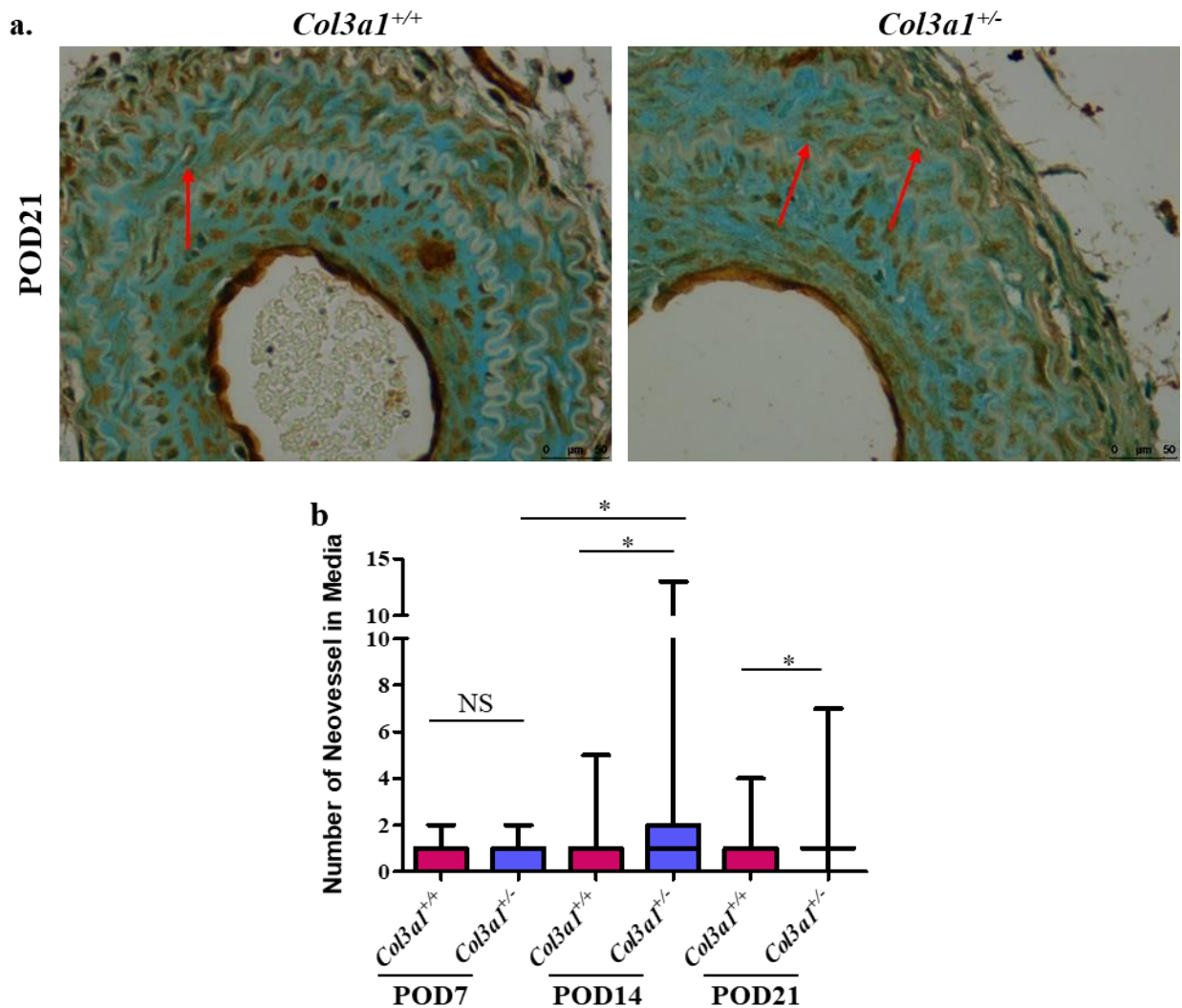


Figure 2.5 Increased medial neovessel formation in *Col3a1*^{+/-} arteries

(a) Representative cross sections with anti-CD31 staining (CD31, for vascular endothelial cells) of carotid arteries from both *Col3a1*^{+/+} and *Col3a1*^{+/-} mice at 7, 14 and 21 days after carotid ligation. The endothelial marker didn't showed any differences between *Col3a1*^{+/+} and *Col3a1*^{+/-} arteries at 7 days after ligation but there was significant increased CD31 positive neovessels in the *Col3a1*^{+/-} arteries compared with that in the *Col3a1*^{+/+} arteries at both 14 and 21 days after ligation. Original magnification 400x, scale bar: 50μm, red arrow was showing the CD31 positive neovessel. (b) Quantitation: showed increased neovessels in the medial layer of the arteries from *Col3a1*^{+/-} mice by POD14 and POD21 compared with that from the *Col3a1*^{+/+} mice. *n* = 6 per group. **p* < 0.05, by Student's *t* test, NS: no significance.

2.4.5 Bone marrow from the *Col3a1*^{+/+} mice rescues the ability of injury repair in *Col3a1*^{+/-} mice

Data from the first section of this chapter confirmed the aberrant injury repair in the *Col3a1*^{+/-} mice. Myofibroblasts which produce collagens to the extracellular matrix are widely accepted to be critical in injury repair⁴⁵. Fibrocytes, which can be differentiated into fibroblasts and further induced into myofibroblasts are derived from fibrocytes in the bone marrow²¹. We hypothesize that deficiency of type III collagen results in an aberrant vascular injury repair in vEDS patients since their myofibroblasts are not producing sufficient type III collagen to effectively and efficiently resolve thrombi after vascular injury. In *Col3a1*^{+/-} carotid ligation mouse model, after induced ligation injury, arteries from *Col3a1*^{+/-} mice showed persistent inflammation and proliferative cells, presumably myofibroblasts, and increased medial neovessel formation. We hypothesize that the extended thrombus resolution seen in *Col3a1*^{+/-} arteries and formation of neovessels in the wall weaken that wall and predispose to arterial events like dissection. We further hypothesize that introducing BMD fibrocytes with *Col3a1*^{+/+} genotype to *Col3a1*^{+/-} mouse, these fibrocytes could then differentiate into myofibroblasts with full expression of procollagen type III and correct the aberrant wound healing in *Col3a1*^{+/-} mice after carotid ligation. Therefore, we performed bone marrow transplant (BMT) of wildtype bone marrow into the *Col3a1*^{+/-} mice to test this hypothesis.

First, bone marrow from the *Col3a1*^{+/+} mice was collected and transplanted to both the *Col3a1*^{+/+} and *Col3a1*^{+/-} mice. **Figure 2.6** shows the flow chart of the forward BMT experiment. After waiting for 4-8 weeks, irradiated mice were sacrificed and the efficiency of BMT was confirmed by flow cytometry to detect the expression of GFP marker on lymphocytes. **Figure 2.7a** showed the expression of GFP on more than 80% of the lymphocytes indicating successful BMT. IHC staining with an anti-GFP antibody (Abcam, Cambridge, United Kingdom) was performed to detect GFP positive cells within the neointima and the arterial lumen to confirm that a chimera was obtained (**Figure 2.7b**). GFP positive cells were detected within the lumen as well as the neointimal layer indicating a contribution of BMDCs to the formation of the neointimal layer. Following the confirmation of successful BMT, IHC staining as stated

in 2.2.1 was performed to examine the proliferation of myofibroblasts in the neointima, inflammation in the neointima and neo-vessel formation in the medial layer. But for this study we only looked at the POD14 and POD21 since the difference between *Col3a1*^{+/+} and *Col3a1*^{+/-} at POD7 is not as dramatic as the difference seen at POD14 and POD21.

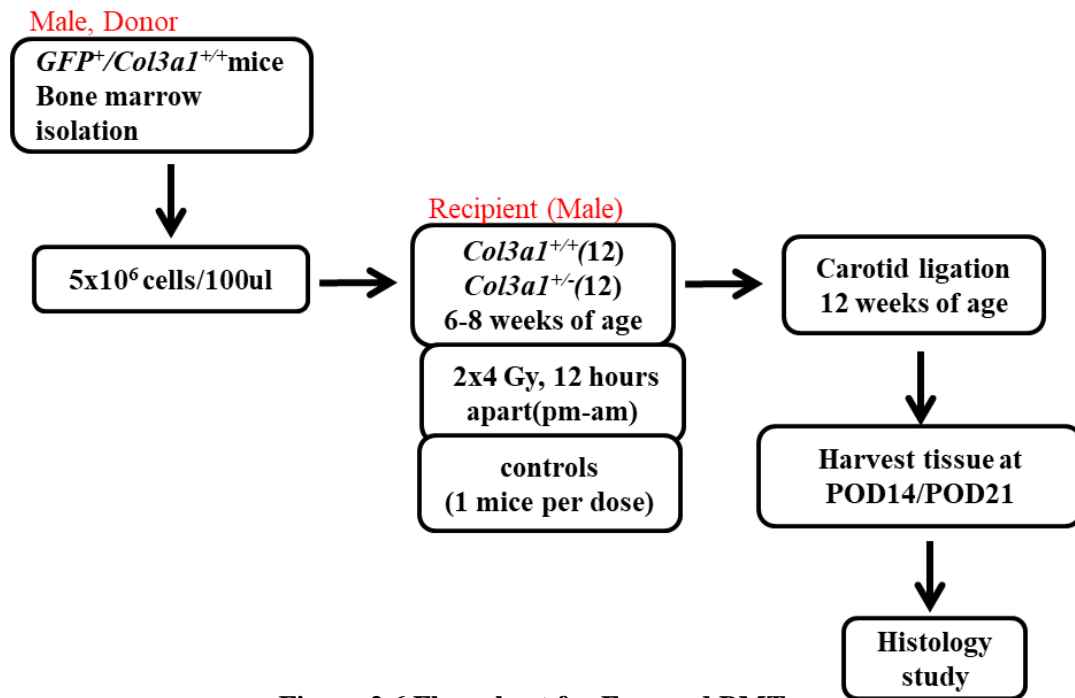


Figure 2.6 Flow chart for Forward BMT

Forward Bone Marrow Transplant (BMT) – F-BMT. Bone marrow was isolated from the *Col3a1*^{+/+} mice and transplanted to both X-ray lethally irradiated *Col3a1*^{+/+} and *Col3a1*^{+/-} recipient mice. Bone marrow repopulated in the recipient mice for 4-8 weeks before performing carotid ligation, mice were sacrificed and carotid arteries harvested for following up histology studies. About 20µl mice peripheral blood from tail vein was saved for flow cytometry to detect the expression of GFP confirm the efficiency of BMT. **F-BMT: Forward bone marrow transplantation**, bone marrow from *Col3a1*^{+/+} mice was transplanted into both *Col3a1*^{+/+} and *Col3a1*^{+/-} mice.

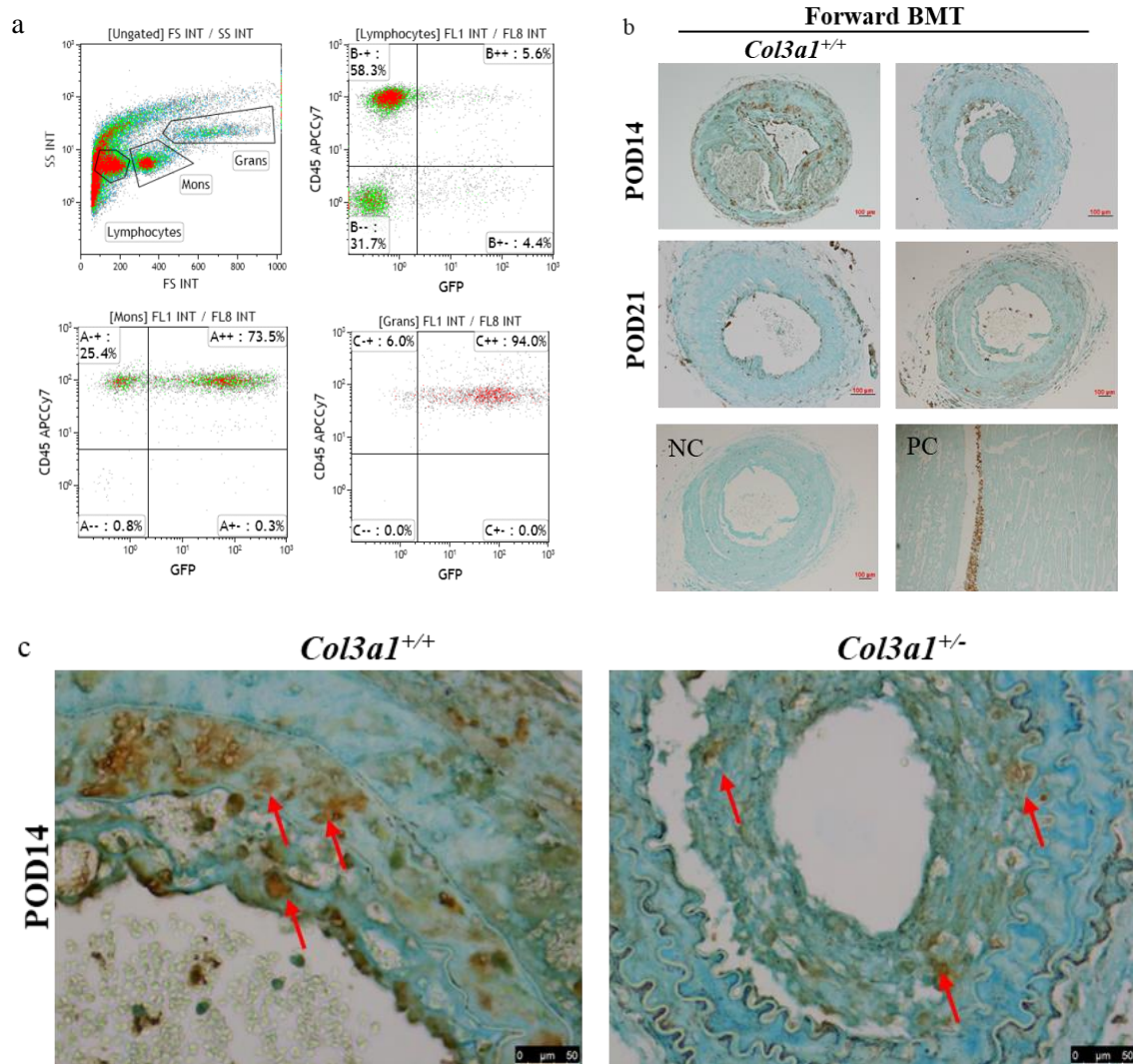


Figure 2.7 Confirmation of F-BMTF-BMT

(a) Expression of GFP in the lymphocytes detected by flow cytometry, positive GFP signal indicated successful BMT. (b) IHC staining to confirm the efficiency of BMT with the detection of GFP in the neointima in ligated arteries. NC: negative control of GFP, PC: positive control of GFP staining. (c): red arrow was showing positive GFP cell. GFP positive cells showed in the neointima indicating that BMD cells circulated to the injury site. **F-BMT: forward bone marrow transplantation**, bone marrow from *Col3a1*^{+/+} mice was transplanted into both *Col3a1*^{+/+} and *Col3a1*^{+/-} mice.

To examine the difference in neointima remodeling between two groups of mice after forward BMT, H & E staining was also performed. Result showed no significant difference after forward BMT at POD14 and POD21 in both *Col3a1*^{+/+} and *Col3a1*^{+/-} mice, indicating the ability of neointimal remodeling was similar in both groups of arteries (**Figure 2.8**). Additionally, cell proliferation ability was again determined by pH3 staining. Again, the number of pH3 positive cells didn't show significant difference within the neointima by POD21, indicating no dramatic difference in the proliferation of cells in the neointima (**Figure 2.9**) after 21 days of injury with forward BMT. Inflammation was also determined by Mac-2 staining. Significant difference was still observed in the inflammation level in the neointima between *Col3a1*^{+/+} and *Col3a1*^{+/-} mice at POD14 and POD21 (**Figure 2.9 and 2.10**). CD31 stained neovessels were also counted and results showed no significant difference in the capability of neovessel formation in the medial layer, indicating that the neovessel formation ability was also reduced back to *Col3a1*^{+/+} levels in *Col3a1*^{+/-} BMT mice at POD14 and POD21 (**Figure 2.11**). These data indicate that transplantation of bone marrow from the *Col3a1*^{+/+} mice could normalize the injury repair in the *Col3a1*^{+/-} mice especially by POD21.

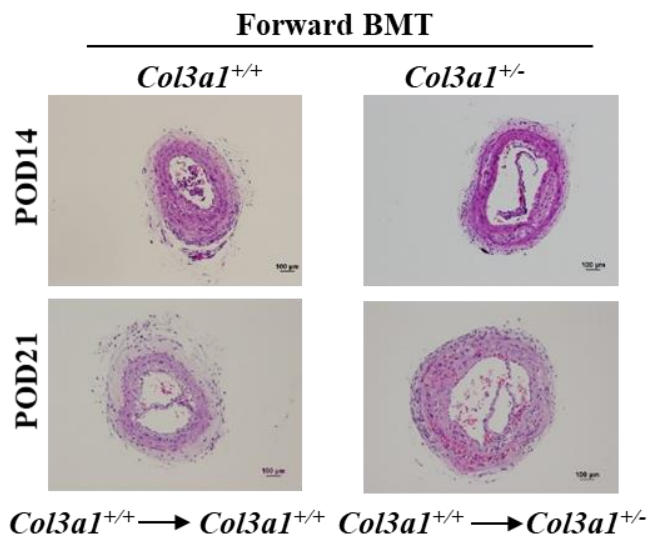


Figure 2.8 Similar ability in neointimal remodeling after F-BMT

Representative H&E-stained cross sections of carotid arteries from both *Col3a1*^{+/+} and *Col3a1*^{+/-} mice after carotid ligation at POD14 (top panel) and POD21 (lower panel), original magnification, 100x. **F-BMT: Forward bone marrow transplantation**, bone marrow from *Col3a1*^{+/+} mice was transplanted into both *Col3a1*^{+/+} and *Col3a1*^{+/-} mice.

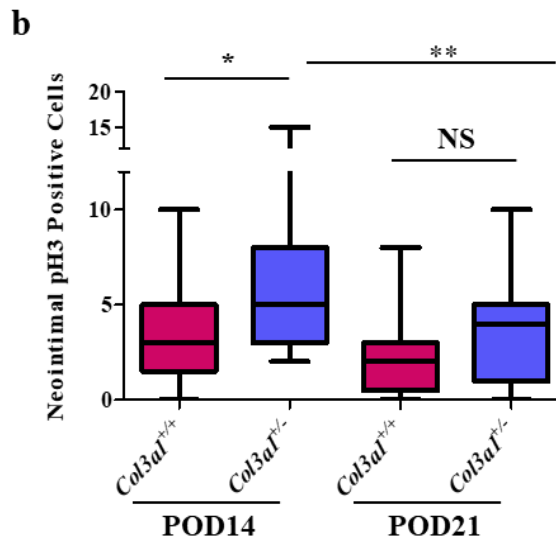
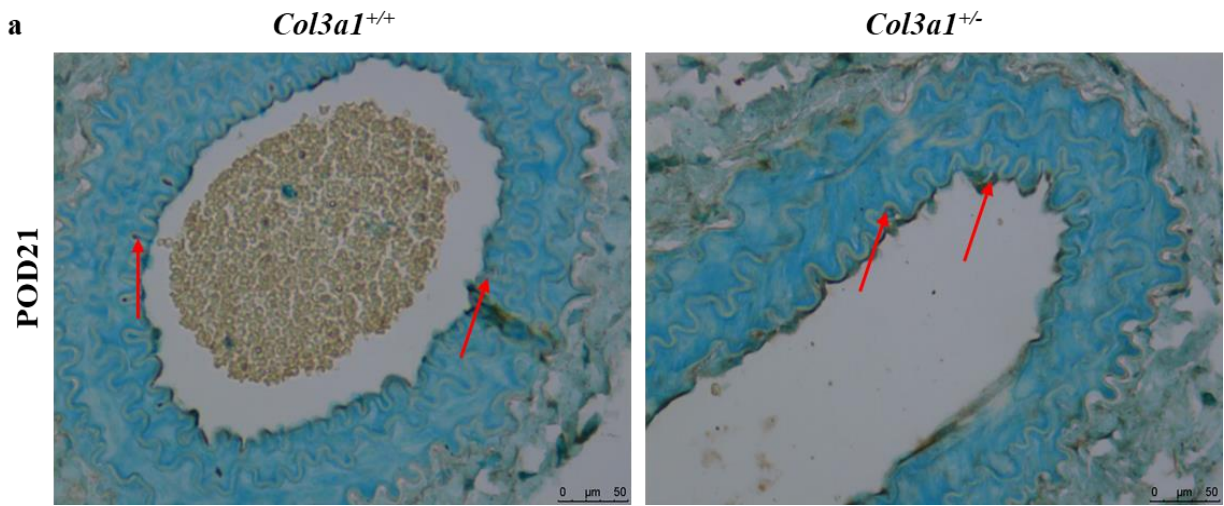


Figure 2.9 Decreased cell proliferation in *Col3a1^{+/-}* arteries after F-BMT

(a) Representative cross sections with anti-p-H3 staining (pH3, for proliferative cells) of carotid arteries from both *Col3a^{+/+}* and *Col3a1^{+/-}* mice at 14 and 21 days after carotid ligation. There was still significant more pH3 positive cells in the neointima of *Col3a1^{+/-}* arteries compared with that in the neointima of *Col3a1^{+/+}* arteries at 14 days after ligation. While there was no differences between *Col3a1^{+/+}* and *Col3a1^{+/-}* arteries at 21 days after ligation from mice with F-BMT. And a significant decrease in pH3 positive cells in the neointima of *Col3a1^{+/-}* arteries at POD21 arteries compared that from the POD14 arteries in *Col3a1^{+/-}* mice. Original magnification 400x, red arrow was showing the pH3 positive cell (b) Quantitation: showed decreased cell proliferation in the *Col3a1^{+/-}* arteries to the level of that in arteries from *Col3a1^{+/+}* mice from POD14 to POD21 indicating decreased neointimal formation after F-BMT in *Col3a1^{+/-}* arteries. $n = 6$ per group. * $p < 0.05$, ** $p < 0.01$ by Student's t test, NS: no significance. **F-BMT: Forward bone marrow transplantation**, bone marrow from *Col3a1^{+/+}* mice was transplanted into both *Col3a1^{+/+}* and *Col3a1^{+/-}* mice.

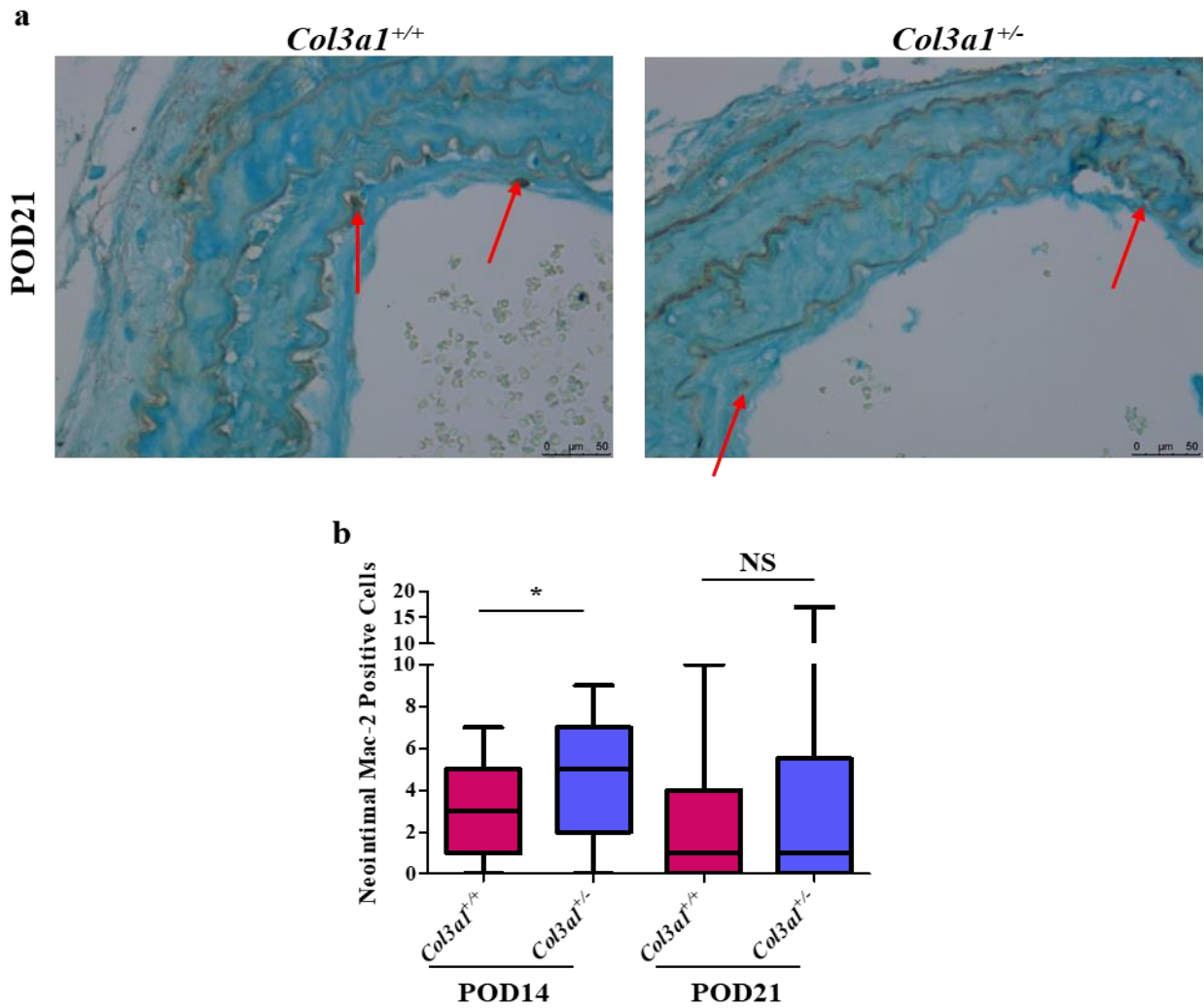


Figure 2.10 Decreased neointimal inflammation in *Col3a1^{+/-}* arteries after F-BMT

(a) Anti-Mac-2 staining (Mac-2, for inflammatory cells) of representative cross sections of carotid arteries from both *Col3a1^{+/+}* and *Col3a1^{+/-}* mice at 14 and 21 days after carotid ligation with F-BMT. The Mac-2 staining showed significant difference in the number of Mac-2 stained cells in the *Col3a1^{+/-}* arteries compared with that in the *Col3a1^{+/+}* arteries at both 14 and 21 days after ligation with F-BMT. Original magnification 400x, scale bars: 50μm. Red arrow was showing the inflammatory Mac-2 positive cell (b) Quantitation: shows decreased inflammation in the *Col3a1^{+/-}* arteries to the level of that in arteries from *Col3a1^{+/+}* mice POD21 indicating similar ability in neointimal inflammation after F-BMT in both *Col3a1^{+/+}* and *Col3a1^{+/-}* arteries at both POD14 and POD21. *n* = 6 per group. NS: no significance by Student's *t*-test, **F-BMT: Forward bone marrow transplantation**, bone marrow from *Col3a1^{+/+}* mice was transplanted into both *Col3a1^{+/+}* and *Col3a1^{+/-}* mice.

2.4.6 Reverse Bone Marrow Transplantation worsens the phenotypes shown in the *Col3a1*^{+/-} mice

Results from the forward BMT showed the potential for *Col3a1*^{+/-} bone marrow to correct the injury repair ability of *Col3a1*^{+/-} mice. This indicated that bone marrow-derived cells from the *Col3a1*^{+/-} mice became myofibroblasts that secrete and lay down collagen fibrils to accelerate the arterial injury repair process which was delayed in the *Col3a1*^{+/-} mice before transplant. Based on these results, we then asked *whether bone marrow from Col3a1^{+/-} mice would worsen post-injury phenotypes in the Col3a1^{+/-} arteries.*

Reverse BMT was performed on both *Col3a1*^{+/+} and *Col3a1*^{+/-} mice. Shown in **Figure 2.12** was the flow chart for the reverse BMT. As before, the recipient mice were lethally irradiated with 8Gy X-ray and bone marrow from female *Col3a1*^{+/-} donor mice was collected and injected retro-orbitally into the recipient male mice. After recovery for 4-8 weeks, carotid artery ligation was also made with the recipient mice.

Carotid arteries from the ligated recipient mice were collected as described before at both POD14 and POD21. Upon harvesting samples, blood was collected from the heart in order to isolate DNA to be used for confirmation of a successful reverse BMT. Liver tissues were collected for isolating DNA to confirm the success of the reverse BMT. Confirmation of reverse BMT was shown in **Figure 2.13**. Sanger sequencing assay on the PCR fragments showed that DNA from a female mouse is homozygous *Zfx* while DNA from a male mouse was heterozygous on some nucleotides that were from the sequence diversity between *Zfx* and *Zfy* (**Figure 2.13, the first row**). The different alleles of each heterozygous nucleotide have similar peak height based on Sanger sequencing, which indicated that the primers had similar efficiency to amplify fragments in *Zfx* and *Zfy* (**Figure 2.13, the first row**).

PCR and sequencing assay were performed with DNA extracted from the blood samples of recipient mice. The results showed that Y chromosome *Zfy* was undetectable in recipients' blood samples (**Figure 2.13, left column, row 2-4**). To validate this finding, we performed PCR and sequencing assay with DNA extracted from livers of recipient mice. The result showed that the amount of Y chromosomes in livers of

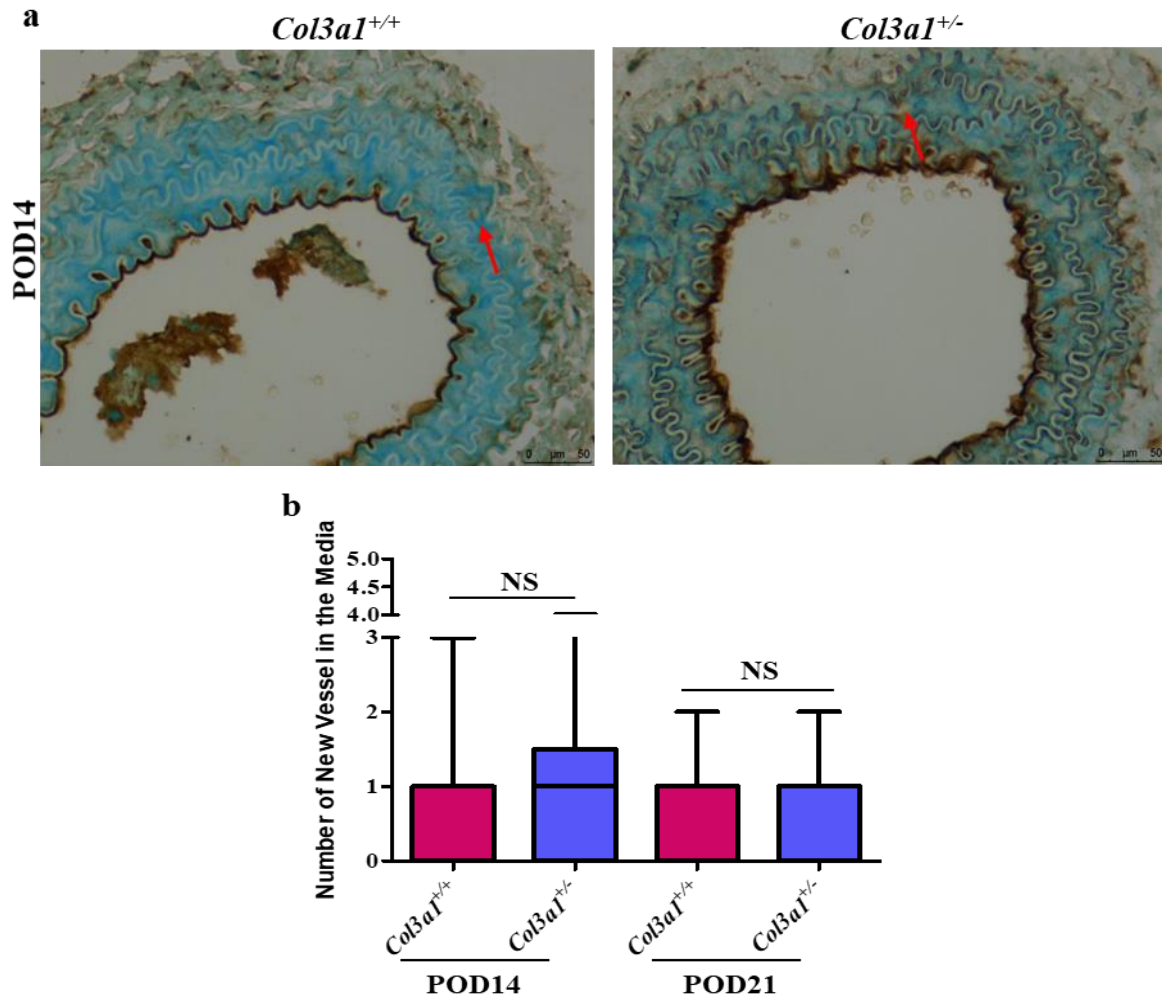


Figure 2.11 Decreased neovessel formation in the *Col3a1*^{+/-} arteries after F-BMT

(a) Representative cross sections with anti-CD31 staining (CD31, marker of endothelial cells) of carotid arteries from both *Col3a1*^{+/+} and *Col3a1*^{+/-} mice at 14 days after carotid ligation with F-BMT. The CD31 staining showed that there was no significant difference in the number of CD31 positive neovessels in the *Col3a1*^{+/-} arteries compared with that in the *Col3a1*^{+/+} arteries at both 14 and 21 days after ligation from mice with F-BMT. Original magnification 400x, and scale bars: 50 μ m. Red arrow was showing the CD31 positive neovessels in the medial layer (b) Quantitation: showed similar number of neovessels in the *Col3a1*^{+/-} arteries compared to *Col3a1*^{+/+} mice after F-BMT. *n* = 6 per group. NS: no significance, by Student's *t*-test. **F-BMT: Forward bone marrow transplantation**, bone marrow from *Col3a1*^{+/+} mice was transplanted into both *Col3a1*^{+/+} and *Col3a1*^{+/-} mice.

the recipient mice were similar to that of X chromosomes (**Figure 2.13, right column, row 2-4**). To further validate this result, we designed a set of primers in *Usp9x* and *Usp9y* genes and the primer sequences on these genes were identical, forward primer: 5'-AACAGAATGAGCAGTCTGAAAG and reward primer: 5'- TCCACCATCTTTTCTGACGCC. The sequencing results confirmed our previous finding that the majority of white blood cells in recipient mice were from donor animals 4-8 weeks after transfusion. (**Figure 2.13, row 5**). Overall, this result suggested that the majority of white blood cells in the recipient mice were from donors 4-8 weeks after the bone marrow transfusion, indicating a successful reverse BMT.

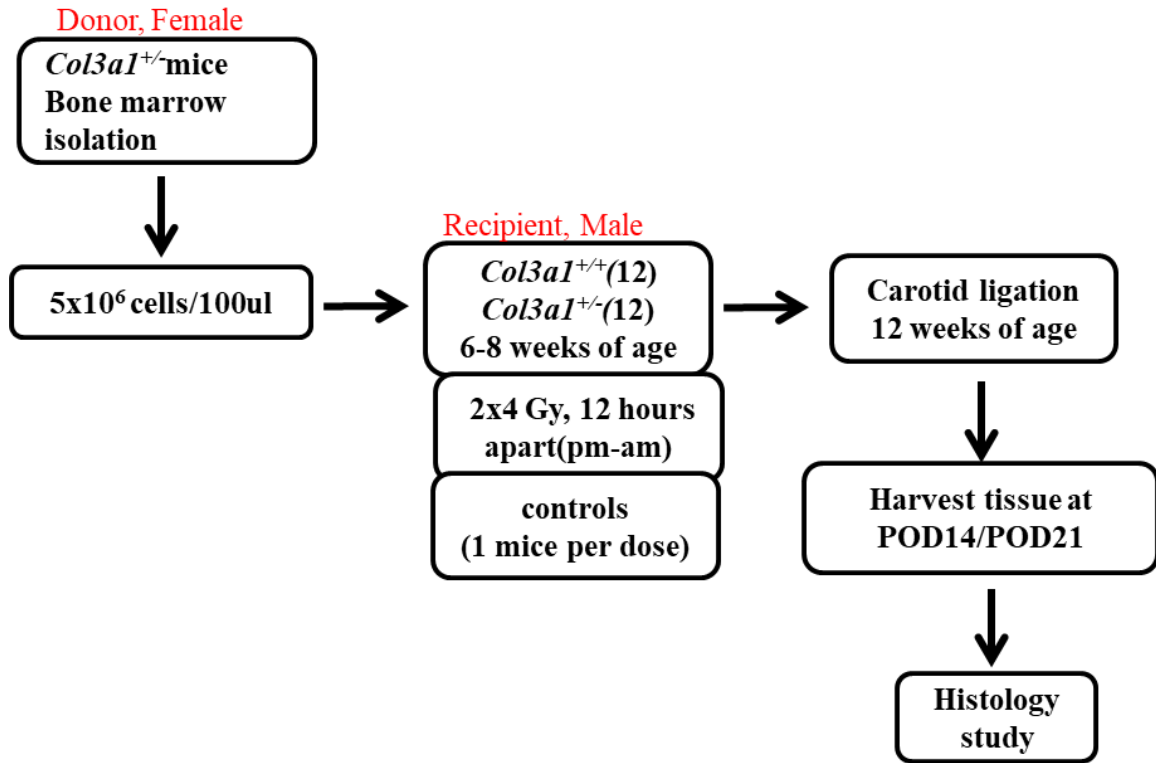


Figure 2.12 Flow chart for Reverse Bone Marrow Transplant (BMT)

Bone marrow was isolated from the *Col3a1*^{+/-} female mice and transplanted to both X-ray lethally irradiated *Col3a1*^{+/+} and *Col3a1*^{+/-} male recipient mice, the bone marrow repopulated in the recipient mice for 4-8 weeks before performing carotid ligation, mice were sacrificed and carotid arteries harvested for following up histology studies. 500ul mice peripheral blood and liver tissue from both donor and recipient mice was saved for the confirmation of R-BMT. **R-BMT: reverse Bone Marrow Transplant, bone marrow from *Col3a1*^{+/-} female mice was transplanted to both *Col3a1*^{+/+} and *Col3a1*^{+/-} male mice.**

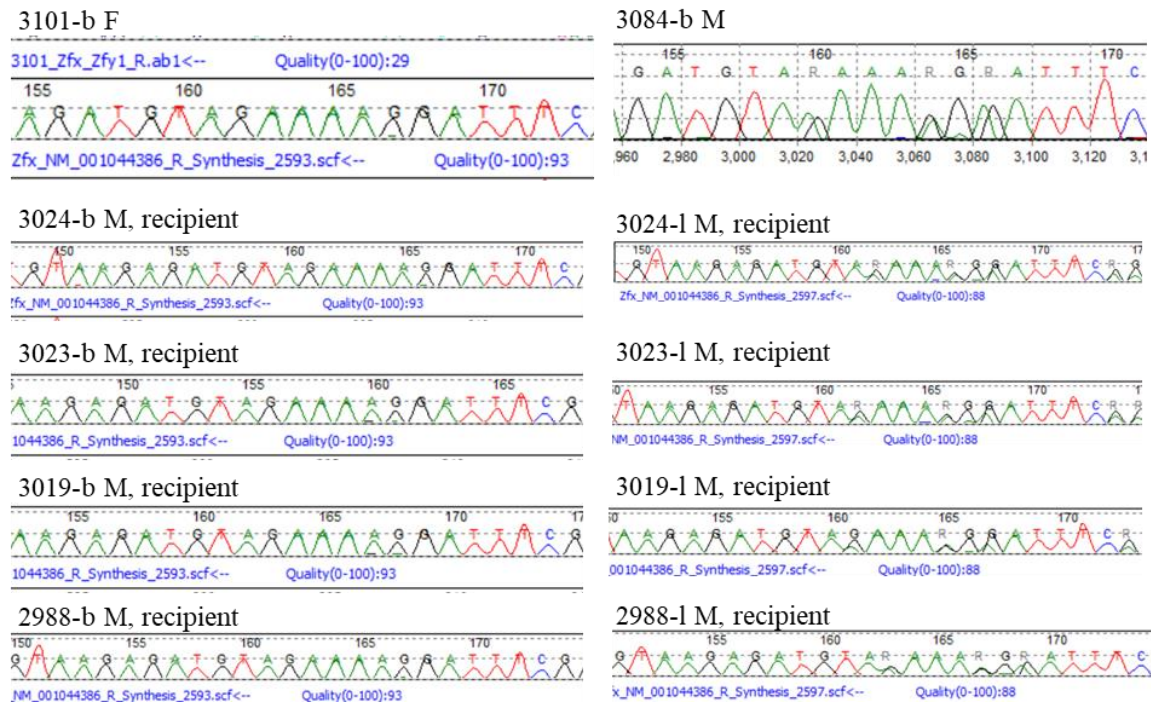


Figure 2.13 Confirmation of R-BMT

PCR and sequencing assay were performed with DNA extracted from both blood and livers of recipient mice. M: male; F: female; b: blood; l: liver, numbers are the mouse identification number. PCR and sequencing results showed that there was donor originated Zfx and Zfy detected in the DNA extracted from recipient blood samples, but not detected in the DNA extracted from recipient liver tissue indicating the repopulation of donor bone marrow in the recipient mice. **R-BMT: reverse Bone Marrow Transplant**, bone marrow from *Col3a1*^{+/-} female mice was transplanted to both *Col3a1*^{+/+} and *Col3a1*^{+/-} male mice.

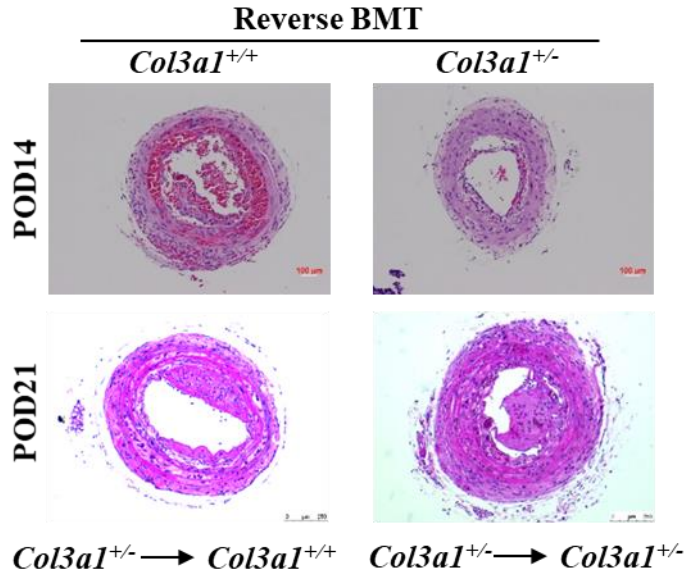


Figure 2.14 Similar ability in neointimal remodeling after R-BMT

Representative H&E-stained cross sections of carotid arteries from both *Col3a1*^{+/+} and *Col3a1*^{+/-} mice after carotid ligation at POD14 (top panel) and POD21 (lower panel). Results show similar ability in neointimal remodeling in the *Col3a1*^{+/+} and *Col3a1*^{+/-} mice after carotid ligation with R-BMT at both POD14 and POD21. Original magnification, 100x. **R-BMT: Reverse bone marrow transplantation**, bone marrow from *Col3a1*^{+/-} female mice was transplanted to both *Col3a1*^{+/+} and *Col3a1*^{+/-} male mice.

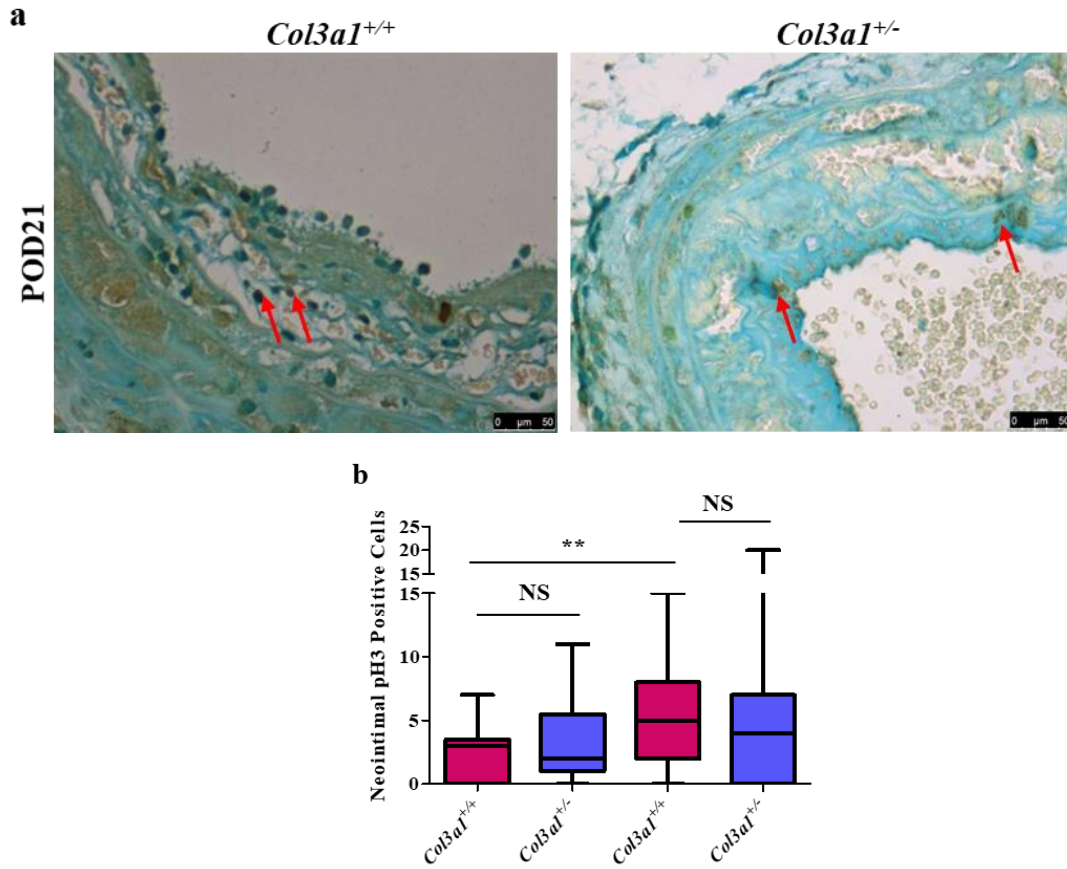


Figure 2.15 No significant difference in cell proliferation after R-BMT

(a) Representative cross sections with anti-p-H3 staining (pH3, for proliferative cells) of carotid arteries from both *Col3a1^{+/+}* and *Col3a1^{+/-}* mice at 14 and 21 days after carotid ligation with R-BMT. No difference between *Col3a1^{+/+}* and *Col3a1^{+/-}* arteries at both 14 and 21 days after ligation from mice with R-BMT was observed. Original magnification: 400x, scale bars: 50μm, red arrow was showing the pH3 positive cell (b) Quantitation: shows no difference in the pH3 positive cell of arteries from both *Col3a1^{+/+}* and *Col3a1^{+/-}* at POD14 and POD21 indicating similar ability in cell proliferation within the arterial lumen after R-BMT. *n* = 6 per group. NS: no significance by Student's *t* test. **R-BMT: Reverse bone marrow transplantation:** bone marrow from *Col3a1^{+/-}* female mice was transplanted to both *Col3a1^{+/+}* and *Col3a1^{+/-}* male mice.

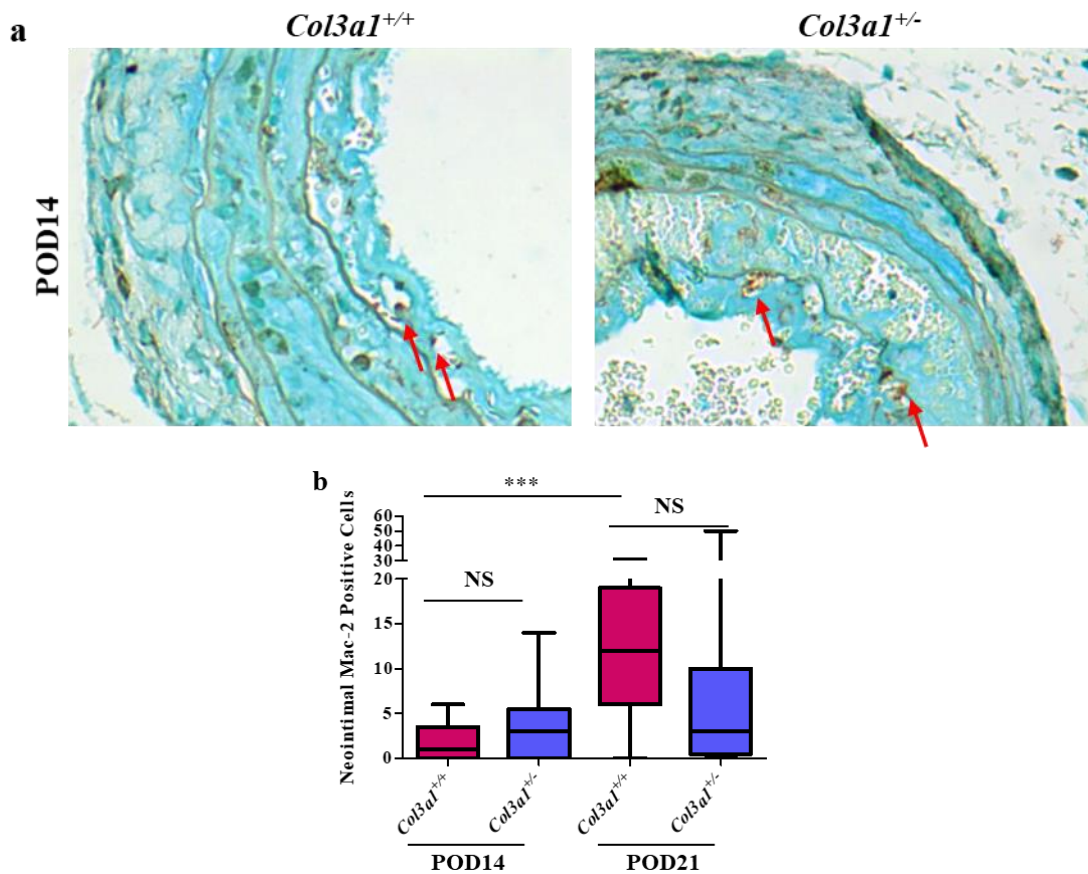


Figure 2.16 No significant difference in neointimal inflammation after R-BMT

(a) Representative cross sections with anti-Mac-2 staining (Mac-2, for inflammatory cells) of carotid arteries from both *Col3a1^{+/+}* and *Col3a1^{+/-}* mice at 14 and 21 days after carotid ligation with R-BMT. The inflammatory marker showed that there was not significant difference in Mac-2 stained cells in the *Col3a1^{+/-}* arteries comparing to that in the *Col3a1^{+/+}* arteries at both 14 and 21 days after ligation with R-BMT, but there was significant increase in Mac-2 positive cells from POD14 to POD21 in the arteries from *Col3a1^{+/+}* compared with that in the *Col3a1^{+/-}* after R-BMT. Original magnification 400x, and scale bars: 50 μ m, red arrow is showing the inflammatory Mac-2 positive cell (b) Quantitation: shows no difference in the neointimal inflammation in arteries from both *Col3a1^{+/+}* and *Col3a1^{+/-}* after R-BMT. $n = 6$ per group. *** $p < 0.001$, by Student's t -test, NS: no significance. **R-BMT: Reverse bone marrow transplantation**, bone marrow from *Col3a1^{+/-}* female mice was transplanted to both *Col3a1^{+/+}* and *Col3a1^{+/-}* male mice.

After reverse BMT, the formation of neointima, cell proliferation, inflammation in the neointima, and neovessel formation in the medial layer were all investigated. First, H&E staining was still performed to examine the neointima hyperplasia. Results from the H&E staining showed increased neointima in sections from both groups of mice from POD14 to POD21 (**Figure 2.14**) and results from the pH3 staining showed that there were significantly more pH3 stained cells in the neointima of arteries from *Col3a1*^{+/+} mice at POD21 compared with that in the neointima of arteries from *Col3a1*^{+/+} arteries at POD14, indicating increased cell proliferation in the *Col3a1*^{+/+} arteries after 21 days of injury (**Figure 2.15**). Interestingly, there was increased quantity of Mac-2 positive cells detected in the neointima layer in *Col3a1*^{+/+} mice after reverse BMT at POD21 compared with that in the *Col3a1*^{+/+} arteries at POD14 (**Figure 2.16**), suggesting increased inflammation in *Col3a1*^{+/+} mice after reverse BMT. There was no difference in neovessel formation after reverse BMT at both POD14 and POD21 in both groups of arteries (**Figure 2.17**). To conclude, after reversal BMT, we found an increase in cell proliferation in the *Col3a1*^{+/+} mice at POD21 compared to POD14, an increase in inflammation in the neointima in the *Col3a1*^{+/+} mice at POD21 compared to POD14, but we were not able to see any difference in the neovessel formation in both groups of mice at both time points.

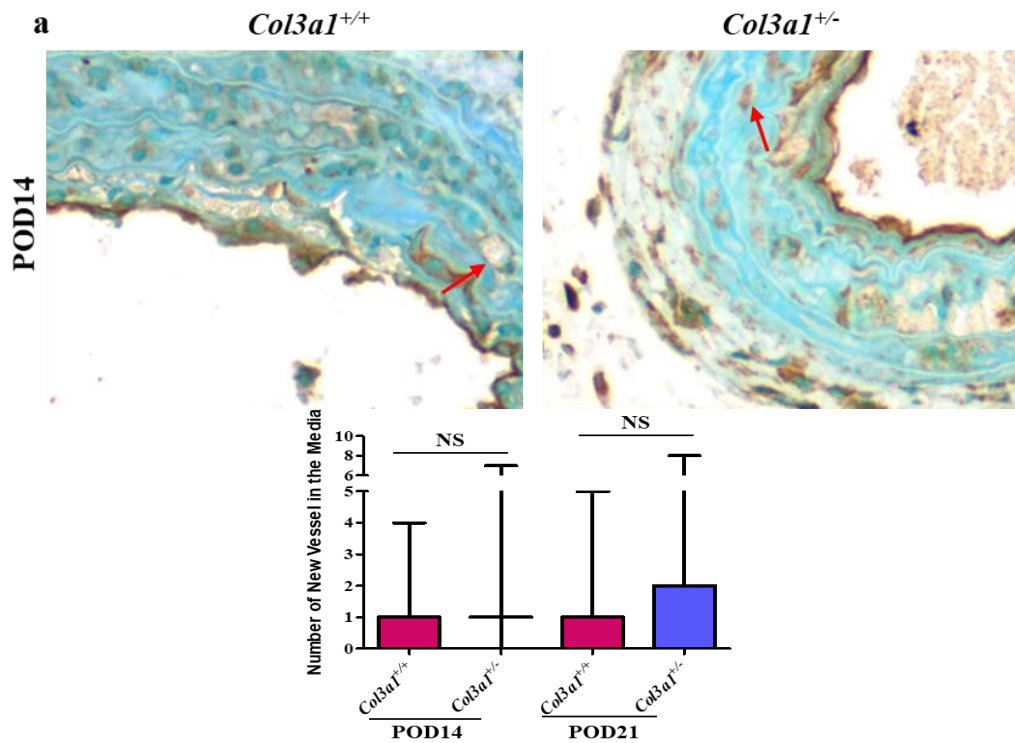


Figure 2.17 No significant in neovessel formation arteries after R-BMT

(a) Anti-CD31 staining (CD31, for endothelial cells) of representative cross sections of carotid arteries from both *Col3a1*^{+/+} and *Col3a1*^{+/-} mice at 14 and 21 days after carotid ligation with R-BMT. The CD31 staining shows that there was no significant difference in the number of CD31 positive neovessel in the *Col3a1*^{+/-} arteries compared with that in the *Col3a1*^{+/+} arteries at both 14 and 21 days after ligation with R-BMT. Original magnification 400x, scale bars: 50 μ m. Red arrow was showing CD31 positive neovessel (b) Quantitation: showed the neovessel formation in the medial layer in the *Col3a1*^{+/-} arteries was similar to the level of that in arteries from *Col3a1*^{+/+} mice both POD14 and POD21 after R-BMT. $n = 6$ per group, NS: no significance by Student's t -test. **R-BMT: Reverse bone marrow transplantation**, bone marrow from *Col3a1*^{+/-} female mice was transplanted to both *Col3a1*^{+/+} and *Col3a1*^{+/-} male mice.

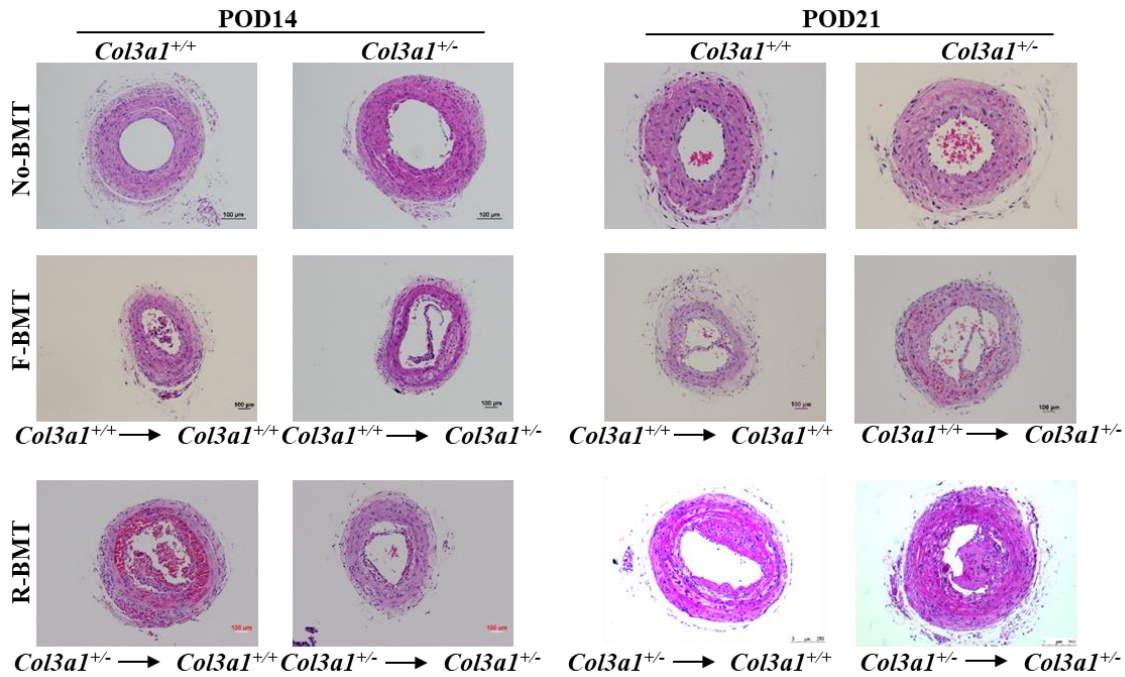


Figure 2.18 H&E staining indicating changes in the neointima remodeling

Representative sections of the *Col3a1*^{+/+} and *Col3a1*^{+/-} mice after carotid ligation with No BMT (top panel), F BMT (middle panel) and R BMT (bottom panel) at both POD14 (left panel) and POD21 (right panel). Showing decreased neointima formation after F-BMT while increased neointima formation after R-BMT compared with that in arteries from mice with no BMT at both POD14 and POD21, especially in *Col3a1*^{+/-} mice at POD21. Scale bar: 100µm. (BMT: bone marrow transplant, F-BMT: forward BMT, R-BMT: reverse BMT).

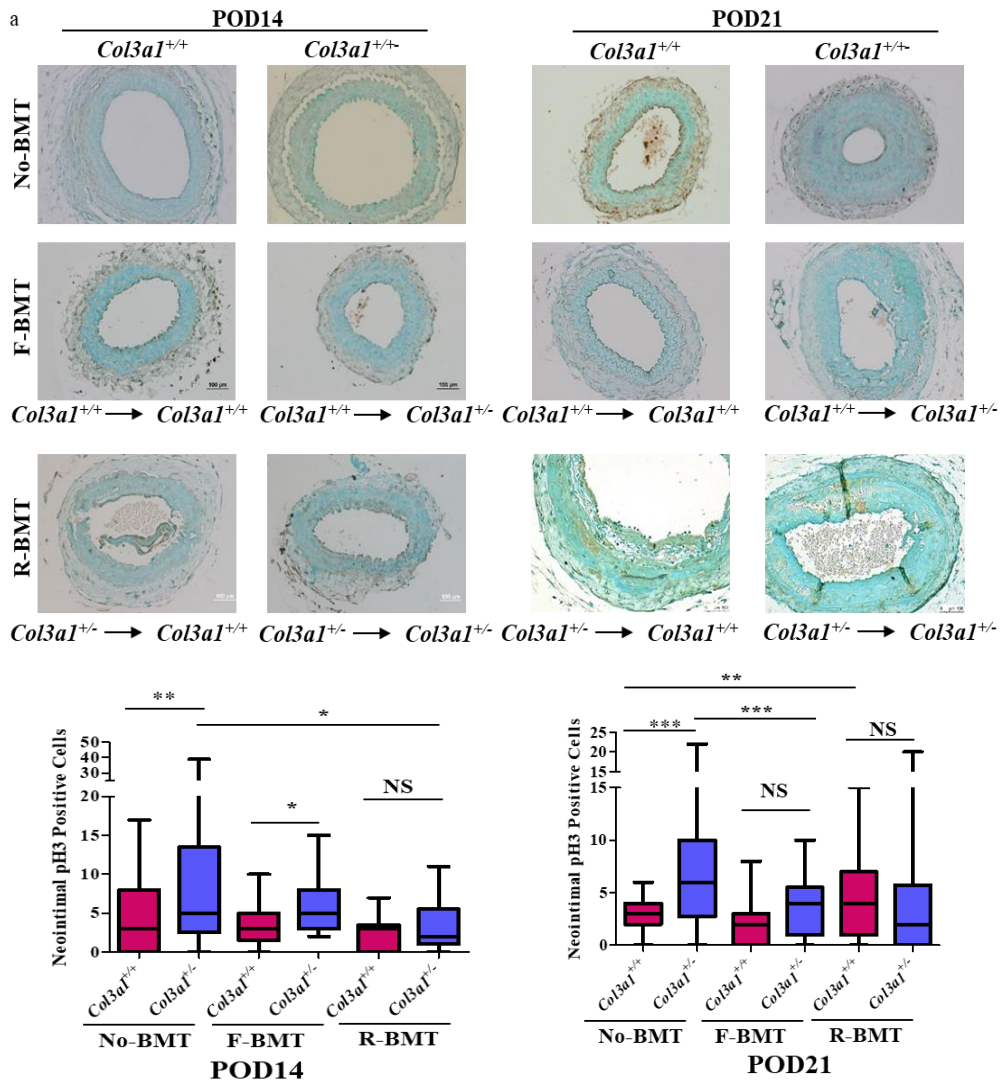


Figure 2.19 Comparison of cell proliferation in the neointima for all groups

(a) pH3 staining showed representative sections of arteries from both *Col3a1*^{+/+} and *Col3a1*^{+/-} mice, after carotid ligation with No-BMT (top panel), F-BMT (middle panel) R-BMT (bottom panel) at both POD14 (left panel) and POD21 (right panel) original magnification 200x. (b) Quantitation showed significantly higher number of pH3 positive cells in arteries from *Col3a1*^{+/-} mice compared with that in arteries from *Col3a1*^{+/+} mice in No-BMT group at both POD14 and POD21. There was no difference in the number of pH3 positive cells in arteries from both *Col3a1*^{+/+} and *Col3a1*^{+/-} mice at both POD14 and POD21 after F-BMT. There was significantly decreased number of pH3 positive cells in arteries from *Col3a1*^{+/-} mice after F-BMT compared with that in No-BMT at POD 21. However, there was significant increase in the number of pH3 cells in arteries from *Col3a1*^{+/+} mice after R-BMT compared with that from No-BMT arteries at POD21. (BMT: bone marrow transplant, F-BMT: forward BMT, R-BMT: reverse BMT), **p*<0.05, ***p*<0.01, ****p*<0.001 by Student's *t*-test, NS: no significance.

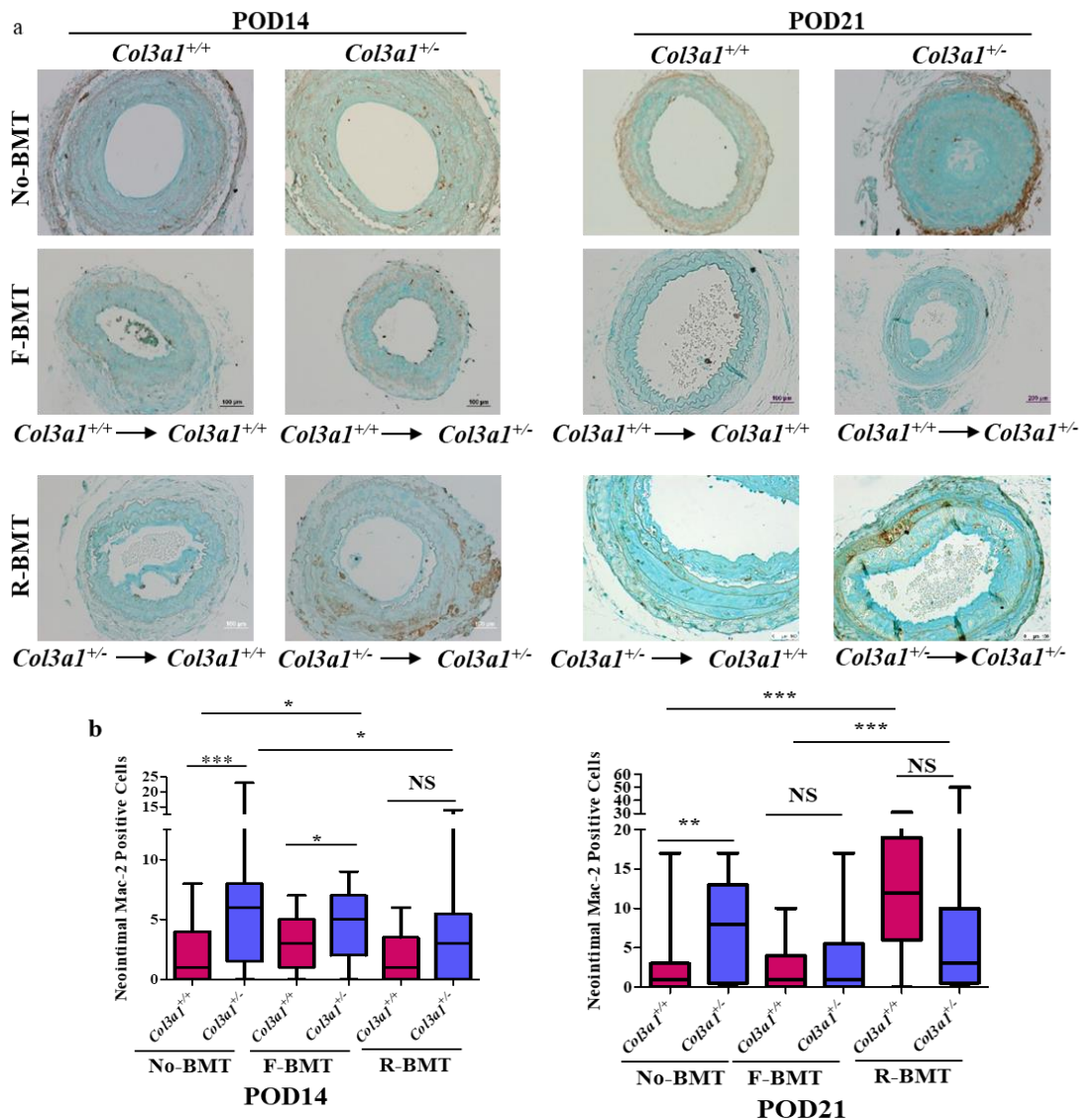


Figure 2.20 Comparison of inflammation in the neointimal layer for all groups

(a) Mac-2 staining showed representative sections of arteries from both *Col3a1*^{+/+} and *Col3a1*^{+/-} mice, after carotid ligation with No-BMT (top panel), F-BMT (middle panel) and R-BMT (bottom panel) at both POD14 (left panel) and POD21 (right panel). (b) Quantitation showed that there was significantly higher number of Mac-2 positive cell in arteries from *Col3a1*^{+/-} mice compared with that in arteries from *Col3a1*^{+/+} mice at both 14 and 21 days after ligation in No-BMT group, and there was no significant difference in the number of Mac-2 positive cells in arteries from *Col3a1*^{+/+} mice compared with *Col3a1*^{+/-} arteries at POD21 after F-BMT. There were significantly more Mac-2 cells in arteries from *Col3a1*^{+/-} mice with R-BMT compared with those from *Col3a1*^{+/+} mice in No-BMT and F-BMT group at POD21. (BMT: bone marrow transplant, F-BMT: forward BMT, R-BMT: reverse BMT), **p*<0.05, ***p*<0.01, ****p*<0.001 by Student's *t* test, NS: no significance.

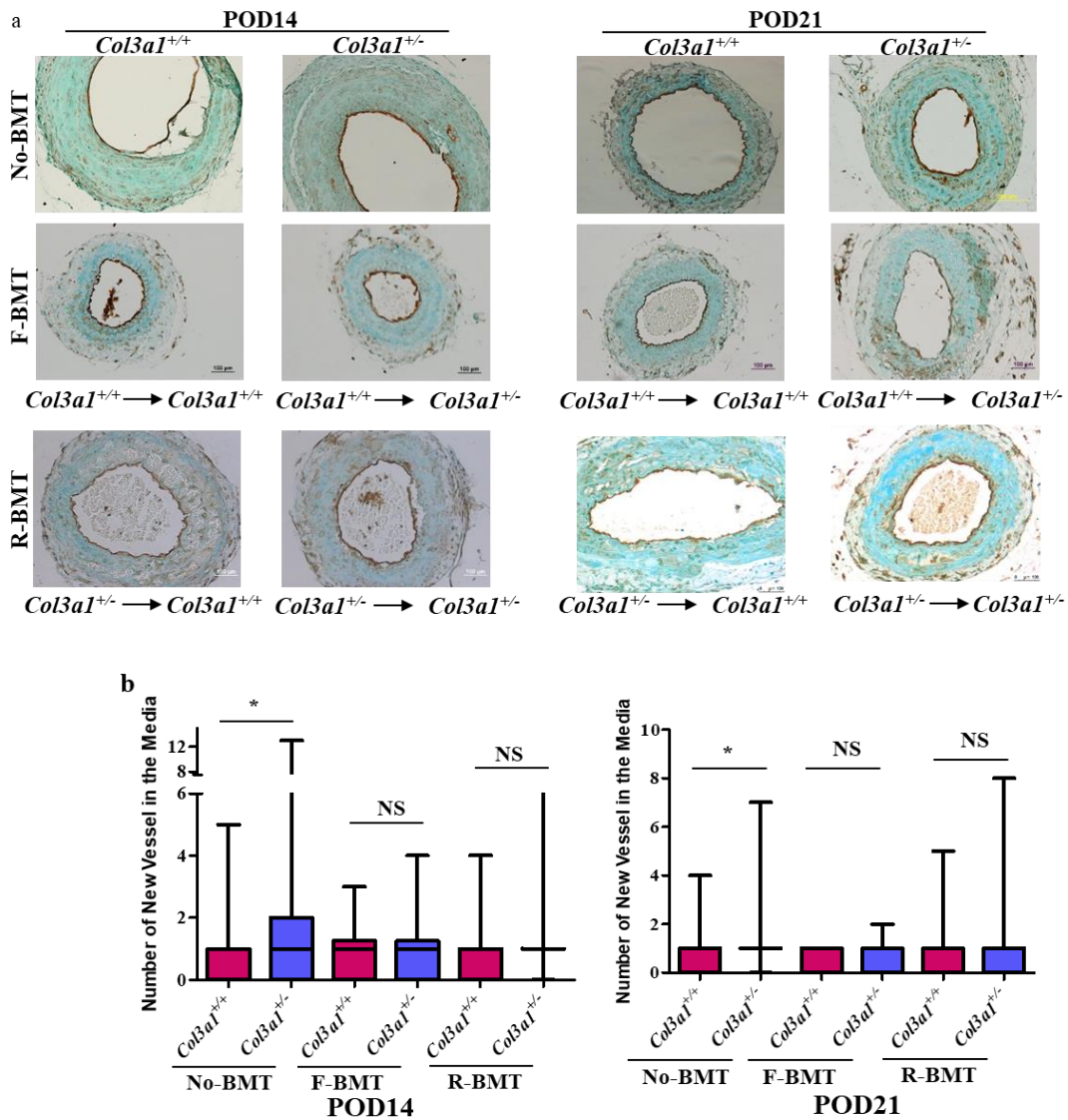


Figure 2.21 Comparison of medial neovessel formation

(a) Representative sections of arteries from both *Col3a1*^{+/+} and *Col3a1*^{+/-} mice after carotid ligation with No-BMT (top panel), F-BMT (middle panel) and R- BMT (bottom panel) at both POD14 (left panel) and POD21 (right panel) (b) Quantitation showed that there was significantly higher number of new vessels in arteries from *Col3a1*^{+/-} mice compared with that from *Col3a1*^{+/+} mice in no BMT group at 14 and 21 days after ligation and there was no significant difference in the number CD31 positive neovessel in arteries from *Col3a1*^{+/+} mice compared with arteries from *Col3a1*^{+/-} mice after F-BMT and R-BMT groups at both POD14 and POD21, indicating no difference in neovessel formation in the medial layer after F- and R-BMT. **p*<0.05 by the Student's t test, NS: no significance.

Discussion

Data generated from *Col3a1*^{+/-} mice showed a decreased expression and production of mature type III collagen by fibroblasts/myofibroblasts in injured carotid arteries, leading to delayed thrombus resolution as described in Dr. Reid's study (Unpublished data). The study described herein confirmed and expanded the finding of delayed thrombus resolution in the *Col3a1*^{+/-} mice. In *Col3a1*^{+/+} mice, there was an initial response that led to the appearance of thrombus at POD7. This was accompanied by the presence of macrophages in the lumen space. However, by POD14, the size of the neointima was already decreasing, and by POD21 the neointima has decreased to a relatively thin layer. By contrast, in the *Col3a1*^{+/-} mice the initial response was slower, such that at POD7 there was actually less neointima than in the *Col3a1*^{+/+}. However, the number of proliferating and infiltrating cells was higher in the *Col3a1*^{+/-} mice. At POD14 and POD21 the size of the neointima continued to increase in the *Col3a1*^{+/-} mice. The thickening of neointimal layers in *Col3a1*^{+/-} tissues at POD14 and POD21 was consistent with results from Dr. Reid's study (Unpublished data). This delayed wound healing in *Col3a1*^{+/-} mice suggested that expression of correct type III collagens was necessary for quick and complete thrombus resolution. Taken together, these results showed that the *Col3a1*^{+/-} mice have delayed thrombus resolution as a result of reduced type III collagen production.

Macrophage participation in inflammation was critical in successful wound healing by secreting inflammatory factors and pro-angiogenic factor-VEGF. Both secure a normal and successful wound healing⁴⁶. However, when there is not enough type III collagen laid down at the wound site, there is a continuous need for myofibroblast proliferation, resulting in a persistent existence of macrophages and inflammation. Extra TGF- β from macrophages are involved in the differentiation of myofibroblasts to produce procollagen type III, while extra VEGF result in medial neovessel formation, which predisposes the arterial dissection and rupture⁴⁷. Macrophages have different functions in wound healing. Expression of growth factors and/or angiogenic factors such as TGF- β and VEGF by macrophages are both critical in persistent wounding and scarring⁴⁶.

We proposed that myofibroblasts functioning at the injury site originated from the circulating fibrocytes in the bone marrow, and therefore hypothesized that BMT could be a potential strategy to correct the defective injury repair in *Col3a1*^{+/-} mice. In principal, transplanted BMD cells from *Col3a1*^{+/-} mice could circulate to the injury site, expressed and lay down mature type III collagen⁴⁸, thus accelerating the process of thrombus resolution. Results from the forward BMT showed that at POD14 and POD21 the neointimal thickening in *Col3a1*^{+/-} arteries was reduced back to the level that was observed in the arteries from *Col3a1*^{+/+} mice (**Figure 2.18**). Additionally, the proliferation and inflammation in the *Col3a1*^{+/-} arteries was reduced to similar levels as *Col3a1*^{+/+} arteries (**Figure 2.19 and 2.20**). Less neovessel formation in the medial layer was also observed, suggesting that preventing the exaggerated proliferative and inflammatory response also reduced expression of angiogenic factors (**Figure 2.21**). These results support our hypothesis that after receiving bone marrow from the *Col3a1*^{+/+} mice, fibrocytes circulate to the wound area and produce type III collagen to promote wound repair by decreasing aberrant cell proliferation and inflammation as well as neovessel formation in the *Col3a1*^{+/-} arteries.

Bone marrow-derived cells as well as resident fibroblasts contribute to the arterial injury process after tissue injury^{38,49}. However, it is still controversial whether the circulating cells or the resident cells contribute to repairing at the injury site. From our forward BMT study, we demonstrated by GFP staining that cells from circulation migrate to the injury site (**Figure 2.7**). To confirm the discoveries, we hypothesized that transplanting bone marrow from the *Col3a1*^{+/-} mice into the *Col3a1*^{+/+} mice would exacerbate the phenotypes in the *Col3a1*^{+/+} arteries by contributing circulating *Col3a1*^{+/-} fibrocytes which will be induced and differentiated into myofibroblasts, this will lead to a delayed arterial injury in the *Col3a1*^{+/+} arteries. To test our hypothesis, reverse BMT was performed.

Results from the reverse BMT validated our hypothesis. We observed increased cell proliferation in the neointima layer in the *Col3a1*^{+/+} mice after reverse BMT at POD21 compared with arteries from non-BMT *Col3a1*^{+/+} mice (**Figure 2.18 and 2.19**). Furthermore, we observed increased inflammation levels in the neointima in the *Col3a1*^{+/+} mice after reverse BMT at POD21 (**Figure 2.20**).

In conclusion, the current study confirmed a novel mechanism for the vascular phenotypes in vEDS patients. More importantly, we have tested a novel therapeutic approach of BMT to treat the vascular complications of vEDS by correcting injury repair ability of vEDS patients. This study provided a possibility to dramatically improve the length and quality of life for vEDS patients and decrease the incidence of sudden death caused by arterial events, including dissections and arterial rupture⁴.

3 Celiprolol Trial on *Col3a1*^{+/-} Mice to Modulate the Thrombus Resolution

3.1 Introduction

3.1.1 β -adrenergic receptors (β -ARs) and wound healing

Beta-adrenergic receptors (β -ARs) are playing a central role to the regulation in cardiac function⁵⁰. These receptors are located on the surface of many cell types and bound to endogenous hormones such as catecholamine and norepinephrine⁵¹. The “ β_2 -AR subtype” of β -ARs is distributed on the membrane of fibroblasts, keratinocytes and melanocytes⁵². Although the expression of β_2 -AR subtype on skin tissues has been identified for more than three decades, their functional significance was not recognized until recently⁵³.

The complicated skin wound healing process requires a series of coordinated procedures. Temporal and orchestration of numerous cell types which parallel with thrombus resolution, as discussed in Chapter 2, all together, they provide a successful wound healing mice model. Although different studies have provided evidences that a β_2 -AR autocrine/paracrine signaling pathway exists, a clear understanding of the specific role for β_2 -AR signaling in wound healing requires more investigation. Studies by Pullar et al. have shown that β_2 -ARs could regulate migration and re-epithelialization of keratinocytes⁵⁴, and that blockade of β_2 -ARs increases keratinocyte migration. Antagonism of β_2 -ARs has many other effects including enhancing angiogenesis, increasing secretion of vascular endothelial growth factor (VEGF) from human keratinocytes, increasing the migration rate of human dermal fibroblasts (HDFs) *in vitro*, and increasing expression of SM- α -actin, production of collagen III. Mice without β_2 -ARs have faster wound healing, at least within the first few days post-injury⁵⁵. Studies from the same group demonstrated that antagonists of β_2 -AR could promote wound re-epithelialization by increasing phosphorylation and activation of ERK signaling, increasing migration rate of keratinocytes, and increasing electric field-directed migration. To conclude, blockade of β_2 -ARs with β -blockers appeared to be a promising strategy for promoting skin wound healing (**Figure 3.1**)⁵⁶.

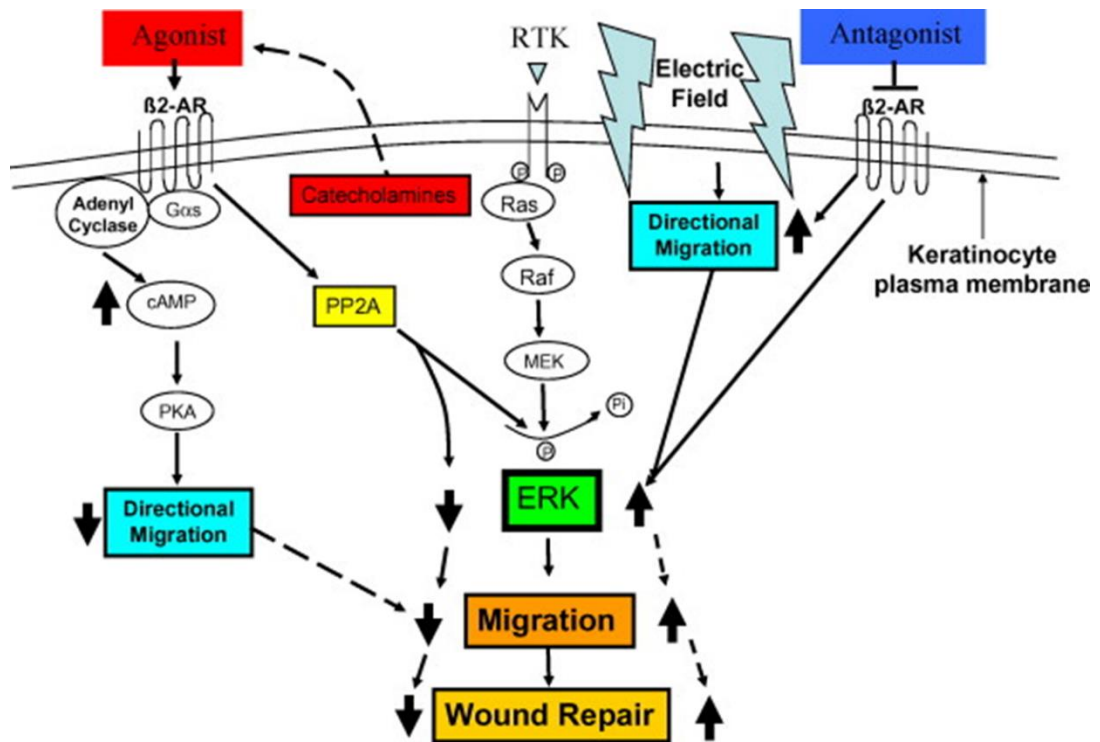


Figure 3.1 Schematic representation of interaction of the β_2 -AR

Agonists and antagonists in keratinocyte cell migration. Agonists of β_2 -AR inhibit directional migration of keratinocytes while antagonists promote the migration, leading to increased wound repair. Reprinted with the permission from Elsevier [β -Adrenergic receptor modulation of wound repair] Volume 58, Issue 2, August 2008, 158-164

3.1.2 Drug: celiprolol

Celiprolol is a relatively cardio-selective β_1 -adrenoceptor blocker, possessing intrinsic sympathomimetic activity, acting as a partial agonist on β_2 -receptors and having a direct vasodilator effect. It is applied clinically for the treatment of mild to moderate level of hypertension⁵⁷. Boutouyrie et al. demonstrated that vEDS patients showed a decrease in the thickness intima to media. This decrease resulted from the mechanical stress especially when the stress was against extremely fragile tissues¹⁴. They postulated that treatment with celiprolol could decrease the mechanical stress which was loaded to the arterial collagen fibrils coming from continuous and pulsatile pressure, ultimately preventing arterial dissection and rupture. Following this publication, Ong et al. initiated a prospective randomized open blinded-endpoint trial to systematically investigate the role of celiprolol in vEDS patients. Patients were classified by their age (≤ 32 years or > 32 years) randomly into two groups with an established and blinded information. Fifty-three patients in this study were randomly grouped for either treatment with celiprolol or as the control group. It is important to emphasize that at the initiation of the trial only thirty-three patients had undergone genetic testing to confirm a mutation in *COL3A1* gene. The dosage of celiprolol was increased from 100mg to a maximum of 400mg twice daily every six months. There was only 100mg for each increase during the six months period. Primary endpoints were set to include rupture or dissection of major arteries, and fatal or not. Results of this clinical trial showed that treatment of vEDS patients with celiprolol reduced arterial events, such as rupture or dissection, three folds when compared with vEDS patients in the control group. Thus, they recommended treating vEDS patients with celiprolol to prevent major complications. However, the mechanisms by which celiprolol was effective at reducing arterial events in vEDS patients was not determined⁶.

In the early wound repair process, myofibroblasts synthesize collagen III but was later replaced by collagen I as the scars mature⁵⁸. Studies by Pullar et al. showed that β_2 -AR antagonist treatment increased the content of collagen III significantly in the wound area compared with no antagonist⁵⁴. Xu et al. showed that a stiffer arterial wall might result from an increase in the expression of type I as well as type III collagen⁵⁹. Celiprolol shows stronger β_1 selective activity compared with β_2 agonist activity⁶⁰ while Ong

et al. showed an increased stiffness of arterial wall in their clinical patients after celiprolol administration⁶, indicating that there was increased production of collagens in the arterial wall of vEDS patients after taking celiprolol. Disrupted arterial wound healing and thrombus resolution after artificial injury were demonstrated in chapter 2 of this dissertation. In conclusion, all the data suggested that celiprolol administration might be able to induce the production of type III collagen to promote injury repair.

Hypothesis: we hypothesize that celiprolol administration in the *Col3a1*^{+/-} mice would increase type III collagen production after arterial injury and correct the aberrant injury repair in the *Col3a1*^{+/-} mice.

Specific aims:

Celiprolol was used to treat both the *Col3a1*^{+/+} and *Col3a1*^{+/-} mice and histology studies were performed to compare the injury repair ability by detecting inflammation, cell proliferation and neovessel formation in *Col3a1*^{+/-} mice after celiprolol administration.

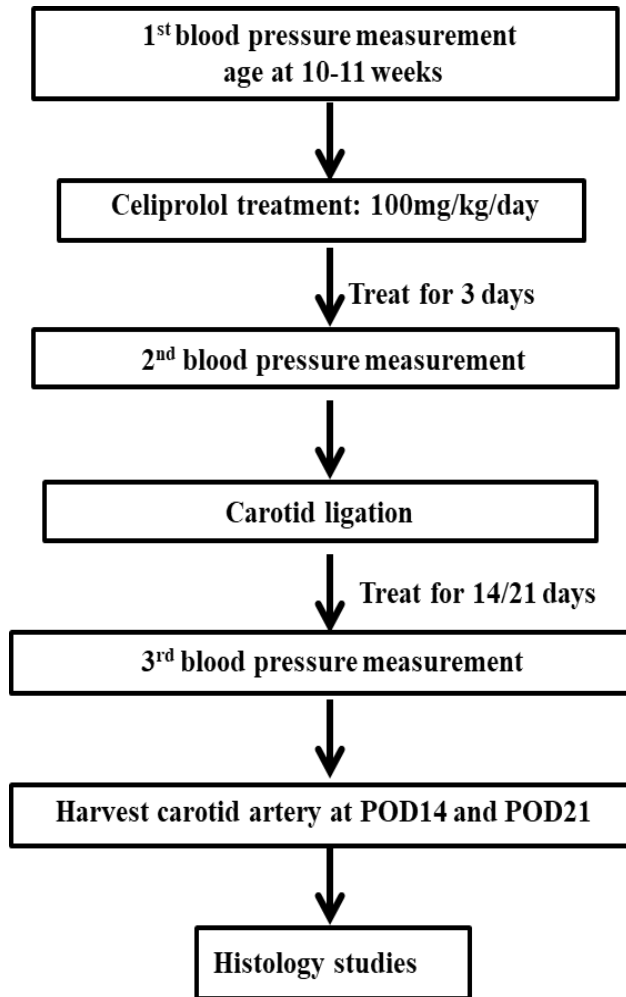


Figure 3.2 Flow chart of celiprolol trial

To modulate arterial injury repair in *Col3a1*^{+/+} and *Col3a1*^{+/-} mice with celiprolol.

3.2 Methods

3.2.1 Measurement of basic blood pressure for *Col3a1* mice

The animal study protocol was approved by Animal Welfare Committee at UThealth at Houston. Mice were surgically ligated at the left common carotid artery at the age of 12-14 weeks (unless otherwise stated) and were weighed between 25 and 30g (same to that described in Chapter of this dissertation).

Experiments were carried out according to the flow chart (**Figure 3.2**). On day 1, basal blood pressure was measured with the Kent Scientific CODA tail-cuff blood pressure machine (Kent Scientific Corporation, CT). Mice were placed into the restraint tubes according to their weight and cuffs were placed on the animal. They then were moved to the Animal Warming Platform that came with the machine and the CODA cover was lifted to measure the tail temperature by pointing an infrared thermometer at the tail base. The temperature was between 32°C and 35°C. The entire length of the animal's tail rested on the warming surface. Mice were measured with the machine for 3 consecutive days to get an average blood pressure value. Mice were treated with celiprolol on day 3 (Friendly gift from Dr. Julie De Backer, M.D., Ph.D., Center for Medical Genetics, Ghent University Hospital, Belgium.) at a dose of 100mg/kg/day by oral gavage delivery for 3 consecutive days. The drug was dissolved in purified water and the dosage was determined in accordance with multiple studies^{61,5,62}. On day six, blood pressure was measured again.

3.2.2 Carotid artery ligation and sample harvesting

The surgery procedure was modified from that described in Dr. Reid's study (Amy Reid unpublished data). Briefly, surgical mice were induced to anesthesia with 4% isoflurane which was maintained at 2-2.5% by a nose cone connected to the mouse. Aseptic techniques were used during the procedure and the fur at the neck area was shaved off with Nair gel and sanitized with alcohol swabsticks. Afterwards, analgesia with subcutaneous bupivacane (2.5 mg/kg) was applied immediately before making a midline incision of 3mm in length in the neck with sterilized scissors. Followed by dissecting away the left common

carotid artery from the carotid sheath and vagus nerve. A ligature was made on the artery with 6-0 silk suture immediately at the bifurcation site where the internal carotid arteries separate from external carotid arteries. It was important to be gentle to avoid bleeding. The open skin area was irrigated with iodine alcohol and closed by 2 interrupted stitches with 5-0 suture which would be absorbed after about one week.

About 10% of animals experienced stroke symptoms of during the first 7 post-operative days (POD7). Mice which failed to maintain 80% of their body weight were sacrificed. About 5% of the mice died before ligation due to massive bleeding caused by the procedure of carotid artery dissection. Mice that did not show neurological phenotypes such as stroke were monitored and treated subcutaneous with ketoprofen (2-5mg/kg) twice a day for 2 days after surgery. They were weighed daily and injected mice as needed with 0.5-1ml lactated Ringer's solution based on their weight for over 10% drops. Normally mice would survive 95% after POD7. Mice were sacrificed on 7, 14 and 21 days after surgery for the different following up experiments.

3.2.3 Histological Analysis: Morphology

For studies and analysis of POD7 arteries (N = 6 *Col3a1*^{+/+}, 6 *Col3a1*^{+/-}), POD14 (N = 6 *Col3a1*^{+/+}, 6 *Col3a1*^{+/-}), and POD21 (N = 5 *Col3a1*^{+/+}, 5 *Col3a1*^{+/-}), mice were first sacrificed, followed by puncturing of the left ventricles with a 27-gauge needle. An incision was made on the right atria to allow the outflow of perfusate. Mice were then perfused with phosphate-buffered saline (PBS) at <20 ml/min until blanching of the liver completely. Mice were then perfused with 10ml of 10% formalin at the similar rate to fix arteries in the native geometry. Both the entire lengths of carotid arteries were harvested for multiple experiments.

Arteries were followed by fixing in 10% buffered formalin for about 24 hours. After fixation, arteries were cleaned up and the connective tissues were removed followed by processing. After processing, the arteries were left in fridge to chill up. Then the arteries were cut three times with a scalpel: one cut was immediate to the ligature to remove the suture; a second cut was at the location of the descending aorta to

remove extra descending aorta; the third cut was in the mid-carotid artery. The remaining two pieces of the artery were embedded with careful attention to maintain correct orientation. The entire block with embedded artery was serial sectioned and three 5- μ m-thick sections were collected per slide all through the entire length of the arteries. Every tenth slide from the entire slides sequence was then performed with hematoxylin and eosin (H&E) staining, followed by imaging a representative section on each slide. This set of sequential images were enough for us to build up an entire arterial length along the axis of the arteries. Each carotid artery could supply approximately 60 to 80 slides. All images in this dissertation were presented at 20x, unless otherwise stated, and scale bars represent 100 μ m.

3.2.4 Immunohistochemical (IHC) staining

The IHC staining method was modified from Dr. Reid's study (unpublished data) and most of the methods were similar with only minor corrections. Briefly, each arterial segments as obtained above from H&E-staining provided a relative location of each segment with neointima formation. Those unstained slide neighboring each neointima positive slide was subjected to IHC probes (Mac-2, pH3 and CD31) to investigate the amount of macrophages, the number of actively proliferating cells locate within the neointima and the neovascularization in the medial layer. The first slide was probed with Mac-2, which showed the number of macrophages. The second local slide was used to measure the number of pH3-positive nuclei. The third slide was subjected to CD31 which was used to detect endothelial cells that are precursors for neovessels. Unstained sections were processed before heat-induced epitope retrieval (HIER citrate pH 6.0) followed by blocking for 1 hour at room temperature.

For detecting the local macrophages, slides with arterial sections were probed with rat anti-mouse Mac-2 primary antibodies (Cedarlane, Burlington, NC) and incubated for 1 hour at room temperature. For detection of proliferative cells, slides with arterial sections were probed with with rabbit anti-mouse pH3 primary antibodies (Millipore, Billerica, MA) followed by incubation overnight at 4°C. To examine

neovessel formation in formalin-fixed paraffin-embedded tissues, slides were left overnight at 4°C with rat anti-mouse CD31 antibodies (Dianova, Hamburg, Germany). Slides with arterial sections were then washed with PBS, followed by incubation at room temperature for 1 hour with the appropriate biotinylated secondary antibodies, and then tissues were probed with peroxidase-conjugated avidin/biotin complexes (Vectastain ABC-AP Kit, Vector Laboratories, Burlingame, CA). Activity of peroxidase was detected using a 3, 3'-diaminobenzidine (DAB) chromogen (Dako, Glostrup, Denmark). Slides were counterstained with methyl green at the last step of staining.

For statistical analysis, slides were counted one by one to get the number of positive cells or vessels independently. And then, for each genotype, a mean \pm SD of positive cells was generated by averaging out all the number from each group from the pooled neointima-positive slides, representing *Col3a1*^{+/+} or *Col3a1*^{+/-}. Significant differences were determined by the Student's *t*-test between the means (**p* < .05).

3.3 Results

3.3.1 No difference in basal systolic or diastolic blood pressure of *Col3a1*^{+/+} and *Col3a1*^{+/-} mice

Celiprolol is known to have β_2 agonist properties, and therefore blood pressure was assessed to determine whether celiprolol lowers mouse blood pressure. We chose a dose of celiprolol based on studies from rat, mice and human beings^{61,5,62}. In these studies, dosages were between 50 to 200mg/kg/day for mice or rats, but celiprolol was given to vEDS patients twice daily at doses from 100mg to 400mg. We therefore chose of 100mg/kg/day for each mouse based on their body weight, a dosage that was encompassed by both of these ranges. Blood pressure (BP) was measured before initiating the trial in 11 to 12-week-old mice. An average value of BP was generated by measuring on three consecutive days. There was not a significant difference in the BP value between the *Col3a1*^{+/+} and *Col3a1*^{+/-} mice at basal level (**Figure 3.3**). Celiprolol was given for three days prior to carotid ligation, and BP was measured again on post treatment day three (POT3), one day before ligation. In both genotypes, there was an average drop

of 15mmHg in basal systolic BP after three days of celiprolol treatment; however, this result was not statistically significant so we cannot conclude that celiprolol lowers blood pressure in mice.

We were curious whether celiprolol might be effective in lowering BP after a longer period of treatment. Therefore, BP value was measured a third time, at POD14 (data not shown) and POD21 (post treatment day 24 (POT24)), immediately before harvesting arteries (**Figure 3.3**). However, there was no dramatic difference in the BP value after celiprolol administration for 24 days either.

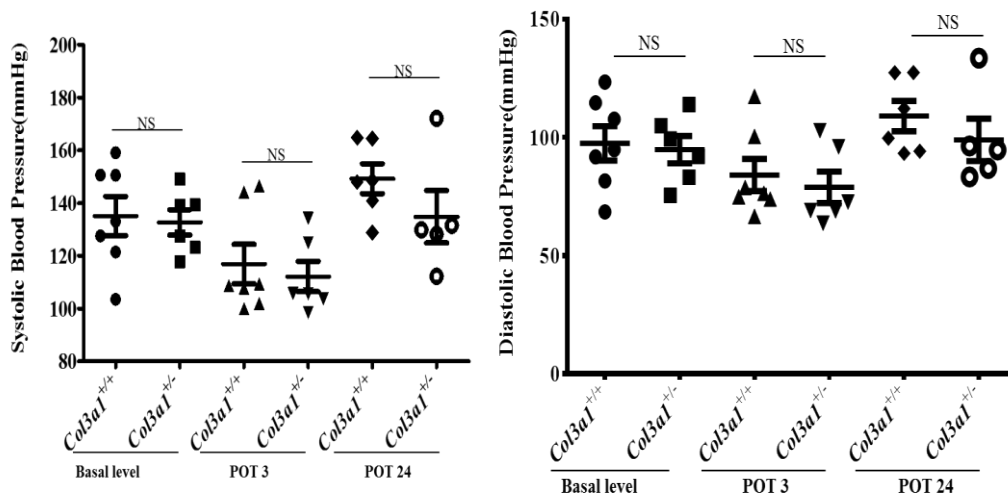


Figure 3.3 Comparison of the systolic blood pressure after celiprolol administration

Data representing 3 post days of treatment (POT3) and 24 days post treatment (POT24) in *Col3a1* mice, NS indicating no significant difference.

3.3.2 Decreased neointimal layer formation in $Col3a1^{+/-}$ mice carotid arteries after celiprolol treatment

As proposed in Chapter 2, to determine if celiprolol corrected the arterial injury repair process in the $Col3a1^{+/-}$ mice, neointima formation was first examined by H&E staining. Since there were only significant differences in pathological changes at POD14 and POD21 when comparing $Col3a1^{+/+}$ and $Col3a1^{+/-}$ mice at basal level, we only looked at these timepoints after celiprolol treatment. Compared with arteries from mice without celiprolol treatment, there was decreased neointima formation in arteries from both $Col3a1^{+/+}$ and $Col3a1^{+/-}$ mice with celiprolol treatment at both POD14 (POT17) and POD21 (POT24) as shown in (Figure 3.4).

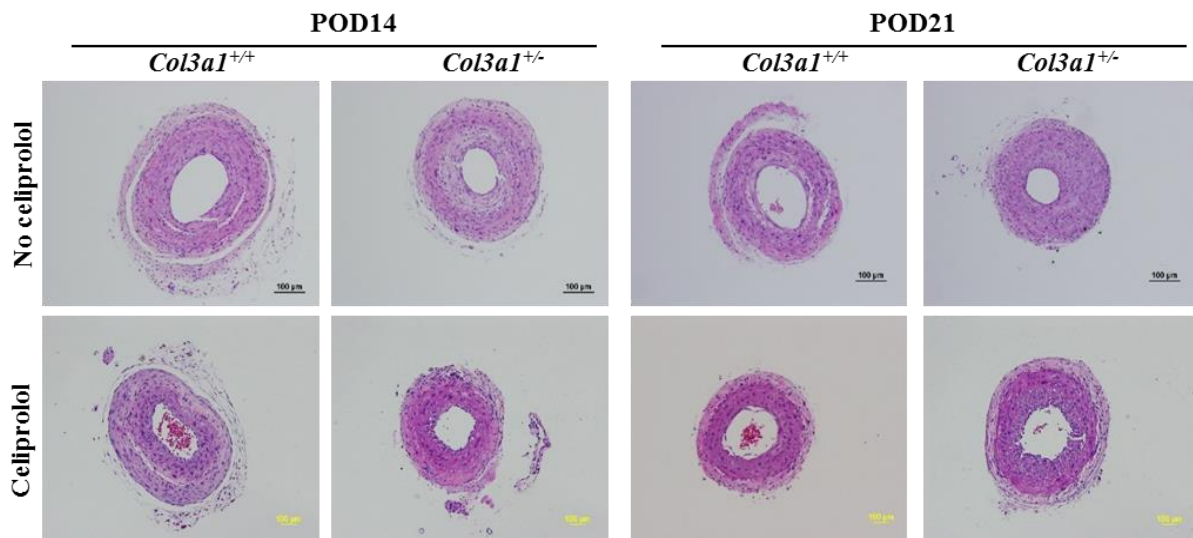


Figure 3.4 Remodeling of neointimal by H&E staining after celiprolol administration

Representative sections of the $Col3a1^{+/+}$ and $Col3a1^{+/-}$ mice both without (top panel) and with celiprolol treatment (bottom panel), showing decreased neointima formation after celiprolol treatment in mice from both groups at both POD14 and POD21. Scare bar: 100 μ m.

3.3.3 Altered cell proliferation and inflammation in the neointimal layer after celiprolol treatment

We further stained the arterial sections with anti-pH3 antibody to detect the cell mitosis marker pH3, which indicated the proliferative cells in the neointima. There were decreased pH3 positive cells in the arteries from celiprolol treated *Col3a1*^{+/-} mice compared with arteries from untreated *Col3a1*^{+/-} mice (**Figure 3.5a**). No significant difference in pH3 positive cells was observed comparing *Col3a1*^{+/+} arteries from no celiprolol and celiprolol treated mice at both POD14 and POD21 (**Figure 3.5b**). This result indicated that celiprolol was more effective in decreasing cell proliferation in the arteries from *Col3a1*^{+/-} mice than in the arteries of *Col3a1*^{+/+} mice.

It was shown by Rough et al. that β_2 -AR blockade could decrease the hyper-inflammatory reaction after traumatic injury in mice⁶³. To look at the inflammation level at the neointima after celiprolol administration, IHC with anti-Mac-2 antibody was used to detect the number of macrophages in the neointima (**Figure 3.6a**). At basal level, prior to celiprolol treatment, there were significantly more Mac-2 stained cells in *Col3a1*^{+/-} arteries compared with arteries from *Col3a1*^{+/+} mice at both POD14 and POD21 (**Figure 3.6b**). However, after celiprolol treatment, a significant decrease was observed after analyzing Mac-2 positive cells in *Col3a1*^{+/-} arteries comparing with those from untreated *Col3a1*^{+/-} arteries (**Figure 3.6b**). No difference was observed for Mac-2 stained cells when comparing *Col3a1*^{+/+} arteries from no celiprolol and celiprolol treated mice at both POD14 and POD21. Again, results showed that celiprolol was more effective in lowering inflammation level in the arteries from *Col3a1*^{+/-} mice.

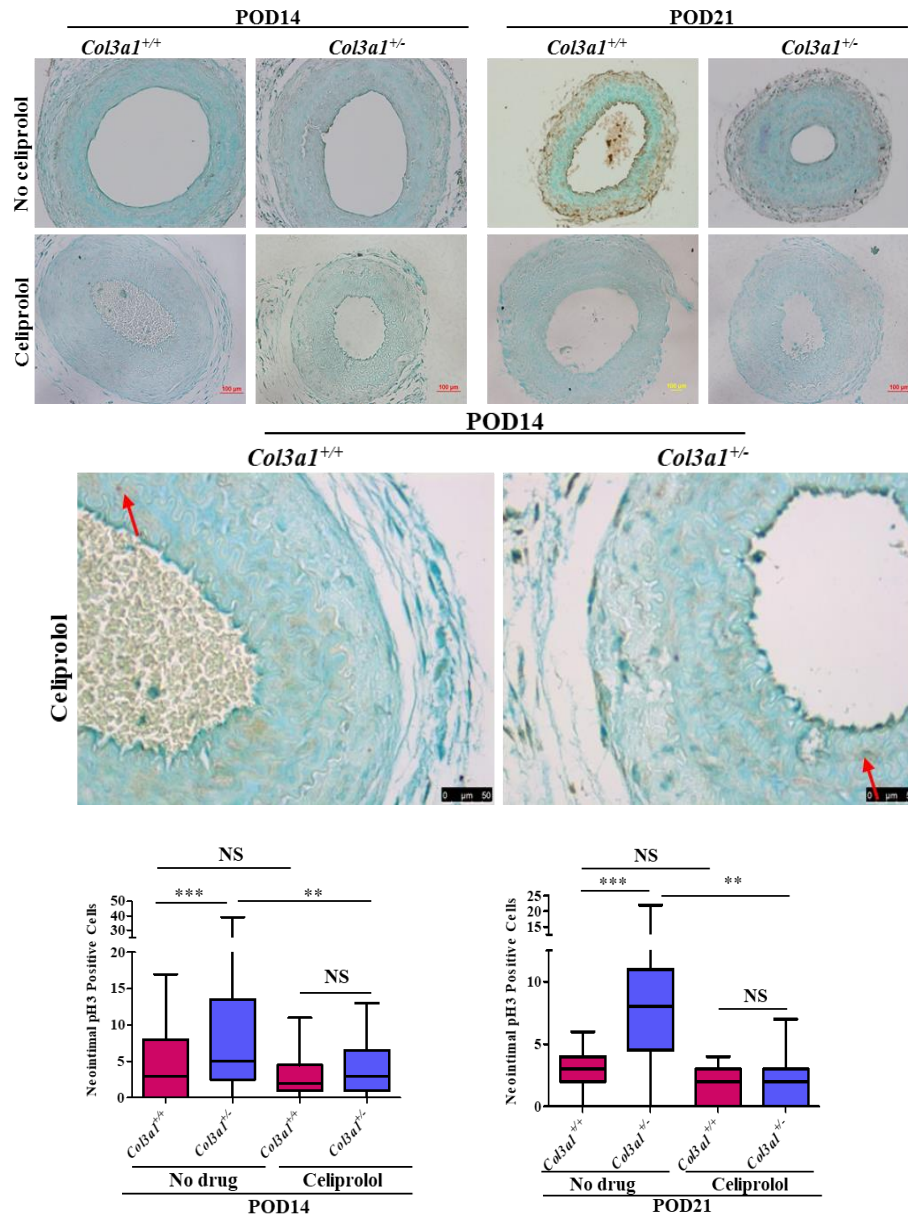


Figure 3.5 Decreased cell proliferation in *Col3a1*^{+/-} arteries after celiprolol administration

(a) Representative sections of arteries from both *Col3a1*^{+/+} and *Col3a1*^{+/-} mice, both without (top panel) and with (bottom panel) celiprolol treatment, (b) Higher power images, red arrow showed the neointimal pH3 positive cells, (c) Quantitation showed significantly decreased number of pH3 positive cells after celiprolol treatment in arteries from *Col3a1*^{+/-} mice at both POD14 and POD21 indicating decreased cell proliferation in the *Col3a1*^{+/-} arteries after celiprolol treatment. NS: no significance, ** $p < 0.01$, *** $p < 0.001$ by Student's *t*-test.

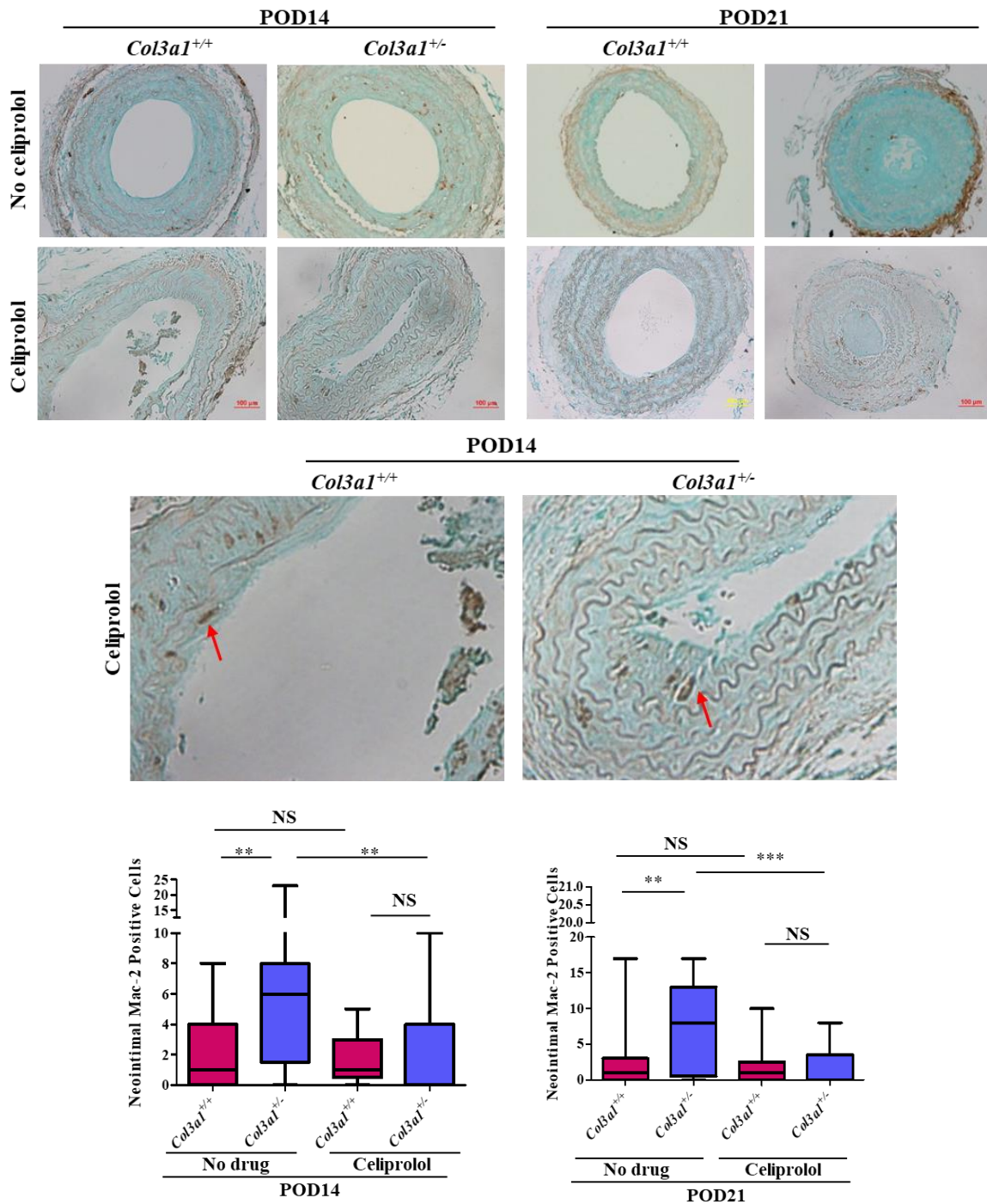


Figure 3.6 Decreased neointima inflammation in *Col3a1*^{+/-} arteries after celiprolol

(a) Representative sections of arteries from both *Col3a1*^{+/+} and *Col3a1*^{+/-} mice, both without (top panel) and with celiprolol treatment (bottom panel) (b) Higher power images, red arrow was showing the neointimal Mac-2 positive cell (c) Quantitation showed significantly decreased number of Mac-2 positive cells after celiprolol treatment in arteries from *Col3a1*^{+/-} mice at both POD14 and POD21 indicating decreased inflammation in the *Col3a1*^{+/-} arteries after celiprolol treatment. NS: no significance, ***p*<0.01, ****p*<0.001 by Student's *t*-test.

3.3.4 No difference in the formation of new vessels in the medial layer after celiprolol treatment at both POD14 and POD21

Similarly, IHC with anti-CD31 antibody was used to detect the presence of CD31 for assessing the formation of neovessels in the medial layer after administration of celiprolol. At basal level, when there was no celiprolol treatment, there were significantly more CD31 positive neovessels in the arteries from *Col3a1*^{+/-} mice compared with those from *Col3a1*^{+/+} mice at both POD14 and POD21 (**Figure 3.7a**). However, after celiprolol treatment, no significant difference was found in the formation of neovessels comparing arteries from *Col3a1*^{+/+} mice with those from *Col3a1*^{+/-} arteries. There was also no statistical difference between the number of neovessels in *Col3a1*^{+/-} arteries treated with or without celiprolol. These results indicated a potential partial blunting of neovessel formation in *Col3a1*^{+/-} mice with celiprolol treatment, but more studies need to be done to confirm the role of celiprolol in affecting neoangiogenesis. (**Figure 3.7b**).

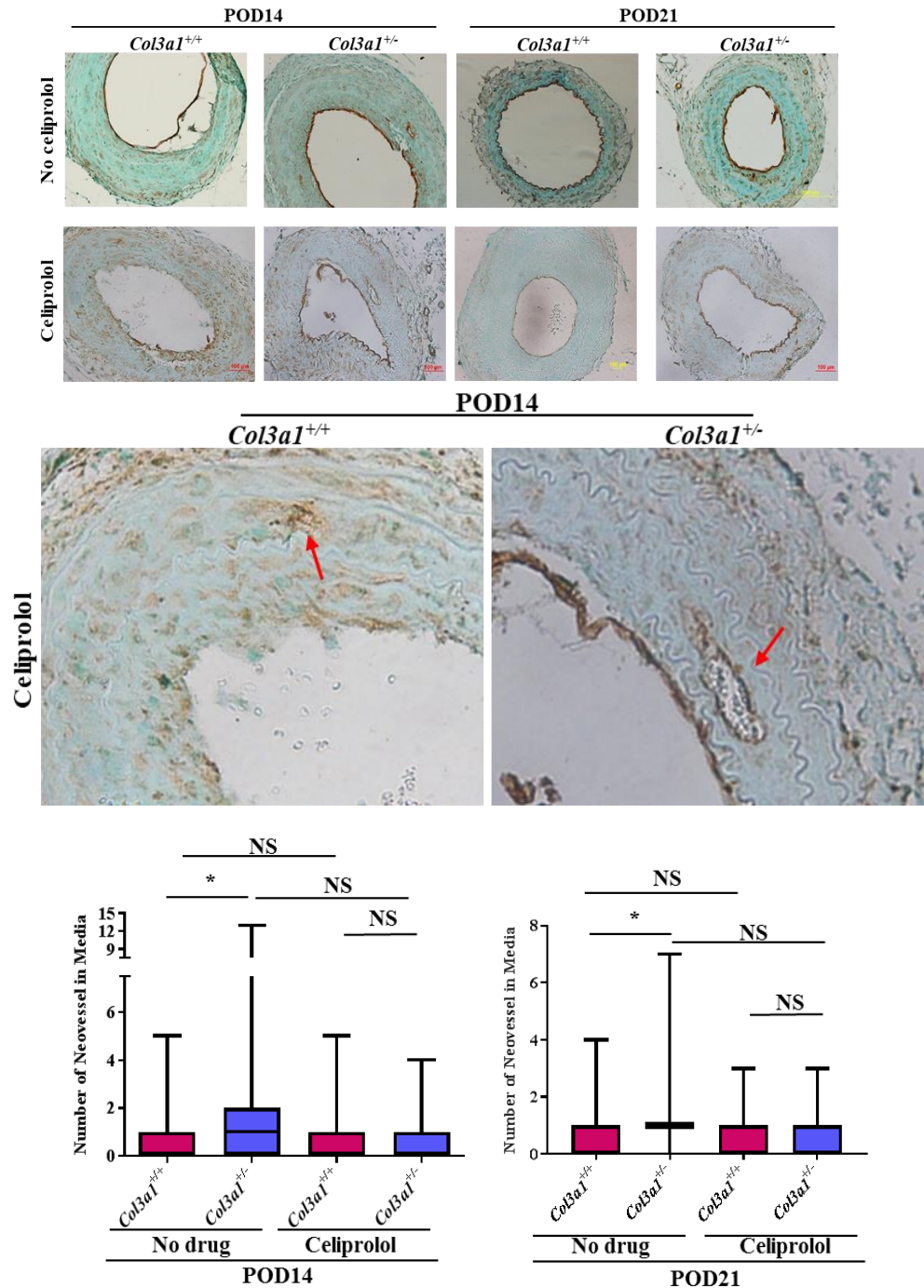


Figure 3.7 No significant difference in neovessel formation after celiprolol

(a) Representative sections of arteries from both *Col3a1*^{+/+} and *Col3a1*^{+/-} mice, both without (top panel) and with celiprolol treatment (bottom panel) (b) Higher power images and red arrow was showing medial layer neovessel by CD31 staining (c) Quantitation showed no difference in the potential of new vessel formation in both mice genotypes after celiprolol treatment. NS: no significant difference by Student's *t*-test.

3.4 Discussion

To better understand the mechanisms leading to vEDS and to discover a possible therapeutic approach for vEDS patients, previous work of Dr. Reid (unpublished data) and studies in the first part of Chapter 2 of this dissertation were conducted which showed a consistent defective in injury repair in *Col3a1*^{+/-} mice compared to that in *Col3a1*^{+/+} mice. These results confirmed a defect of injury repair in the *Col3a1*^{+/-} mice when there was not sufficient type III collagen. This suggested that there was aberrant injury repair in vEDS patients, resulting in both aberrant skin wound healing and also problems with arterial injury repair causing frequent arterial events such as dissection or aneurysms of vEDS patients and leading to a decreased life expectancy for these patients⁶⁴.

Ong et al. speculated that patients taking celiprolol would have alleviated high blood pressure in hypertensive people which could lead to a decreased in stress formed against arterial collagen fibers resulting in decreased incidence of arterial dissections and ruptures, and showed that taking celiprolol, a β -blocker, could decrease the arterial events in vEDS patients threefold⁶. They initiated a clinical trial to investigate the effects of celiprolol on vEDS patients. Instead however, their findings proved that celiprolol could have demonstrated more stable haemodynamic resistance which lead to a more strenuous arterial wall. Data generated from this current study did not show the effect of celiprolol to lower blood pressure at both 3 days and 24 days after administration, which was consistent with the discoveries by Ong et al. However, we could not conclude that celiprolol did not show β_2 agonist activity in this study due to absent data from a critical group-regular ligation without celiprolol treatment, as the ligation procedure itself might have lead to an increase in systematic blood pressure.

Inflammation following arterial injury plays a critical role in both cutaneous and arterial injury repair²⁰. Secretion of TGF- β by macrophages and platelets would induce the differentiation of myofibroblasts from fibroblasts both of local origin and from bone marrow derived (BMD) fibrocytes³⁷. After the expression of type III collagen by myofibroblasts, contracting cells would pull open the fibrin clot resulting in successful thrombus resolution after arterial injury. Unpublished data from our laboratory

has shown a significant increase in inflammation of POD14 and POD21 arteries in the *Col3a1*^{+/-} mice without celiprolol treatment, compared with that in the *Col3a1*^{+/+} mice in the neointima layer (p<0.05).

Morissette et al. harvested both plasma as well as dermal fibroblasts from vEDS patients and investigated the role of inflammation and the expression of proteins for TGF- β pathways⁶⁵. They demonstrated that vEDS patients usually have a chronic inflammation going on all through their life. Results from the pathological data of the current study also showed that there was decreased inflammation in the neointima in the *Col3a1*^{+/-} arteries after ligation indicating the potential of *Col3a1*^{+/-} mice in repairing arterial injury after celiprolol treatment.

Other studies have shown that celiprolol was effective in cardiovascular diseases effects through the antioxidative properties to increase the function of vascular endothelial progenitor cells (EPCs), resulting in a decreased intimal thickening after vascular injury^{66,67}. Previous data showed in Chapter 2 of this dissertation that there was an increase in the potential of cell proliferation POD14 and POD21 with carotid injury in the *Col3a1*^{+/-} mice when comparing to that in the *Col3a1*^{+/+} mice in the neointimal layer. However, after treating both groups of mice with celiprolol, a dramatic decrease was observed in cell proliferation in injured *Col3a1*^{+/-} arteries with celiprolol treatment compared with that of no celiprolol injured *Col3a1*^{+/-} arteries (**Figure 3.7**). Yao et al. also showed the decreased proliferative cell activity in the vein graft neointima after celiprolol administration⁶⁶, which was consistent with data from the current study. However, we were not able to determine the mechanism beyond the pathological change with celiprolol administration.

From our unpublished study, there was dramatic neovessel formation in the medial layer after carotid injury at both POD14 and POD21 in *Col3a1*^{+/-} mice, compared to that in *Col3a1*^{+/+} mice in the medial layer. This neovessel formation may predispose arteries to fragility, resulting in dissection and arterial rupture. We sought to use celiprolol to modulate the thrombus resolution and neovessel formation procedure in the *Col3a1*^{+/-} mice, we didn't get any difference in neovessel formation in the media with celiprolol treatment. Although the neovessel data is inconclusive, we were able to decrease the

inflammation and cell proliferation in the *Col3a1*^{+/-} mice. Though there were limitations for the current study in that no cellular/molecular work has been done to prove why and how celiprolol does these things.

Pullar et al. concluded that β -adrenergic receptor modulation of wound repair through a variety of signaling pathways by both *in vivo* and *in vitro* models^{50,56} (**Figure 3.1**). As with their studies, future studies should be focused on investigating the role of celiprolol on inflammatory responses and cell proliferation by *in vitro* models. Cells should be explanted from *Col3a1*^{+/+} and *Col3a1*^{+/-} mice to understand the cellular/molecular mechanisms and explain the data generated from the current study.

In conclusion, celiprolol was effective in decreasing the inflammation and persistent cell proliferation in the neointima of the *Col3a1*^{+/-} arteries but not in decreasing the neovessel formation in the medial of those arteries. Indicating that it might be used to alleviate the symptoms of vEDS patients.

4 Dysregulated Myofibroblasts from *Col3a1*^{+/-} Mice Contribute to the Abnormal Injury Repair

4.1 Introduction

4.1.1 Myofibroblasts in wound healing

Characteristics of vascular Ehlers-Danlos Syndrome (EDS) include thin, translucent, and often, bruised skin. This easy bruising indicates aberrant injury repair in vEDS patients⁶⁴. Myofibroblasts are key players in normal injury repair³⁷. After a tissue has been wounded, myofibroblasts are involved in a few events in remodeling tissues⁶⁸: (1) secretion of ECM proteins (2) tension sensation and transduction and (3) apoptosis, through which they disappear from the wounding area.

Myofibroblasts are differentiated from fibroblasts demonstrated by the expression of α -SMA, which is one of the major mechanosensitive proteins that is recruited to stress fibers under high mechanical stress. With the expression of α -SMA, myofibroblasts gain highly contractile potential⁶⁹. Myofibroblasts can not only produce procollagen type I and III, but also other ECM components, such as collagens⁷⁰. With the expression α -SMA, myofibroblasts assemble bundles of contractile microfilaments that stretch across the cell and attach to different cell surface protein complexes that link the intracellular filaments to the surrounding area of extracellular matrix (ECM)⁷¹.

Secondly, contraction of myofibroblasts is accomplished by the motor mechanism of the myosin head domain sliding along the actin filaments, and this sliding mechanism creates a tension that is transferred to the surrounding ECM⁷⁰. An extended network of stress fibers results in the formation of large focal adhesion sites, also called super-mature focal adhesions (FAs)⁷². The size of the FAs is critical to control differentiation and contracture of myofibroblasts⁶⁹.

Lastly, after wound closure, myofibroblasts undergo automatic cell apoptotic procedure and disappear gradually from the site of injury. Normal procedure of myofibroblasts apoptosis results in formation of scar from granulation tissues while abnormal apoptosis leads to the development of pathological scarring⁷³. This balance ensures to tissue integrity³¹. Disturbances such as abnormality in tissue contraction to excessive deposition of ECM, could severely impair skin function. Common problems include hypertrophic scar formation, scleroderma, skin contractures after a burn⁷³. Fibrosis in the in the kidney,

heart or lung also rely on these same cells functioning in the same way, but pathologically²¹. It is promising that many studies suggest that myofibroblasts are bone marrow-derived (BMD), as perhaps modulating the bone marrow could address many of these health problems³⁷.

4.1.2 Role of TGF- β in differentiation of fibroblasts and arterial injury

TGF- β 1 is a cytokine secreted by platelets, fibroblasts and macrophages. Injection of TGF- β 1 to rats subcutaneously resulted in a granulation tissue formation in which there are particularly abundant amount of myofibroblasts with α -SMA expressing while injection of other growth factors or cytokines such as TNF- α or PDGF did not induce α -SMA expression in myofibroblasts⁷⁴. This suggests the importance for TGF- β 1 in myofibroblast differentiation in the procedure of wound healing and fibro-contractile diseases by the regulation of α -SMA expression in those cells. A study from James et al. also demonstrated that TGF- β 1 played a significant role in cutaneous wound repair: wounds were made by an incision on the skin of a pig and expression of TGF- β 1 and integrin was examined. Expression of TGF- β 1 within the extracellular matrix area was finely coordinated with an increased expression of different integrin subunits⁷⁵. Thus, they concluded that in the different steps of wound repair procedure, TGF- β 1 could induce the expression of integrins by epidermal keratinocytes to facilitate the migration for re-epithelialization.

In the classical TGF- β signaling, three different isoforms of TGF- β ligands are believed to bind two TGF- β receptors (T β RI and T β RII) through which signal is transduced (**Figure 4.1**). T β RII is constitutively phosphorylated and they phosphorylate T β RI once bind to the ligand. Once phosphorylated, the ligand and receptor complex will activate the intracellular SMAD signaling pathway. The SMAD proteins will then be translocated to the nucleus for regulation of other targets genes²².

Studies by Roberto et al. proposed that TGF- β 1 secreted by macrophages and platelets at sites of injury would not only recruit fibroblast but also induce the differentiation of them to form myofibroblasts. Formation of myofibroblasts ensures the production of major ECM components such as collagens and the

contraction to close the wound⁷⁶. Taken together, these studies and others showed that TGF- β 1 is one of the key players in modulating the wound healing process described above, in part by regulating the function of myofibroblasts.

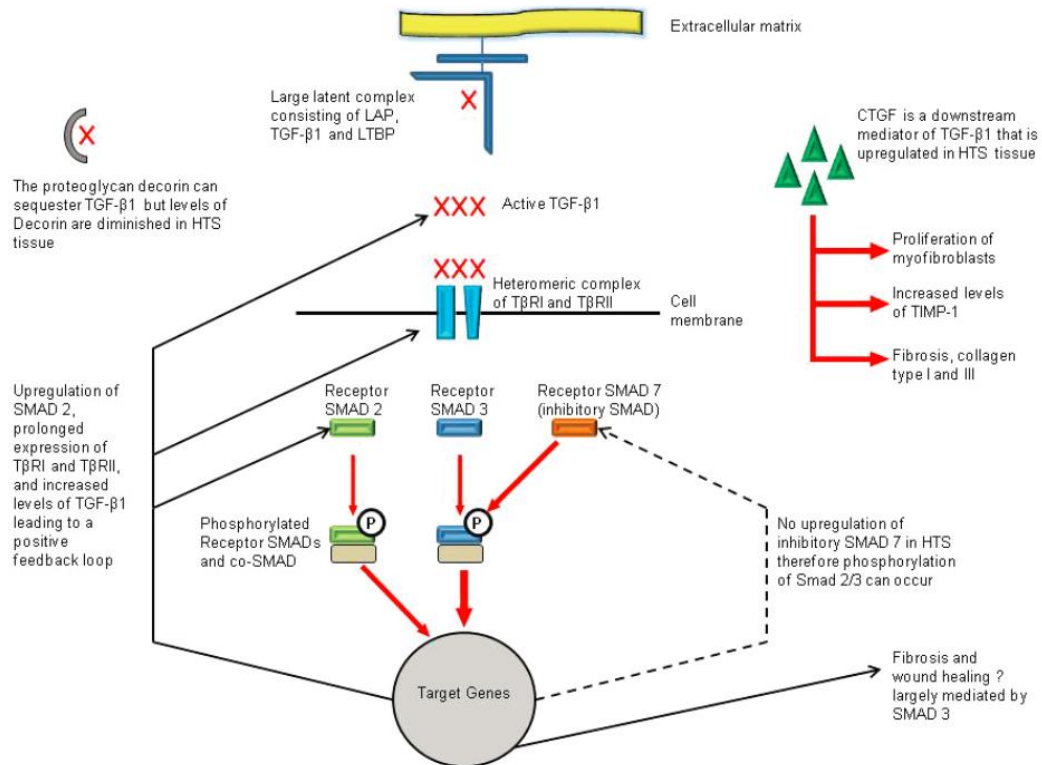


Figure 4.1 Summary of TGF- β signaling in hypertrophic scarring

4.1.3 Focal adhesions (FAs) and focal adhesion kinase (FAK) in the differentiation of fibroblasts

Focal adhesions are located at the convergence of integrin receptors. They transduce signal to other cell adhesions and actin cytoskeleton⁷². They are within the site where integrin receptors and proteoglycan attach to cytoskeleton formed by actin. According to the subcellular location, composition and size, focal adhesions are mainly classified into four different groups: focal adhesions, focal complexes, three-dimensional (3D) matrix adhesions, and fibrillary adhesions⁷⁷.

Thannickal et al. showed that in addition to TGF- β 1, myofibroblast phenotype was dependent on adhesion-dependent signals²³. Increased expression of α -SMA is first activated by TGF- β signaling and followed by FAK signaling pathway. In this study, they demonstrated that both TGF- β 1 and adhesion-dependent signals were required for a stable expression of the myofibroblast phenotype. TGF- β 1-induced myofibroblast differentiation would be inhibited in non-adherent cells even if the existence of TGF-receptor-Smad2 phosphorylation signaling. Tyrosine phosphorylation of FAK induced by TGF- β 1 which including Tyr-397 was also delayed in relative to early TGF- β 1-Smad signaling. Blockage of FAK or induced expression of kinase-mutated FAK, inhibited expression of α -SMA as well as stress fiber formation and cellular hypertrophy induced by TGF- β 1. Their working model was illustrated in **Figure 4.2**.

4.1.4 MRTFA and fibroblasts differentiation

Myocardin-related transcription factor-A (MRTF-A) and -B (MRTF-B) are widely distributed. Both of them interact with G-actin and are sequestered in the cytoplasm^{78,79}. Once there is stress, the actin dynamics would be altered for the formation of F-actin fibers and further enhance nuclear MRTFs accumulation⁸⁰. Within nuclear, SRF/MRTF binding together to form a complex which specifically binds to short element of CArG locating within the promoters of contractile related genes. Smooth muscle α -actin (SMA, ACTA2) and transgelin (TAGLN, SM22) are the two genes most responsive to stress⁸¹. Thus, MRTFs play a critical role for SMCs to respond to stress. It was also shown that MRTFA contributes to myofibroblast differentiation and contractility⁸².

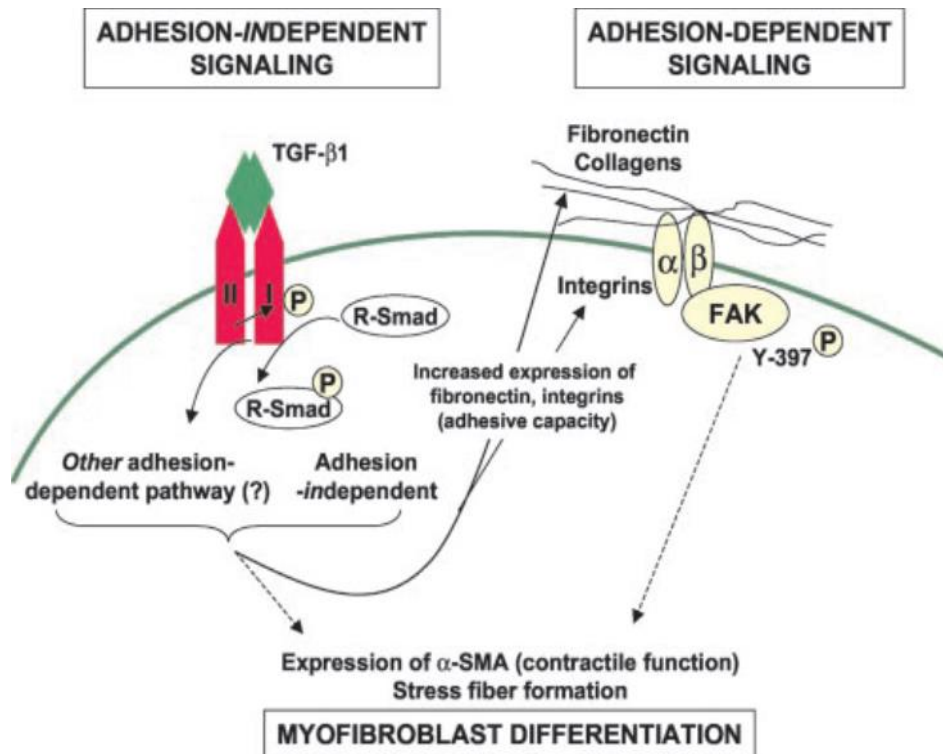


Figure 4.2 Schematic of the proposed regulatory pathways involved in myofibroblast differentiation.

TGF- β receptor(s) signaling is primarily mediated by rapid phosphorylation/activation of Smad proteins, which occurs by an adhesion-independent mechanism. Other unidentified non-Smad pathways may also be activated early post-TGF- β receptor(s) activation. FAK autophosphorylation/activation is delayed relative to Smad signaling and is associated with TGF- β 1-induced expression of both integrin subunits and fibronectin/collagens. Integrin signaling via FAK autophosphorylation/activation is essential for induction/maintenance of the stably differentiated myofibroblast phenotype. With permission from American Society for Biochemistry and Molecular Biology.

4.1.5 Studies with fibroblasts from *Col3a1*^{+/-} mice and unpublished data on mice embryonic fibroblasts (MEF) and fibroblasts from vEDS patients

Studies by Volk et al. showed that deficiency of type III collagen promoted differentiation of myofibroblast and increased scar formation after cutaneous wounding. They showed that aged *Col3a1*^{+/-} mice had was quicker in wound healing comparing with *Col3a1*^{+/+} mice using an *in vivo* wounding model. Wounds were made on both *Col3a1*^{+/+} and *Col3a1*^{+/-} mice, and wound area (WA) was measured at different time points. By using fibroblasts explanted from *Col3a1*^{+/+} and *Col3a1*^{+/-} mice skin tissues, they demonstrated that *Col3a1*^{+/-} mice showed increased ability in wound closure compared with that of *Col3a1*^{+/+} mice⁸³. The *in vitro* data showed that fibroblasts from *Col3a1*^{+/-} and *Col3a1*^{-/-} mice express more α -SMA compared with cells from *Col3a1*^{+/+} mice by immunofluorescent staining (**Figure 4.3**). In conclusion, their study demonstrated that a type III collagen was important in modulating myofibroblast differentiation and activity during cutaneous repair. They also identified a possible mechanism *in vivo* for an increased scar formation in wounded *Col3a1* deficient skin. Unpublished *in vitro* data from Dr. Reid showed dysregulated fibroblasts in the *Col3a1*^{+/-} mice by increasing expression of α -SMA, increasing collagen I fibril formation in 3D fibrinogen gel experiment. Finally, results from Chapter 2 in this dissertation demonstrated that BMD fibrocytes were critical in the correction of injury repair in *Col3a1*^{+/-} mice.

SMCs:

As we discussed in chapter 2, introduction section that SMCs migrating from arterial wall contribute to the neointima formation followed by thrombus resolution³⁹.

Hypothesis

Taken together, we hypothesize that myofibroblasts from the *Col3a1*^{+/-} mice predispose a persistent differentiated status due to the defects in contracture, leading to an aberrant wound healing in the *Col3a1*^{+/-} mice after arterial injury. To address the hypothesis, fibroblasts from mouse lungs were explanted

according to protocol adapted from Dr. Blackburn's laboratory, and *in vitro* studies were performed with the fibroblasts. **SMCs were explanted from the ascending aorta of *Col3a1*^{+/-} mice⁸⁴.**

Specific aims:

- 1. Is there any difference in phenotype between *Col3a1*^{+/+} and *Col3a1*^{+/-} fibroblasts/myofibroblasts?**
 - a) Test the myofibroblasts differentiation and compare if there is any difference between *Col3a1*^{+/+} and *Col3a1*^{+/-} fibroblasts by detecting the expression of RNA and protein for SMC markers, collagens and integrins.
 - b) Examine the formation of F-actin of fibroblasts by actin IF staining and F/G actin assay.
- 2. Is there any difference in phenotype of *Col3a1* SMCs?**
 - a) Expression of RNA and protein for SMC markers, collagens and integrins.
 - b) Test the potential of SMC proliferation by BrdU assay, MTT assay.
 - c) Examine the formation of stress fiber by F-actin IF staining.
- 3. Why there is the difference between cells explanted from both *Col3a1*^{+/+} and *Col3a1*^{+/-} cells? Is there any focal adhesions link collagen and actin expression/polymerization in both, is there any difference?**
 - a) Focal adhesion staining by vinculin IF
 - b) Focal adhesion signaling to detect activity of pFAK by both Western blots and IF staining

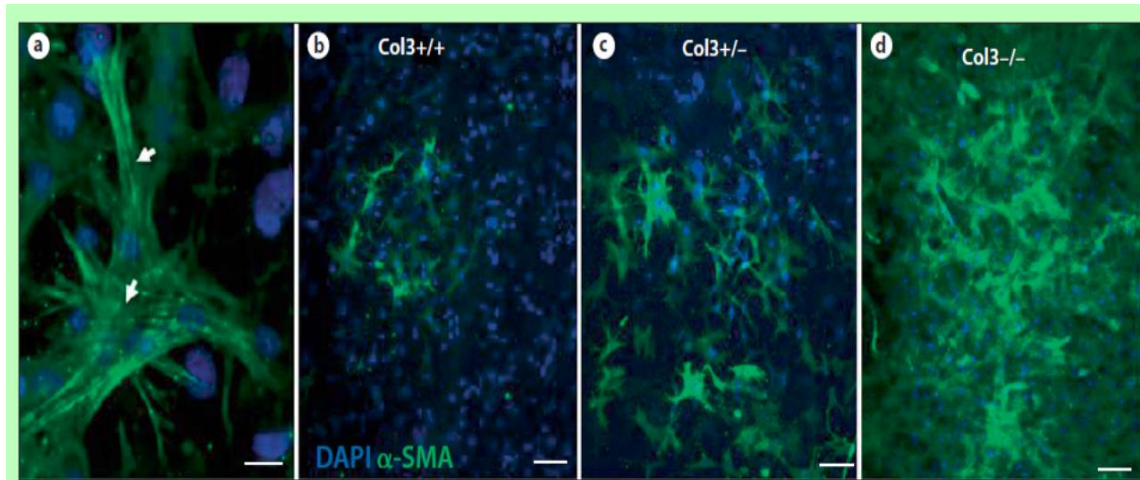


Figure 4.3 Increased α -SMA expression by $Col3^{+/-}$ and $Col3^{-/-}$ cells compared to $Col3^{+/+}$ cells

Cells from all 3 genotypes, utilized in the attached fibroblast-populated collagen gel assay, were immune-stained for α -SMA (green) and counterstained with DAPI (blue). Collagen lattices seeded with cell isolates from at least 3 embryos per genotype were analyzed. **a** Myofibroblasts within collagen lattices were identified by α -SMA expression. α -SMA incorporation into stress fibers (arrows) could be visualized in cells from all 3 genotypes. **b-d** Representative images showing the percentage of myofibroblasts in cultures of $Col3^{+/+}$ (**b**), $Col3^{+/-}$ (**c**), and $Col3^{-/-}$ (**d**). Copyright (1997) National Academy of Sciences, U.S.A

4.2 Methods

4.2.1 Fibroblast explant from mouse lung tissues

To explant fibroblasts, mice were sacrificed humanely at 4-6 weeks. Mouse was then perfused with 10ml cold-sterile PBS at the right ventricle, the whole lung tissues were taken out and put into a clean petri-dish with PBS. Then tissues were rinsed to remove blood cells, cleaned up to remove connective tissues and brought to tissue culture hood. The tissues were rinsed with 70% ethanol and PBS followed by cutting into very small pieces (0.1-0.5mm) with an autoclaved blade. Small pieces of lung tissues were re-suspended with 10ml PBS and transferred to 75mm² flask. PBS was aspirated and the tissues were left to attach to the bottom of the flasks, followed by leaving the flasks vertically in the incubator for 2 hours. After incubation, extra PBS was aspirated from the bottom of the flask followed by adding 10ml high glucose DMEM with 10% FBS and 1% antibiotics. Leave the flasks incubated for 14 days and media was changed very other day. Cells were split from one T75 flask to two T75 flasks when they were about 80-90% confluence and labelled as passage 1(P1). Experiments were set up for harvesting protein, RNA, immunofluorescent (IF) and BrdU samples with cells which were at 90% confluence and less than P4.

Two independent cell lines were generated from *Col3a1*^{+/+} and *Col3a1*^{+/-} mice, using lungs pooled from two mice for each genotype per explant. Results presented in this dissertation were representative of two independent experiments replicated on each line of fibroblasts. Fibroblasts used in this study were passage- and sex-matched explanted from *Col3a1*^{+/+} and *Col3a1*^{+/-} mice. Fibroblasts were used at no more than passage 3.

4.2.2 Isolation of Vascular SMCs from *Col3a1*^{+/+} and *Col3a1*^{+/-} mice

4-6-week old *Col3a1*^{+/+} and *Col3a1*^{+/-} mice were used for isolating mouse aortic SMCs according to the protocol developed by our lab⁸⁴. Briefly, aortas were pooled from at the aortic root and up until the bifurcation of the renal artery. Whole aortas collected were treated under sterile techniques and transferred to media for collecting biopsy. (**Table 1**). Ascending aorta was collected from each mouse. Followed by

removing the connective tissues. The aorta was washed and then cut into 1mm pieces. All the aortic tissues were collected and put into digestion medium for 16 hours. The medium was prepared as shown in **Table 1**. Followed by spinning down cells and small tissues. Cells and tissue pallets were then re-suspended in complete SMC medium and put into petri-dishes for another 14 days of incubation. The expression of α -actin was used to define the cell identity explanted.

Two lines of fibroblasts from *Col3a1*^{+/+} and *Col3a1*^{+/-} mice were generated independently, using aortas pooled from four mice for each genotype per explant. The results presented in this study were representative of two independent replicates. Passage-and-sex-paired SMCs from *Col3a1*^{+/+} and *Col3a1*^{+/-} mice were used at no more than passage 4 for all the experiments.

Table 1 Media and buffer used in this project

Media/Buffer	Composition
Aortic biopsy medium	Waymouth's MB 752/1 medium supplemented with 100U/ml penicillin, 100ug/ml streptomycin, 250 ng/ml amphotericin, 2.5 mM L-glutamine, 1 mM MEM non-essential amino acids, 100 mM Hepes buffer, and sodium bicarbonate
Complete SMC medium	SmBm basal media (Lonza/Cambrex) supplemented with 20% FBS, 100 U/ml of penicillin, 100 ug/ml of streptomycin, 250 ng/ml of amphotericin, 0.5 ml of insulin, 1.0 ml of rhEGF, 0.5 ml of rhFGF, 2 mmol/l of l-glutamine, 20 mmol/l of HEPES, 1 mmol/l of sodium pyruvate
1% serum medium	SmBm basal media (Lonza/Cambrex) supplemented with 1% FBS, 100 U/ml of penicillin, 100 ug/ml of streptomycin, 250 ng/ml of amphotericin, 2 mmol/l of l-glutamine, 20 mmol/l of HEPES, 1 mmol/l of sodium pyruvate
RIPA buffer	50 mm of Tris, pH 7.5, 150 mm of NaCl, 1% NP-40, 0.5% sodium deoxycholate and 0.1% SDS) supplemented with protease inhibitor cocktail P8340 (Sigma) and phosphatase inhibitor cocktails 2 and 3 (Sigma)

4.2.3 Isolation of RNA and q-PCR

RNA extraction kit (Invitrogen, Carlsbad, CA) was used to collect entire cellular RNA. Briefly, RNA lysis buffer with 1% β -Mercaptoethanol was prepared, cells cultured in 6cm petri-dish were washed with PBS for 2 times. 700ul lysis buffer was put into each petri-dish and incubated at 4°C or on ice for 30 minutes. The mixture was transferred to 1.5ml eppendorf tube, thoroughly mixed with 21gauge syringe for 10 times, followed by adding 0.7 volume 70% ethanol and vortexing to mix thoroughly. The mixture

was transferred to the mini-column with the kit, spun down at 12,000 rpm for 15 seconds, the column was washed 3 times before adding 30-100ul sterile water to dissolve RNA on the column. The concentration of the samples was between 100-300ng/ul. IScript supermix kit (Bio-rad laboratories, Hercules, CA) was applied for reverse transcription directed by protocol from the manufacturer. Q-PCR analysis was applied for target genes expression with TaqMan probes. TaqMan probes for target genes were purchased from Applied Biosystems and results of q-PCR was analyzed with an Applied Biosystems Prism 7900 HT Sequence Detection System (Applied Biosystems, Foster City, CA) using the manufacture's protocol. Results were generated by three independent times. Endogenous control was referred to the expression of *Gapdh*. Data was analyzed by $2^{-\Delta\Delta CT}$ method to generate a p-values Student's *t*-test.

4.2.4 Protein preparation and Western blotting

Cells cultured in 6cm petri-dish were washed 2 times with PBS. After washing, 120ul cell lysis buffer for western blot was added to each petri-dish then lysed cells cultured in petri-dish. Samples were incubated at 4°C in fridge or on ice for 30 minutes and followed by manually vortexed 3 times. Supernatant was collected and then quantitated by a Bradford assay. After quantitation, equal amount (5ug or 10µg) of protein was prepared and loaded onto 4-20% protein gels (Bio-Rad laboratories, Hercules, CA). A standard way of western-blotting in this laboratory was used. Briefly, membranes with complete proteins from SDS page gel were put into 5% non-fat milk blocking buffer for 1 hour. After blocking, the membranes were probed with appropriate primary antibodies, usually 1:1000 dilution in 5% TBST/milk buffer followed by washing before probing with appropriate secondary antibodies, usually 1:5000 dilution in 5% TBST/milk buffer. See **Table 2** for information of antibodies. Immunoblots were developed to see the expected bands of target proteins using regular or enhanced chemiluminescence technique (GE Healthcare, Piscataway, NJ).

Table 2 Antibody information

Antigen	Company	Species	Uses
SM-actin	Sigma	Mouse	WB, IF
SM-MHC	Biomedical Technologies, Inc	Rabbit	WB
Calponin	Novus Biologicals	Rabbit	WB
MRTF-A	Santa Cruz Biotechnology	Rabbit	IF
Vinculin	Sigma	Mouse-FITC conjugate	IF
SM-22 α	Santa Cruz Biotechnology	Rabbit	WB
Phospho-FAK (Y397)	Millipore	Mouse	WB, IF
FAK	Santa Cruz Biotechnology	Rabbit	WB
Phospho-Akt (S473)	Cell Signaling Technology	Rabbit	WB
Akt	Cell Signaling Technology	Rabbit	WB
Phospho-Histone 3 (S10)	Upstate (Millipore)	Rabbit	IHC
Mac-2			IHC
CD-31			ICH

4.2.5 Cell proliferation assay

5,000 cells (Mice lung fibroblasts or SMCs) were put in a 96-well plate and incubated 20-24 hours before serum-starvation with DMEM containing 1% FBS. After starving 24 hours, TGF- β 1 (2 ng/mL) was added and kept for 24 hours before addition of BrdU reagent to each well and incubating for 24 more hours. BrdU ELISAs assay was performed with the instruction from the manufacture (Millipore, Bedford, MA.) BrdU ELISA assay was applied in replicates. $p^* < 0.05$ using Student's t-tests was generated as

statistical significance.

4.2.6 TGF- β 1 administration to fibroblasts and immunofluorescent staining (IF)

Fibroblasts or SMCs were seeded onto 18mm glass coverslips. And about 5,000 cells suspended in complete media were seeded on a single coverslip. Cells were starved with 1% FBS media after incubation for 20-24 hours. Fresh media containing 1% FBS with TGF- β 1 (2ng/mL) was used to replace the starvation media. 4% paraformaldehyde (PFA) was added to fix cells after 72 hours TGF- β 1 induction. For focal adhesion staining, PBS with 0.2% saponin and 10% FBS was applied to permeabilize cells on coverslips, which were incubated at room temperature for 10 minutes before blocking in PBS with 5% donkey serum for 30 minutes. Coverslips were then probed with vinculin antibody (1:200, Sigma-Aldrich, St. Louis, MO) at 4°C overnight. The following day, coverslips were washed before adding Vectashield mounting medium with DAPI (Vector Labs, Inc., Burlingame, CA). Then nail polish was used to seal coverslips which were then stored in cold room until they were taken out for images. **Table 1** provides information of the antibodies used.

Analysis of Immunofluorescence Images

For vinculin staining and pFAK staining, images were obtained on Olympus Fluoview 300 confocal microscope using a PL APO LSM2 40x water immersion objective with NA=0.9. The image statistics and masking tools coming with the SlideBook software (Intelligent Imaging Innovations, Denver, CO) were used to measure area of cell and focal adhesions. To compare sufficient cell number, area of vinculin staining and focal adhesions was normalized to each total cell area of each cell followed statistical analysis. A $p < 0.05$ was generated by the Student's t -test and was determined as significant difference.

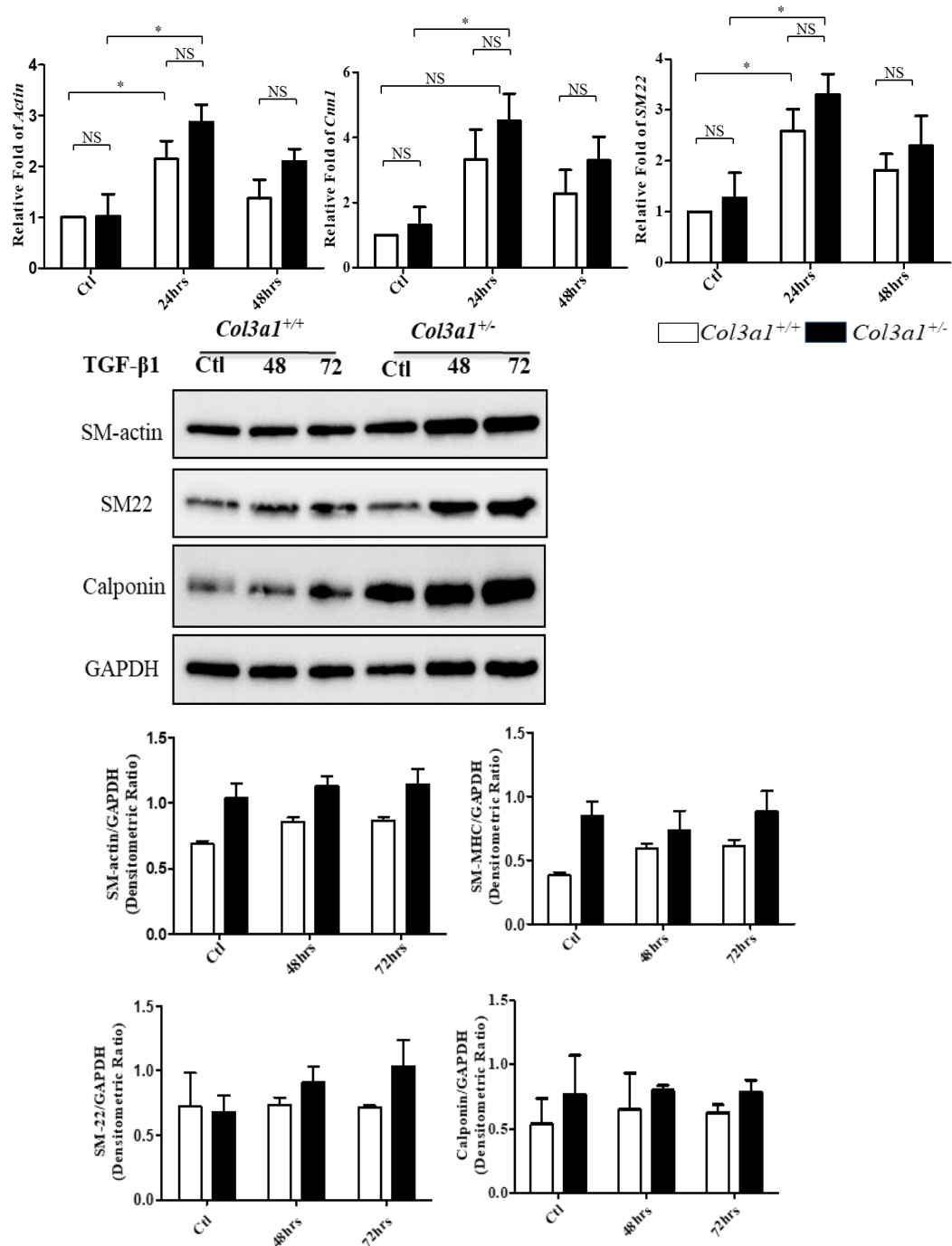


Figure 4.4 Expression level of contractile proteins

□ *Col3a1*^{+/+} ■ *Col3a1*^{+/-}

RNA was isolated from both TGF- β 1 treated and control cells at different time points. qPCR was performed according to the protocol, statistics was generated by Student's t test and * $p < 0.05$, NS: no significance.

4.3 Results

4.3.1 Both the *Col3a1*^{+/+} and *Col3a1*^{+/-} fibroblasts respond to stimulation by TGF-β1

At the injury site, immediately after thrombi formation, there is increased secretion of TGF-β1 by platelets and activated macrophages⁴⁶, resulting in a TGF-β1 rich environment. TGF-β1 is widely accepted as a chemokine that promotes differentiation of myofibroblasts from fibroblasts as assayed by expression of contractile proteins. To examine the differentiation of fibroblasts, *in vitro* experiments were conducted by examining the expression of contractile proteins with fibroblasts explanted from mouse lung tissues. Expression of three most common contractile proteins, *Acta2* (SM-actin), *Cnn1* (calponin), and *SM22* (*transgelin*) were detected. Both *Acta2* and *SM22* genes were expressed at significantly higher levels after 24 hours of TGF-β1 treatment (**Figure 4.4a**). But *Cnn1* gene was only expressed significantly higher in the *Col3a1*^{+/-} cells. The expression of all the contractile proteins decreased at 48 hours. We next examined their protein accumulation by westernblot. Interestingly, there was increased expression for all three proteins after 48 hours of TGF-β1 treatment and persistent up until after 72 hours in *Col3a1*^{+/-} cells (**Figure 4.4b**). The results indicating stable increased protein accumulation of contractile targets in the *Col3a1*^{+/-} fibroblasts after TGF-β1 treatment.

We then examined the expression of collagens genes, *Colla1*, *Colla2* and *Col3a1* as well as collagen receptors, *Itga2* and *Itgb1* (**Figure 4.5a**). There was not any significant difference between *Col3a1*^{+/+} and *Col3a1*^{+/-} cells after TGF-β1 for either 24 or 48 hours for both *Colla1* and *Colla2*, but there was significant decreased expression of *Col3a1* in *Col3a1*^{+/+} cells after 24 hours treatment.

There was significant less *Itga2* expression in *Col3a1*^{+/-} cells compared to that in *Col3a1*^{+/+}

cells at basal level while expression of *Itga2* decreased dramatically in *Col3a1*^{+/+} cells after 48 hours. And there was significantly increased expression of *Itgb1* in *Col3a1*^{+/-} cells compared to that in *Col3a1*^{+/+} after both 24 and 48 hours treatment (Figure 4.5b).

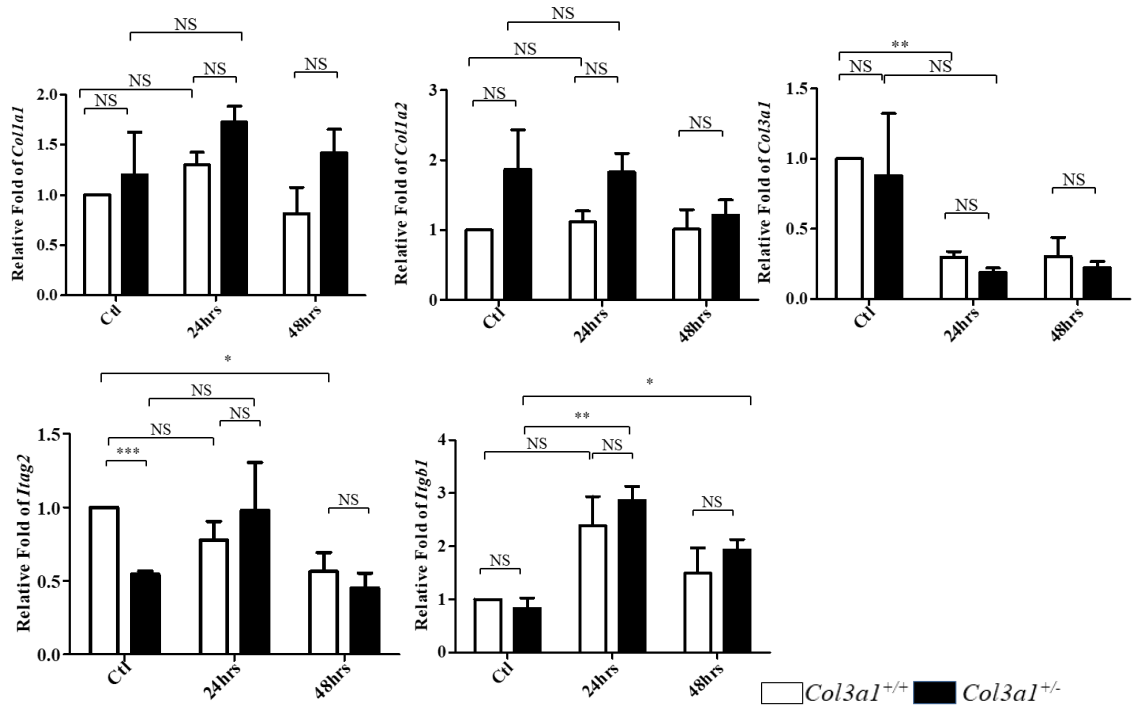


Figure 4.5 Expression of collagens (a) and two collagen receptors(b)

RNA was isolated from both TGF- β 1 treated and control cells at different time points. qPCR was performed according to the protocol, statistics was generated by Student's t test and * $p < 0.05$, ** $p < 0.01$, NS: no significance.

4.3.2 More formation of stress fibers in *Col3a1*^{+/-} cells at basal level but not after TGF-β1 stimulation

To validate the more differentiated status of *Col3a1*^{+/-} cells after TGF-β1 stimulation, we performed IF staining to examine the F-actin polymerization in both *Col3a1*^{+/+} and *Col3a1*^{+/-} fibroblasts (**Figure 4.6**). It was shown that both *Col3a1*^{+/+} and *Col3a1*^{+/-} cells significantly expression more a-actin, but in *Col3a1*^{+/-} cells, a-actin were not assembled into F-actin fibers normally.

4.3.3 Significantly increased activity of focal adhesion signaling in the *Col3a1*^{+/-} cells after TGF-β1 stimulation for 72 hours

Focal adhesions (FAs) are widely distributed at the plasma adjacent to the membrane area and to sense forces against cells. Size of FA and maturation of them has been shown to demonstrate the degree of myofibroblasts differentiation⁷². We then asked whether the FAs in *Col3a1*^{+/-} cells might be more mature compared to those from the *Col3a1*^{+/+} cells. Vinculin is one of the components of FAs and has been used

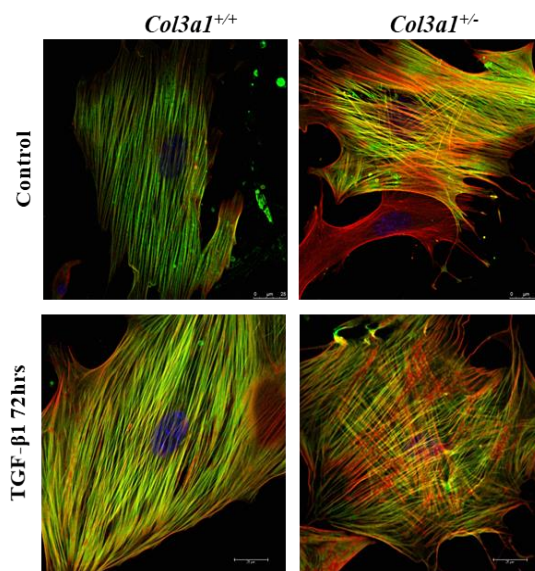


Figure 4.6 Abnormal actin polymerization in *Col3a1*^{+/-} myofibroblasts

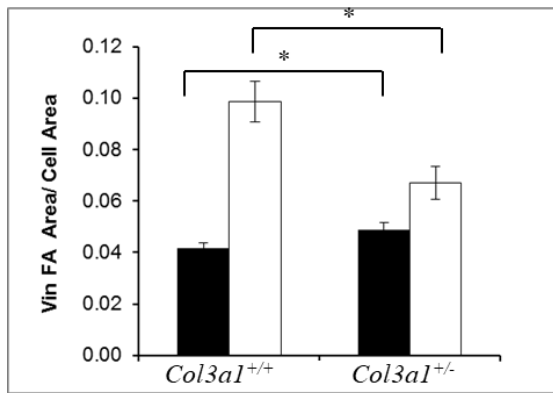
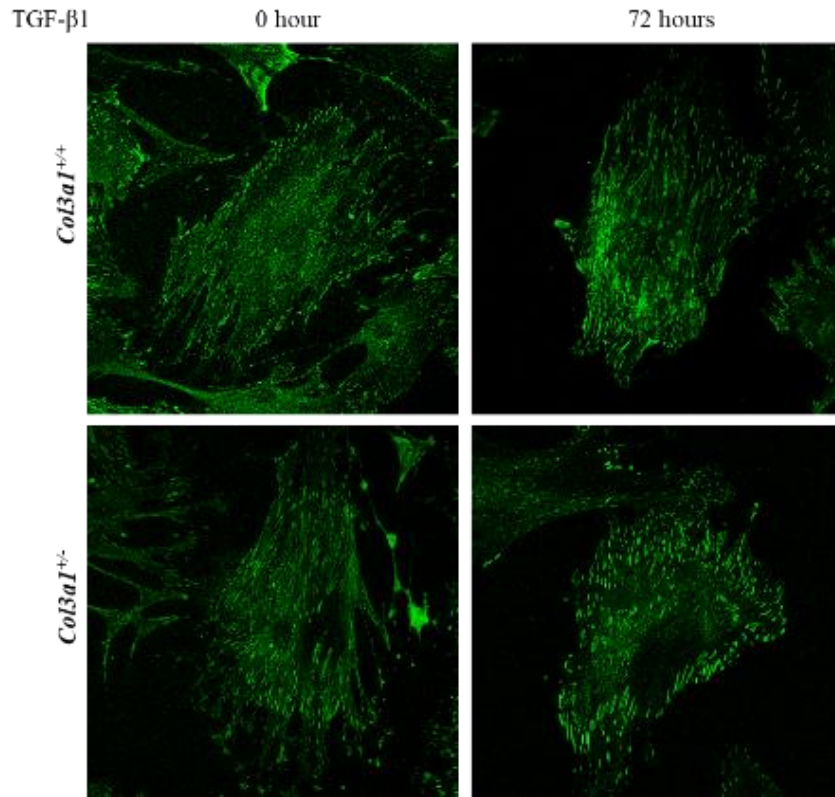
Abnormal actin polymerization in *Col3a1*^{+/-} fibroblasts after treatment with TGF-β1 for 72hrs. Images are from IF staining showing merge of a-actin (green), DAPI (blue) and F-actin (red).

as a marker of FAs. IF of vinculin was used to show the size and location of focal adhesions. Results

showed an increase in area of vinculin/area of cell in *Col3a1*^{+/-} comparing with that in *Col3a1*^{+/+} fibroblasts at basal level, but there was significant increase in vinculin area/cell area in *Col3a1*^{+/+} cells compared with that in *Col3a1*^{+/-} cells with 72 hours TGF-β1 induction. (**Figure 4.7a**), indicating the size of FAs in the *Col3a1*^{+/-} cells was not increased after TGF-β1 treatment.

4.3.4 No activation of pFAK in *in vitro* tissue culture of *Col3a1*^{+/-} fibroblasts

Focal adhesion kinase (FAK) locates at FAs and function as a protein to transduce signaling. A group of different signaling pathways are activated by FAK, such as MAPK and PI3K-AKT. Activity of FAK was assayed to determine if there was increased kinase activity in the *Col3a1*^{+/-} fibroblasts. Western blot analyses showed that there was not significant difference in phosphorylation of FAK comparing *Col3a1*^{+/+} cells to *Col3a1*^{+/-} cells after TGF-β1 treatment (**Figure 4.7c**). However, immunofluorescent staining (IF) of pFAK revealed a smaller pFAK area/cell area in *Col3a1*^{+/-} cells compared with *Col3a1*^{+/+} cells at both basal level and after TGF-β1 treatment for 72 hours (**Figure 4.7b**). This indicated that *Col3a1*^{+/-} cells were not further responding to TGF-β1 compared to *Col3a1*^{+/+} cells.



■ No TGF- β 1

□ TGF- β 1 for 72hours

4.3.5 Increased translocation of MRTFA into the nucleus of *Col3a1*^{+/-} myofibroblasts

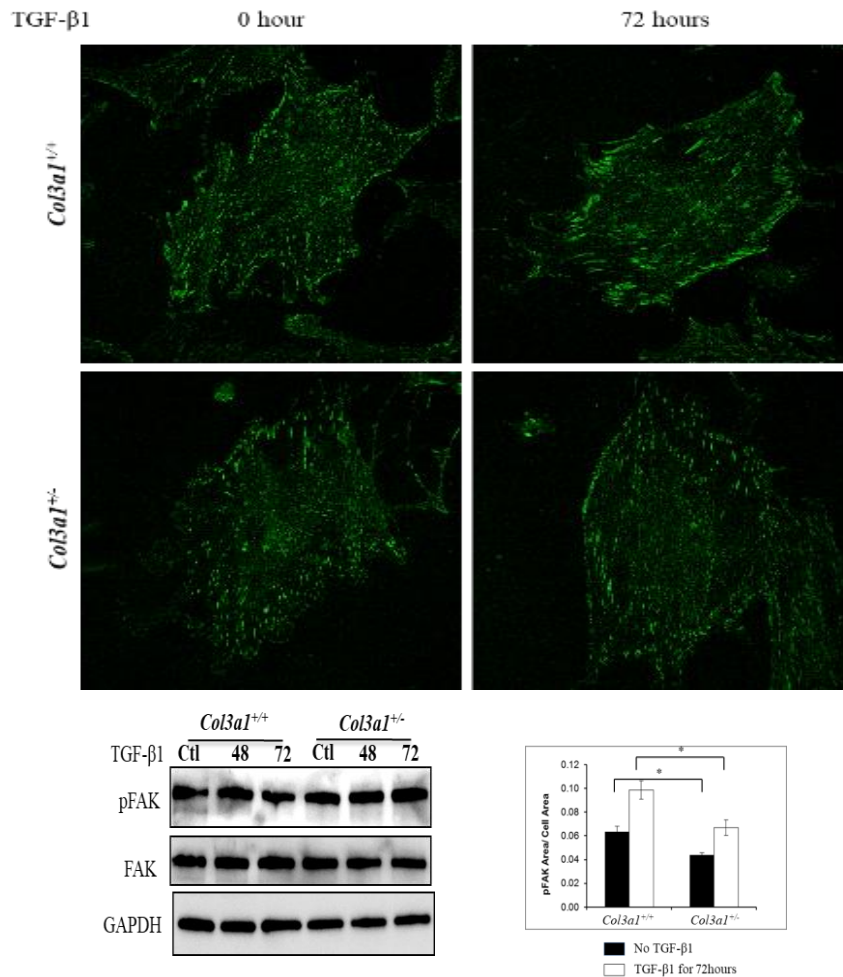


Figure 4.7 Altered focal adhesions in both *Col3a1*^{+/+} and *Col3a1*^{+/-} cells

(a) Immunofluorescent staining (IF) to detect vinculin, marker for focal adhesions, results showed an increase in vinculin area/cell area in *Col3a1*^{+/-} cells compared to that in *Col3a1*^{+/+} at basal level, but there is significant increase in vinculin area/cell area in *Col3a1*^{+/+} cells compared with that in *Col3a1*^{+/-} cells after TGF-β1 treatment for 72 hours (b) IF to detect pFAK results showed that there was increase in pFAK area/cell area in *Col3a1*^{+/+} cells compared with that in *Col3a1*^{+/-} cells at both basal level and after TGF-β1 treatment for 72 hours. Cells were treated with TGF-β1, followed by IF staining, and images were obtained on Olympus Fluoview 300 confocal microscope using a PL APO LSM2 40x water immersion objective with NA=0.9. Significance was evaluated at $p < 0.05$.

MRTFA which was shown to be responsible TGF-β1 induced myofibroblasts differentiation by multiple studies⁸². In order to find out the reason for the differentiation of *Col3a1*^{+/-} fibroblasts, we

conducted IF staining of MRTFA with *Col3a1*^{+/+} and *Col3a1*^{+/-} fibroblasts with 72-hour TGF-β1 induction to determine the translocation of MRTFA from cytoplasm to nucleus. Quantitation was done by measuring the intensity of the staining. Result showed the increased MRTFA intensity in the nucleus of *Col3a1*^{+/-} cells compared with the *Col3a1*^{+/+} cells (**Figure 4.8**), indicating that after stress exposed to fibroblasts, *Col3a1*^{+/-} cells were more dependent on MRTFA signaling to further drive differentiation instead of FAK signaling.

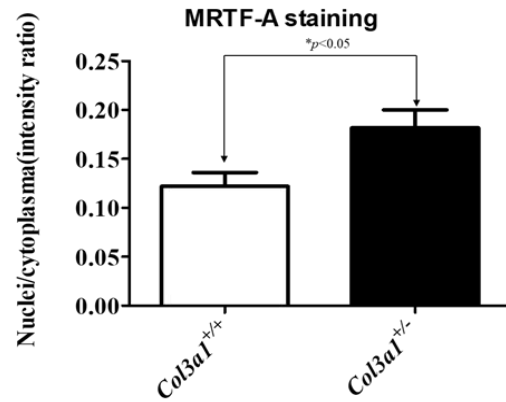
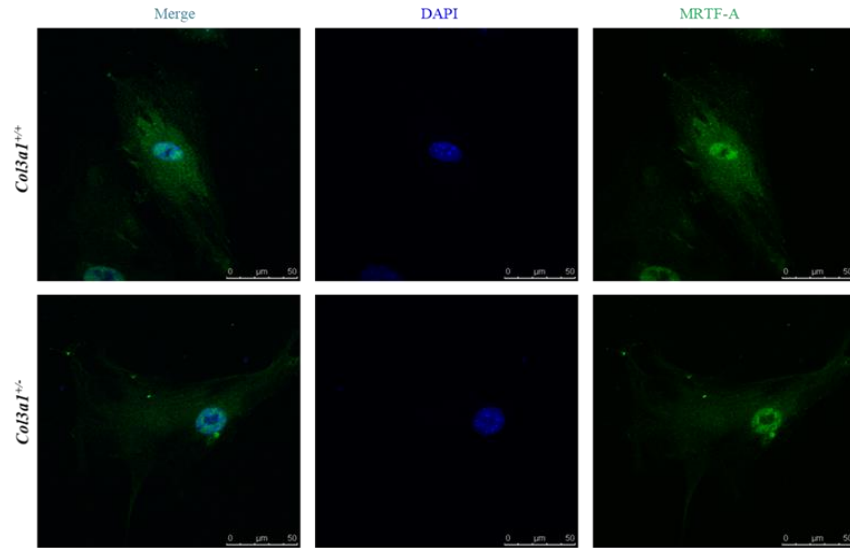


Figure 4.8 Increased translocation of MRTFA into the nucleus of *Col3a1*^{+/-} myfibroblasts

Immunofluorescent staining (IF) to detect MRTFA, marker for focal adhesions, results showed that there was an increase in translocation of MRTFA in *Col3a1*^{+/-} cells compared to that in *Col3a1*^{+/+} cells after TGF-β1 treatment for 72 hours. Significance was evaluated at **p* < 0.05.

4.3.6 Increased differentiation of *Col3a1*^{+/-} SMCs after stimulation with TGF-β1

Since SMCs migrated from arterial wall also play a critical role in neointimal formation, we also examined phenotypes of SMCs in both *Col3a1*^{+/+} and *Col3a1*^{+/-} mice. Multiple experiments were performed with SMCs explanted from both *Col3a1*^{+/+} and *Col3a1*^{+/-} aortas. As with fibroblasts, expression of contractile markers was also detected. Results showed more dramatic increased messenger RNA (Figure 4.9a) and protein accumulation (Figure 4.9b) of contractile markers in *Col3a1*^{+/-} SMCs after stimulation with TGF-β1 for 24 hours.

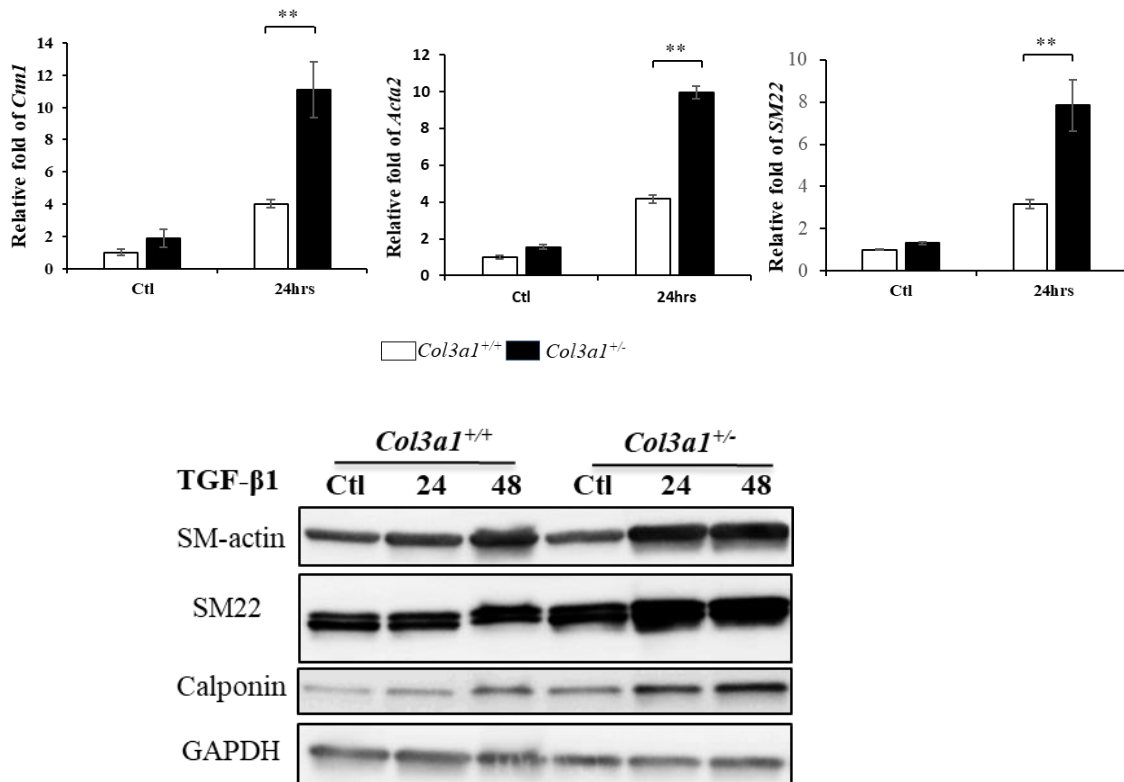


Figure 4.9 Increased expression of contractile proteins in *Col3a1*^{+/-} myofibroblasts

RNA was isolated from both TGF-β1 treated and control SMCs cells at different time points. There was increased messenger RNA expression of contractile proteins and accumulation of protein level in both *Col3a1*^{+/-} SMCs after TGF-β1 stimulation compared with control cells, but was more dramatic in SMCs. qPCR was performed according to the protocol, $p^{**} < 0.001$, by the Student's *t*-test.

4.3.7 Altered focal adhesion by vinculin staining and increased differentiation of *Col3a1*^{+/-} SMCs

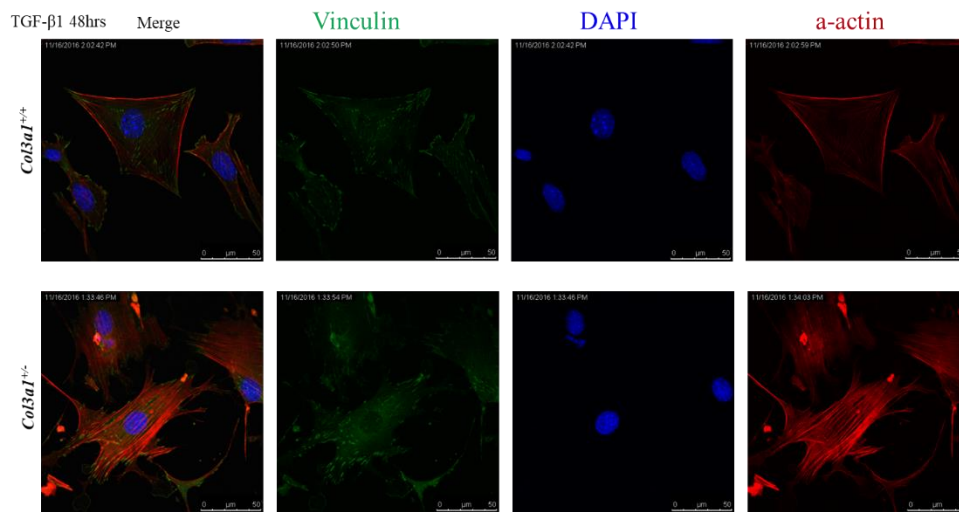


Figure 4.10 Altered focal adhesion signaling in *Col3a1*^{+/-} SMCs

Immunofluorescent staining (IF) to detect vinculin, marker for focal adhesions, results showed that there was an alteration in distribution of focal adhesions in *Col3a1*^{+/-} cells compared to that in *Col3a1*^{+/+} with TGF- β 1 treated for 48 hours.

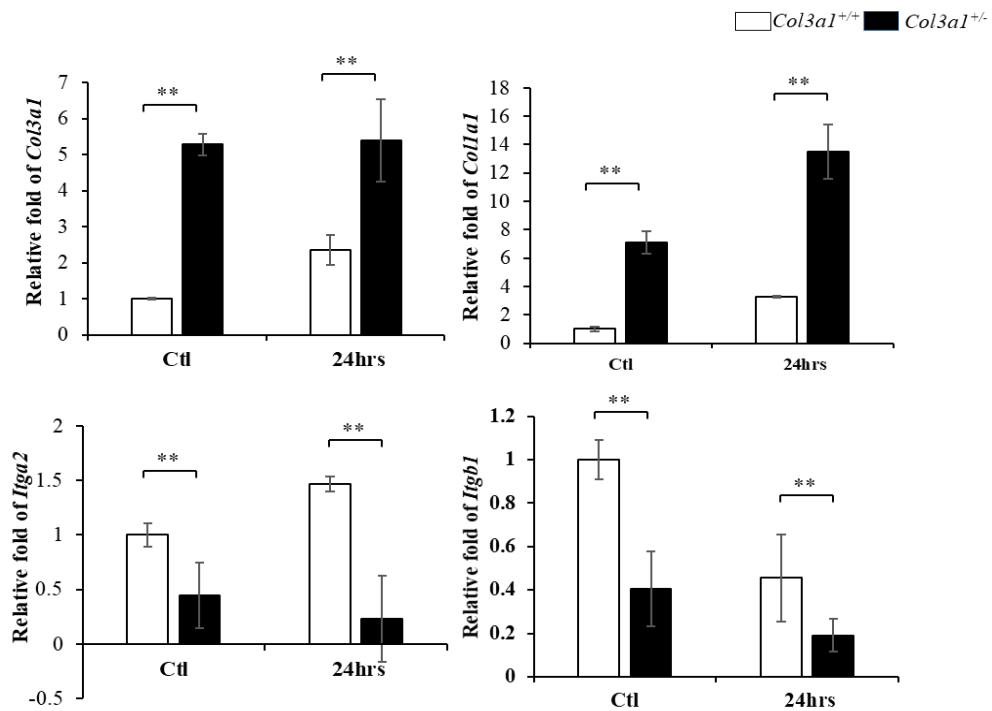


Figure 4.11 Expression of collagens and collagen receptors at RNA level in SMCs

RNA was isolated from both TGF- β 1 treated and control SMCs cells at different time points. There was increased *Col3a1* and *Colla1* expression after TGF- β 1 stimulation compared with in *Col3a1*^{+/-} SMCs. And decreased of *Itga2* and *Itgb1* in *Col3a1*^{+/-} SMCs qPCR was performed according to the protocol, $p^{**}<0.001$, by the Student's *t*-test.

Whether the FAs in *Col3a1*^{+/-} cells might be more mature compared to those from the *Col3a1*^{+/+} SMC cells? To answer this question, IF of vinculin was conducted to show the size and location of focal adhesions. Results showed an increase in vinculin intensity in *Col3a1*^{+/-} SMCs visually (**Figure 4.10**), indicating activation of FAK signaling and the maturation of FAs in the *Col3a1*^{+/-} SMCs after TGF- β 1 treatment.

4.3.8 Altered production of collagen and their receptors *Col3a1*^{+/-} SMCs

As with fibroblasts, expression of collagens, *Col3a1*, *Colla1* as well as collagen receptors *Itga2*, *Itgb1* was also detected. results showed a dramatic increase in expression of both *Col3a1* and *Colla1* after 24 hours stimulation with TGF- β 1 in both *Col3a1*^{+/-} SMCs compared with *Col3a1*^{+/+} SMCs (**Figure 4.11a**), a decreased expression of *Itga2* and *Itgb1* in *Col3a1*^{+/-} SMCs compared with *Col3a1*^{+/+} SMCs after stimulation with TGF- β 1 for 24 hours (**Figure 4.11b**). Indicating a decreased integrin signaling transduction in the *Col3a1*^{+/-} SMCs.

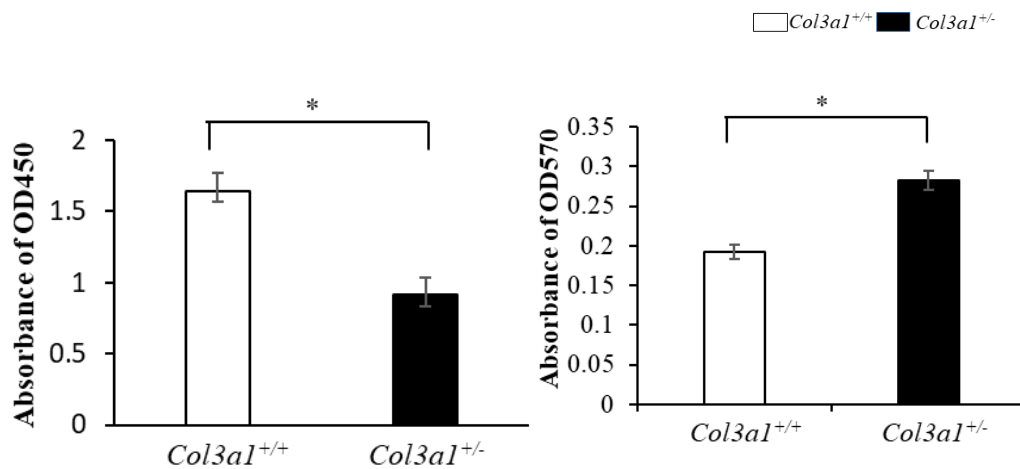


Figure 4.12 Decreased cell proliferation while increased viability of *Col3a1*^{+/-} SMCs

BrdU and MTT assay was performed according to assay protocols, and absorbance was generated with plate reader at different wave length. There was decreased *Col3a1*^{+/-} SMCs proliferation compared to that of *Col3a1*^{+/+} SMCs (a) however, there was increased cell viability in *Col3a1*^{+/-} SMCs compared with *Col3a1*^{+/+} SMCs after stimulation with TGF- β 1 for 24 hours (b). Statistical analysis: Student's *t*-test, **p*<0.05

4.3.9 Decreased cell proliferation and increased viability of *Col3a1*^{+/-} SMCs

To determine the difference of SMCs in proliferation, BrdU assay and MTT assay on cells stimulated with TGF- β 1 for 24 hours (**Figure 4.12a and b**) were conducted. Data showed decreased *Col3a1*^{+/-} SMCs

proliferation compared to *Col3a1*^{+/+} SMCs. However, there was increased cell metabolic activity in *Col3a1*^{+/-} SMCs compared with *Col3a1*^{+/+} SMCs after stimulation with TGF-β1 for 24 hours. Indicating their difference in cell metabolism (**Figure 4.12 b**).

4.4 Discussion

Dysregulated function of myofibroblasts was shown from *in vitro* data by Dr. Amy Reid previously (unpublished data from our lab). In her 3D fibrinogen culture model, there was increased contractile protein expression as well as increased assembly of fibrillar collagens in the *Col3a1*^{+/-} cells after induction with TGF-β1. Results from Reid's study and another study showing the differentiated *Col3a1*^{+/-} fibroblasts phenotype⁸³ lead to the hypothesis that in the *Col3a1*^{+/-} mouse model after carotid ligation, fibroblasts might be showing a persistent differentiation status at the injury site due to the diminished content of type III collagen resulting in delayed thrombus resolution and aberrant injury repair. To further elucidate the phenotype of *Col3a1*^{+/-} fibroblasts, we studied myofibroblast differentiation more closely.

Results showed that there was increased contractile protein expression at both RNA and protein level the *Col3a1*^{+/-} fibroblasts which was consistent with results from Amy's study. The F/G actin assay showed an increased proportion of F-actin polymerized in the *Col3a1*^{+/-} cells after TGF-β1 treatment (**Figure 4.5**). Under normal condition, fibroblasts will be activated and recruited to the injury site where they will be differentiated into myofibroblasts by TGF-β1⁸⁶. TGF-β1 as a chemokine secreted mostly by platelet and macrophages is critical for the entire process of wound healing⁸⁷. Secretion of TGF-β1 at an early stage of the healing prompts recruitment of inflammatory cells into the injury site, which are later involved in a negative feedback via macrophages⁸⁸. At the same time, TGF-β1 induced the expression of ECM components like collagens by myofibroblasts. All these behaviors secure a successful wound healing after injury. This is what we speculate to be happening in the *Col3a1*^{+/+} mice after carotid injury. In mice lung tissues, this process is accompanied by the activation of pFAK signaling pathway followed the activation of TGF-β1 and SMAD signaling pathway²³. Therefore, we also looked at the size of the focal adhesions (FAs) using IF staining of a representative FA marker, vinculin, as well as pFAk^{72,69}. There was increased vinculin area/cell area in *Col3a1*^{+/-} cells compared to that in *Col3a1*^{+/+} at basal level, which indicated that *Col3a1*^{+/-} fibroblasts were more differentiated even when there was no stimulation with TGF-β1, which was not shown by the data for the contractile proteins. But a dramatic increased vinculin area/cell area (Indicating size of FAs) in *Col3a1*^{+/+} cells compared with that in *Col3a1*^{+/-} cells after 72-hour TGF-β1

induction. Also, there was significantly increased pFAK area/cell area in *Col3a1*^{+/+} cells compared with that in *Col3a1*^{+/-} cells at both basal level and after TGF-β1 treatment for 72 hours, indicating continuous response of *Col3a1*^{+/+} cells to drive expression of α-SMA to form stress fibers, as shown by IF data (**Figure 4.6**). When it was related to the *in vivo* situation, *Col3a1*^{+/+} myfibroblasts proliferate and produce normal procollagen type III with help from TGF-β1 for the earlier wound healing phase and followed by producing contractile proteins, especially α-SMA for a wound contracture and normal wound healing²³. By contrast, we hypothesize that *in vivo* in the *Col3a1*^{+/-} mouse, although there is sufficient TGF-β1 secreted by the persistent activated macrophages, the myfibroblasts are not producing enough procollagen type III. Thus, although the cells are able to respond to TGF-β1 to stimulate pFAK and FA growth as well as initial expression of contractile proteins (**Figure 4.7**), the FAs are linking up to aberrant collagen in the extracellular matrix and they are unable to stimulate stress fiber formation to complete the differentiation. Instead they activate MRTFA signaling pathway for F-actin formation and keep the producing α-SMA (**Figure 4.8**). Even though, they are still not confident for contracture. We hypothesize that not only are the cells failing to complete contracture due to the lack of collagen, but the myfibroblasts are failing to undergo apoptosis and instead persistent differentiation and attempting to heal the wound long after the process should be completed (**Figure 4.13**)

Due to the contribution of SMCs from arterial wall to the remodeling of arterial wall after injury⁸⁹, we also investigated if there is any difference between SMCs from *Col3a1*^{+/+} and *Col3a1*^{+/-} mice. Results showed that *Col3a1*^{+/-} SMCs present a more differentiated status by increasing expression of contractile markers at both RNA and protein level compared with the *Col3a1*^{+/+} SMCs (**Figure 4.9**). Although there was a decrease in *Col3a1*^{+/-} SMCs proliferation, there was increased cell metabolic activity of *Col3a1*^{+/-} SMCs (**Figure 4.12**). Proliferation of SMCs is critical in intimal hyperplasia after arterial injury⁹⁰. Results from the SMC data showed that deficit of type III collagen impaired the neointima hyperplasia procedure after arterial injury.

In conclusion, I was able to find consistently demonstrated that there was persistent myfibroblasts differentiation status in the *Col3a1*^{+/-} mice by the *in vitro* study. And study from the SMCs validate that

the impaired arterial injury wound healing in the *Col3a1*^{+/-} mice. In the future, studies should be focused on whether any approaches could be applied to modulate the secretion of type III collagen in *Col3a1*^{+/-} fibroblasts, and then put the cells back to mouse model to correct their aberrant injury repair. Another future study should be directed to more completely (mechanistically) link the collagen defect to the cellular defects seen in the current study.

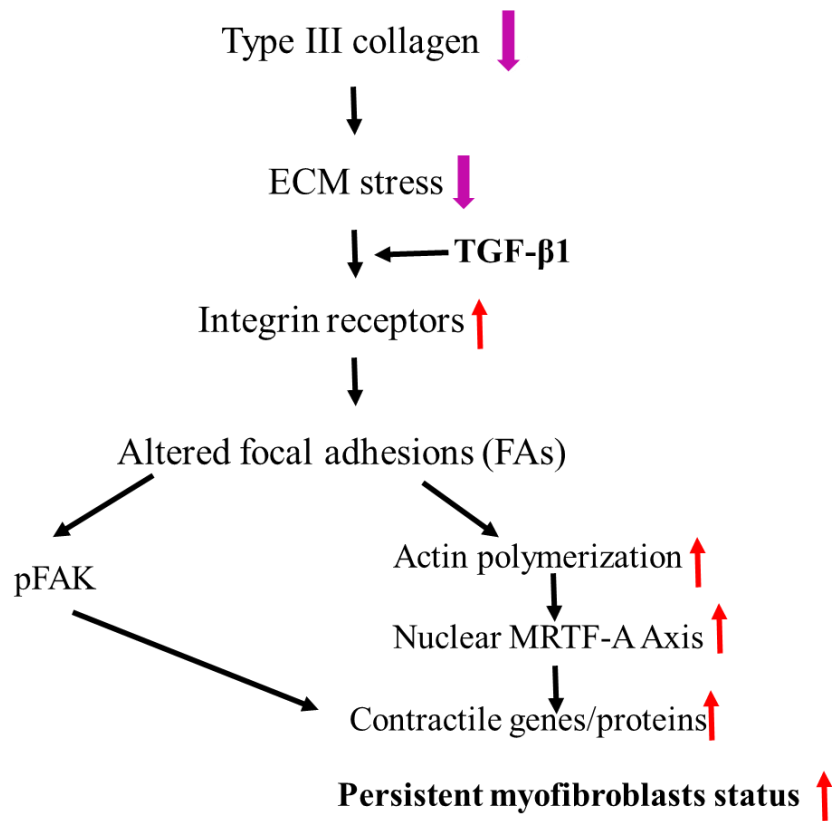


Figure 4.13 Proposed mechanisms for the persistent *Col3a1*^{+/-} myfibroblasts status

5 Discussion

5.1 Discussion of the project

vEDS is the most severe type of EDS, with no effective therapeutic approach for patients. The widely accepted dogma of vEDS pathogenesis is that defective production and a deficit of type III collagen leads to a weakened arterial wall⁶⁴. The deficit of collagen is mainly caused by the mutation at the Gly-X-Y site of the type III collagen gene, *Col3a1*. Multiple studies suggest that arterial wall weakness and fragility are the main causes of arterial aneurysm and dissection.

A review by Oderich et al. found 90 vEDS patients who showed bruised and translucent skin³, indicating their aberrant injury repair ability. The focus of this dissertation research is to confirm how the deficiency of type III collagen contributes to the pathogenesis of vEDS. Specifically, we explored the mechanisms of aberrant arterial wound healing. We used a haploinsufficient *Col3a1*^{+/-} mouse model, which resembles vEDS patients by showing arterial and other phenotypes as seen in human patients¹⁷. Previous studies from our lab linked vEDS with dysfunctional fibroblasts in the *Col3a1*^{+/-} mice. Additionally, fibrocytes that are bone marrow-derived (BMD) differentiate into wound-healing myofibroblasts with the expression of α -SMA^{27,48}. Thus, we hypothesized that a bone marrow transplant (BMT) could correct the ability of injury repair and alleviate the phenotypes in the *Col3a1*^{+/-} mice after induced injury.

Previous studies from our lab have proposed a dis-regulated arterial wound healing process in the *Col3a1*^{+/-} mouse model. Our bone marrow transplant (BMT) data confirmed this finding. In the *in vitro* study on fibroblasts, explanted *Col3a1*^{+/-} mice validated our *in vivo* findings by showing a less mature myofibroblasts phenotype.

The work presented in this dissertation showed the effectiveness of two potential approaches for vEDS treatment, bone marrow transplantation and celiprolol trial, both of which improved post-injury phenotypes in the *Col3a1*^{+/-} mice.

Studies by Morissette et al. demonstrated that a chronic inflammation in vEDS patients⁹¹. They detected markers of the TGF- β signaling pathways, using both patients' plasma and dermal fibroblasts.

According to the classification of vEDS severity and a correlation of phenotype-genotype as well as and fat deposited in patients, they discovered an increased amount of TGF- β 1, TGF- β 2, MCP-1, CRP, ICAM-1), VCAM-1 in vEDS patients. A higher mean platelet volume was also found in vEDS patients, which suggested an increase in their platelet turnover result from persistent vascular damage, and adiposity⁶⁵. Results from the current study could be partially explained by persistent inflammation in vEDS patients. In this current study, we also performed an ELISA assay on plasma to detect inflammatory factors in the *Col3a1*^{+/-} mice. We specifically detected ICAM1, VCAM-1 and MCP-1 at different time points, basal level, POD3, POD7 and POD14. However, we were not able to show any conclusive findings from the ELISA assays (Data not shown). Therefore, we cannot confirm increased circulating inflammatory factors in this mouse model, and we cannot conclude that inflammation plays a role in the disease process.

Attention should be paid to our use of the painkiller drug ketoprofen which was administered to these mice. There are multiples studies showed ketoprofen had anti-platelet activity of aspirin^{92,93}. In contrast, ibuprofen showed effects in inhibiting the platelet aggregation potency of aspirin compared with other nonsteroidal anti-inflammatory drugs (NASIDs)⁹⁴. Immediately after injury, platelets aggregation ensures a normal thrombus formation and initiates successful wound healing³¹; thus while ketoprofen might promote the very early stage of wound healing, ibuprofen inhibits it. As a result of this early difference, for future studies, attention should be paid to which painkiller drug to use and to interpret the results very accurately.

The findings from the current study can also be applied to cerebrovascular diseases, which have been manipulated by endovascular techniques⁹⁵. But there have to be other techniques used at the same time to minimize complications such as thromboembolic events, which is as high as 12.5%⁹⁶. Platelets contribute to both hemostasis and thrombosis⁹⁵. Thromboembolic events also happen to people with acute coronary diseases⁹⁵. Although approaches for antiplatelet activity drugs have been applied, they can lead to either ischemic or bleeding complications, respectively due to the different potency of the antiplatelet drugs and their interactions⁹⁷. For stroke happen to patients especially who are not older than 45 years, spontaneous

dissection of brain vascular plays a huge role. Patients have vascular pathologies usually have experienced trivial trauma, which resembles the carotid ligation we induced to *Col3a1*^{+/-} mice⁹⁸, through which a wound healing process was initiated, persistent inflammation, not timely resolved thrombus leading to the medial neovessel formation, finally predispose the rupture or dissection of the artery. And there was no optimal medical treatment for cerebrovascular dissection. Currently, there are no data from clinical trials who has confirmed antithrombotic with either anticoagulation or antiplatelet drugs⁹⁸. To conclude, two big problems in cerebrovascular disease are thrombosis and trauma, which are both relevant to the arterial injury repair pathways described in this dissertation. The findings from this current study could therefore be applied to those patients with cerebrovascular diseases, specifically, to reduce the inflammation and decrease thrombosis by increasing resolution of thrombus after arterial injury.

On a broader scale, the therapies proposed in the current study can also be used to treat those diseases which are characterized by defects in wound healing or disrupted scar formation, such as defective burn wound healing, persistent burns with type II diabetes and fibrosis by modulating the hyperactivity of fibroblasts/myofibroblasts²¹. Study by Duchesneau et al. showed that BMT could rescue function of lung tissue using a cystic fibrosis (CF) model⁹⁹, which is a fatal genetic disease resulting from mutation in CFTR protein.. They found that transplant of wild type bone marrow into CFTR deleted recipient rescued the phenotypes in CFTR^{-/-} mice. Taken together, their results suggest that BMC can improve overall lung function and may have potential therapeutic benefit for the treatment of CF. Thus, we further propose that together with their studies, findings from the current study could be applied to multiple of other diseases.

However, there were still limitations to the current study. First, transgenic mouse model(s) with specific *Col3a1* mutation(s) are still not available, instead we used a haploinsufficient *Col3a1* mouse model. Although *Col3a1*^{-/-} mice recapitulate syndromes of vEDS more closely, these mice rarely survive after birth. *Col3a1*^{+/-} mice have a milder phenotype¹⁰⁰. Second, although BMT rescued the phenotypes showed in the *Col3a1*^{+/-} mice, we were not able to examine or exclude the immune responses after BMT. Third, there might be some technique limitations of the BMT procedure. Since we transplanted the whole

bone marrow cells into each recipient mouse without isolating specific a fibrocyte population, even though we speculate that BMD fibrocytes are involved in wound healing, we cannot whether it was possible for there to be other cells like macrophage or other BMD cells actually participating in rescuing the phenotypes. There is therefore still a lot of work to be done before a clinical study on vEDS patients could be initiated.

The mouse model used for this current project provides a basic idea which will direct future studies on vEDS patients with severe mutations and their roles in the disease. It also provides a strong early data which links mechanisms of vEDS patients and the role of decreased production of type III collagen. Most importantly, the current work provides us with two potential therapeutic approaches for this deadly disease. In the long run, we expect that these studies will be applied to clinical use after further work solving the above stated limitations.

5.2 Future direction

5.2.1 *In vitro* studies on *Col3a1*^{+/+} and *Col3a1*^{+/-} fibroblasts to test their metabolism and cell interaction

The *in vitro* data from chapter 4 showed increased MTT incorporation in *Col3a1*^{+/-} fibroblasts; it could be possibly explained by the changes in cell metabolism, which is regulated mainly by the mammalian target of rapamycin (mTOR) signaling¹⁰¹. We will look at differences in mTOR signaling between *Col3a1*^{+/-} and *Col3a1*^{+/+} fibroblasts, and will do further studies to mechanistically link these signaling changes with adhesion-based pathways.

5.2.2 Investigating the role of specific bone marrow derived cell types in *Col3a1*^{+/-} mouse model

There are multiple different functions of macrophages in wound healing, including host defense, the inflammatory responses, cell apoptosis and tissue restoration⁴⁶. Specifically, first, it would be of great interest to isolate fibrocytes, macrophages and fibroblasts from *Col3a1*^{+/-} and *Col3a1*^{+/+} mice by flow

cytometry with their differentiated cell surface markers^{102,103}. We could use these cells *in vitro* to study any changes in phenotype and any interaction between these cell types. We expect macrophage phenotype not to be affected and fibrocyte phenotype to be similar to the reported findings in Chapter 4 for lung fibroblasts. Finally, after *in vitro* culture of isolated fibrocytes, both *Col3a1*^{+/+} and *Col3a1*^{+/-} fibroblasts/macrophages would be injected into both two groups of mice respectively, and then compare if there is any correction in the injury repair ability of *Col3a1*^{+/-} mice by using the carotid ligation injury model.

5.2.3 Specialized cell therapy for vEDS.

In developmental biology and cancer biology as well as vascular biology, cell therapy has been widely studied and accepted as an effective approach for a variety of diseases¹⁰⁴. It is of great interest for us to try similar method for vEDS patients. First, gene cloning technique should be used to establish the stable protein expression system of procollagen type III. Then the system could be induced into immortalized fibroblasts/myofibroblasts, followed by injecting the cells into both *Col3a1*^{+/+} and *Col3a1*^{+/-} mice, to check if there is increased injury repair ability of *Col3a1*^{+/-} mice by same mouse model.

5.2.4 Effects of celiprolol on cells explanted from *Col3a1* mouse.

One last, but not least future study is highly proposed to investigate the role of celiprolol using *in vitro* tissue cultured fibroblasts or even macrophages. Phenotypes such as cell migration, proliferation and the secretion of inflammatory factors as well as neo-angiogenesis of these cells should be examined on both *Col3a1*^{+/+} and *Col3a1*^{+/-} cells. This study is of great importance to illustrate the mechanisms underlie how celiprolol could decrease the severity of vEDS and how celiprolol could be best applied for vEDS patients.

References:

1. Pepin M. Clinical and genetic features of Ehlers-Danlos Syndrome Type IV, the vascular type.pdf. *N Engl J Med.* 2000;342(10).
2. Eagleton MJ. Arterial complications of vascular Ehlers-Danlos syndrome. *J Vasc Surg.* 2016;64(6):1869-1880. doi:10.1016/j.jvs.2016.06.120.
3. Oderich GS, Panneton JM, Bower TC, et al. The spectrum, management and clinical outcome of Ehlers-Danlos syndrome type IV: A 30-year experience. *J Vasc Surg.* 2005;42(1):98-106. doi:10.1016/j.jvs.2005.03.053.
4. Shalhub S, Black JH, Cecchi AC, et al. Molecular diagnosis in vascular Ehlers-Danlos syndrome predicts pattern of arterial involvement and outcomes. *J Vasc Surg.* 2014;60(1):160-169. doi:10.1016/j.jvs.2014.01.070.
5. Nawarskas JJ, Cheng-Lai A, Frishman WH. Celiprolol: A Unique Selective Adrenoceptor Modulator. *Cardiol Rev.* 2017;25(5):247-253. doi:10.1097/CRD.000000000000159.
6. Ong KT, Perdu J, De Backer J, et al. Effect of celiprolol on prevention of cardiovascular events in vascular Ehlers-Danlos syndrome: A prospective randomised, open, blinded-endpoints trial. *Lancet.* 2010;376(9751):1476-1484. doi:10.1016/S0140-6736(10)60960-9.
7. Wagenseil JE, Mecham RP. Vascular Extracellular Matrix and Arterial Mechanics. *Physiol Rev.* 2009;89(3):957-989. doi:10.1152/physrev.00041.2008.
8. Byers PH, Murray ML. Heritable Collagen Disorders: The Paradigm of the Ehlers—Danlos Syndrome. *J Invest Dermatol.* 2012;132:E6-E11. doi:10.1038/skinbio.2012.3.
9. Hulmes DJS. Collagen diversity, synthesis and assembly. *Collagen Struct Mech.* 2008:15-47. doi:10.1007/978-0-387-73906-9_2.

10. Lees JF, Tasab M, Bulleid NJ. Identification of the molecular recognition sequence which determines the type-specific assembly of procollagen. *1997;16(5):908-916.*
11. Stenbridge NS, Vandersteen AM, Ghali N, et al. Clinical, structural, biochemical and X-ray crystallographic correlates of pathogenicity for variants in the C-propeptide region of the COL3A1 gene. *Am J Med Genet Part A.* 2015;167(8):1763-1772. doi:10.1002/ajmg.a.37081.
12. Lucero HA, Kagan HM. Lysyl oxidase: An oxidative enzyme and effector of cell function. *Cell Mol Life Sci.* 2006;63(19-20):2304-2316. doi:10.1007/s00018-006-6149-9.
13. Smith LT, Schwarze U, Goldstein J, Byers PH. Mutations in the COL3A1 gene result in the Ehlers-Danlos syndrome type IV and alterations in the size and distribution of the major collagen fibrils of the dermis. *J Invest Dermatol.* 1997;108(3):241-247. doi:10.1111/1523-1747.ep12286441.
14. Boutouyrie P, Germain DP, Fiessinger JN, Laloux B, Perdu J, Laurent S. Increased Carotid Wall Stress in Vascular Ehlers-Danlos Syndrome. *Circulation.* 2004;109(12):1530-1535. doi:10.1161/01.CIR.0000121741.50315.C2.
15. Liu X, Wu H, Byrne M, Krane S, Jaenisch R. Type III collagen is crucial for collagen I fibrillogenesis and for normal cardiovascular development. *Proc Natl Acad Sci.* 1997;94(5):1852-1856. doi:10.1073/pnas.94.5.1852.
16. Liu X, Wu H, Byrne M, Krane S, Jaenisch R. Type III collagen is crucial for collagen I fibrillogenesis and for normal cardiovascular development. *Proc Natl Acad Sci U S A.* 1997;94(5):1852-1856. doi:10.1073/pnas.94.5.1852.
17. Cooper TK, Zhong Q, Krawczyk M, et al. The Haploinsufficient *Col3a1* Mouse as a Model for Vascular Ehlers-Danlos Syndrome. *Vet Pathol.* 2010;47(6):1028-1039. doi:10.1177/0300985810374842.

18. Ananthaseshan S, Grudzinska MK, Bojakowski K, et al. Locally Transplanted CD34+ Bone Marrow-Derived Cells Contribute to Vascular Healing After Vascular Injury. *Transplant Proc.* 2017;49(6):1467-1476. doi:10.1016/j.transproceed.2017.01.081.
19. Zhao W, Wang C, Liu R, et al. Effect of TGF- β 1 on the Migration and Recruitment of Mesenchymal Stem Cells after Vascular Balloon Injury: Involvement of Matrix Metalloproteinase-14. *Sci Rep.* 2016;6. doi:10.1038/srep21176.
20. Singer AJ, Clark RA. Cutaneous wound healing. *N Engl J Med.* 1999;341(10):738-746. doi:10.1056/NEJM199909023411006.
21. Wynn T a, Yugandhar VG, Clark M a. Cellular and molecular mechanisms of fibrosis. *J Pathol.* 2013;46(2):26-32. doi:10.1002/path.2277.Cellular.
22. Penn JW, Grobbelaar AO, Rolfe KJ. The role of the TGF- β family in wound healing, burns and scarring: a review. *Int J Burns Trauma.* 2012;2(1):18-28.
<http://www.pubmedcentral.nih.gov/articlerender.fcgi?artid=3415964&tool=pmcentrez&rendertype=abstract>.
23. Thannickal VJ, Lee DY, White ES, et al. Myofibroblast differentiation by transforming growth factor- β 1 is dependent on cell adhesion and integrin signaling via focal adhesion kinase. *J Biol Chem.* 2003;278(14):12384-12389. doi:10.1074/jbc.M208544200.
24. Yancopoulos GD, Davis S, Gale NW, Rudge JS, Wiegand SJ, Holash J. Vascular-specific growth factors and blood vessel formation. *Nature.* 2000;407(6801):242-248. doi:10.1038/35025215.
25. Hanahan D, Folkman J. Patterns and emerging mechanisms of the angiogenic switch during tumorigenesis. *Cell.* 1996;86(3):353-364. doi:10.1016/S0092-8674(00)80108-7.

26. Keeley EC, Schutt RC, Marinescu MA, Burdick MD, Strieter RM, Mehrad B. Circulating fibrocytes as predictors of adverse events in unstable angina. *Transl Res.* 2016;172:73-83. doi:10.1016/j.trsl.2016.02.013.
27. Reilkoff RA, Bucala R, Herzog EL. Fibrocytes: emerging effector cells in chronic inflammation. *Nat Rev Immunol.* 2011;11(6):427-435. doi:10.1038/nri2990.
28. Kim ST, Brinjikji W, Lanzino G, Kallmes DF. Neurovascular manifestations of connective-tissue diseases: A review. *Interv Neuroradiol.* 2016;22(6):624-637. doi:10.1177/1591019916659262.
29. Loeys BL, Schwarze U, Holm T, et al. Aneurysm Syndromes Caused by Mutations in the TGF- β Receptor. *N Engl J Med.* 2006;355(8):788-798. doi:10.1056/NEJMoa055695.
30. Lee D, Yuki I, Murayama Y, et al. Thrombus organization and healing in the swine experimental aneurysm model. Part I. A histological and molecular analysis. *J Neurosurg.* 2007;107(1):94-108. doi:10.3171/JNS-07/07/0094.
31. Martin P. Wound Healing--Aiming for Perfect Skin Regeneration. *Science (80-).* 1997;276(5309):75-81. doi:10.1126/science.276.5309.75.
32. Tomasek JJ, Gabbiani G, Hinz B, Chaponnier C, Brown RA. Myofibroblasts and mechano: Regulation of connective tissue remodelling. *Nat Rev Mol Cell Biol.* 2002;3(5):349-363. doi:10.1038/nrm809.
33. Gabbiani G, Le Lous M, Bailey AJ, Bazin S, Delaunay A. Collagen and myofibroblasts of granulation tissue - A Chemical, ultrastructural and immunologic study. *Virchows Arch B Cell Pathol.* 1976;21(1):133-145. doi:10.1007/BF02899150.
34. Majesky MW, Lindner V, Twardzik DR, Schwartz SM, Reidy MA. Production of transforming growth factor β 1 during repair of arterial injury. *J Clin Invest.* 1991;88(3):904-910.

35. Suga H, Rennert RC, Rodrigues M, et al. Tracking the elusive fibrocyte: Identification and characterization of collagen-producing hematopoietic lineage cells during murine wound healing. *Stem Cells*. 2014;32(5):1347-1360. doi:10.1002/stem.1648.
36. Bucala R, Spiegel LA, Chesney J, Hogan M, Cerami A. Circulating fibrocytes define a new leukocyte subpopulation that mediates tissue repair. *Mol Med (Cambridge, Mass)*. 1994;1(1):71-81.
<http://eutils.ncbi.nlm.nih.gov/entrez/eutils/elink.fcgi?dbfrom=pubmed&id=8790603&retmode=ref&cmd=prlinks%5Cnpapers2://publication/uuid/0795ED84-A885-440D-973E-317834B0B326>.
37. Abe R, Donnelly SC, Peng T, Bucala R, Metz CN. Peripheral Blood Fibrocytes: Differentiation Pathway and Migration to Wound Sites. *J Immunol*. 2001;166(12):7556-7562.
doi:10.4049/jimmunol.166.12.7556.
38. Han C-I · Campbell G.R. · Campbell J.H. Circulating Bone Marrow Cells Can Contribute to Neointimal Formation. *J Vasc Res* 2001;38113–119. 2001;4072:113-119.
39. Daniel JM, Sedding DG. Circulating smooth muscle progenitor cells in arterial remodeling. *J Mol Cell Cardiol*. 2011;50(2):73-279. doi:10.1016/j.yjmcc.2010.10.030.
40. Albiero M, Menegazzo L, Fadini GP. Circulating Smooth Muscle Progenitors and Atherosclerosis. *Trends Cardiovasc Med*. 2010;20(4):133-140. doi:10.1016/j.tcm.2010.12.001.
41. Kawasaki T, Dewerchin M, Lijnen HR, Vreys I, Vermynen J, Hoylaerts MF. Platelet-Leukocyte – Dependent Luminal Fibrin , Required for Neointima Development. 2015:159-167.
42. Nosaka M, Ishida Y, Kimura A, Kuninaka Y, Masanori I, Mukaida N KT. Absence of IFN-gamma accelerates thrombus resolution. *J Clin Invest*. 2011;121(7). doi:10.1172/JCI40782DS1.

43. Lee PC, Salyapongse a N, Bragdon G a, et al. Impaired wound healing and angiogenesis in eNOS-deficient mice. *Am J Physiol.* 1999;277(4 Pt 2):H1600-8.
<http://www.ncbi.nlm.nih.gov/pubmed/10516200>.
44. The role of neovascularisation in the resolution of venous Thrombus.pdf.
45. Bochaton-Piallat M-L, Gabbiani G, Hinz B. The myofibroblast in wound healing and fibrosis: answered and unanswered questions. *F1000Research.* 2016;5(0):752.
doi:10.12688/f1000research.8190.1.
46. Koh TJ, DiPietro LA. Inflammation and wound healing: the role of the macrophage. *Expert Rev Mol Med.* 2011;13(July):1-12. doi:10.1017/S1462399411001943.
47. Nissen NN, Polverini PJ, Koch AE, Volin M V, Gamelli RL, DiPietro LA. Vascular endothelial growth factor mediates angiogenic activity during the proliferative phase of wound healing. *Am J Pathol.* 1998;152(6):1445-1452.
<http://www.ncbi.nlm.nih.gov/pubmed/9626049>
<http://www.pubmedcentral.nih.gov/articlerender.fcgi?artid=PMC1858442>.
48. Quan TE, Cowper S, Wu SP, Bockenstedt LK, Bucala R. Circulating fibrocytes: Collagen-secreting cells of the peripheral blood. *Int J Biochem Cell Biol.* 2004;36(4):598-606.
doi:10.1016/j.biocel.2003.10.005.
49. Sata M, Saiura A, Kunisato A, et al. Hematopoietic stem cells differentiate into vascular cells that participate in the pathogenesis of atherosclerosis. *NatMed.* 2002;8(4):403-409.
doi:10.1038/nm0402-403.
50. Pullar CE, Rizzo A, Isseroff RR. β -adrenergic receptor antagonists accelerate skin wound healing: Evidence for a catecholamine synthesis network in the epidermis. *J Biol Chem.* 2006;281(30):21225-21235. doi:10.1074/jbc.M601007200.

51. Steinkraus V, Mak JCW, Pichlmeier U, Mensing H, Ring J, Barnes PJ. Autoradiographic mapping of beta-adrenoceptors in human skin. *Arch Dermatol Res.* 1996;288(9):549-553. doi:10.1007/s004030050101.
52. Schallreuter KU, Wood JM, Pittelkow MR, Swanson NN, Steinkraus V. Increased in vitro expression of beta2-adrenoceptors in differentiating lesional keratinocytes of vitiligo patients. *Arch Dermatol Res.* 1993;285(4):216-220. doi:10.1007/BF00372012.
53. Steinkraus V, Steinfath M, Korner C, Mensing H. Binding of Beta-Adrenergic Receptors in Human Skin. *J Invest Dermatol.* 1992;98:475-480.
54. Pullar CE, Le Provost GS, O'Leary AP, Evans SE, Baier BS, Isseroff RR. β 2AR antagonists and B2AR gene deletion both promote skin wound repair processes. *J Invest Dermatol.* 2012;132(8):2076-2084. doi:10.1038/jid.2012.108.
55. Toda N. Vasodilating β -adrenoceptor blockers as cardiovascular therapeutics. *Pharmacol Ther.* 2003;100(3):215-234. doi:10.1016/j.pharmthera.2003.09.001.
56. Pullar CE, Manabat-hidalgo CG, Bolaji RS, Isseroff RR. α -Adrenergic receptor modulation of wound repair. 2008;58:158-164. doi:10.1016/j.phrs.2008.07.012.
57. Celiprolol and its properties.pdf.
58. Hinz B. Formation and function of the myofibroblast during tissue repair. *J Invest Dermatol.* 2007;127(3):526-537. doi:10.1038/sj.jid.5700613.
59. Xu C, Zarins CK, Pannaraj PS, Bassiouny HS, Glagov S. Hypercholesterolemia superimposed by experimental hypertension induces differential distribution of collagen and elastin. *Arterioscler Thromb Vasc Biol.* 2000;20(12):2566-2572. doi:10.1161/01.ATV.20.12.2566.

60. Wachter SB, Gilbert EM. Beta-adrenergic receptors, from their discovery and characterization through their manipulation to beneficial clinical application. *Cardiol*. 2012;122(2):104-112. doi:10.1159/000339271.
61. Liao Y, Asakura M, Takashima S, et al. Celiprolol, a vasodilatory β -blocker, inhibits pressure overload-induced cardiac hypertrophy and prevents the transition to heart failure via nitric oxide-dependent mechanisms in mice. *Circulation*. 2004;110(6):692-699. doi:10.1161/01.CIR.0000137831.08683.E1.
62. Hayashi T, Juliet PAR, Miyazaki-Akita A, et al. β_1 antagonist and β_2 agonist, celiprolol, restores the impaired endothelial dependent and independent responses and decreased TNF α in rat with type II diabetes. *Life Sci*. 2007;80(6):592-599. doi:10.1016/j.lfs.2006.10.018.
63. Rough J, Engdahl R, Opperman K, Yerrum S, Monroy MA, Daly JM. β_2 Adrenoreceptor blockade attenuates the hyperinflammatory response induced by traumatic injury. *Surgery*. 2009;145(2):235-242. doi:10.1016/j.surg.2008.09.013.
64. Beridze N, Frishman WH. Vascular ehlers-Danlos syndrome: Pathophysiology, diagnosis, and prevention and treatment of its complications. *Cardiol Rev*. 2012;20(1):4-7. doi:10.1097/CRD.0b013e3182342316.
65. Morissette R, Schoenhoff F, Xu Z, et al. Transforming growth factor- β and inflammation in vascular (Type IV) ehlers-danlos syndrome. *Circ Cardiovasc Genet*. 2014;7(1):80-88. doi:10.1161/CIRCGENETICS.113.000280.
66. Yao EH, Fukuda N, Matsumoto T, et al. Effects of the antioxidative β -blocker celiprolol on endothelial progenitor cells in hypertensive rats. *Am J Hypertens*. 2008;21(9):1062-1068. doi:10.1038/ajh.2008.233.

67. Hattori K, Yamanouchi D, Banno H, et al. Celiprolol reduces the intimal thickening of autogenous vein grafts via an enhancement of nitric oxide function through an inhibition of superoxide production. *J Vasc Surg.* 2007;46(1):116-123. doi:10.1016/j.jvs.2007.03.044.
68. Moulin V, Tam BYY, Castilloux G, et al. Fetal and adult human skin fibroblasts display intrinsic differences in contractile capacity. *J Cell Physiol.* 2001;188(2):211-222. doi:10.1002/jcp.1110.
69. Goffin JM, Pittet P, Csucs G, Lussi JW, Meister JJ, Hinz B. Focal adhesion size controls tension-dependent recruitment of α -smooth muscle actin to stress fibers. *J Cell Biol.* 2006;172(2):259-268. doi:10.1083/jcb.200506179.
70. Hinz B. Masters and servants of the force: The role of matrix adhesions in myofibroblast force perception and transmission. *Eur J Cell Biol.* 2006;85(3-4):175-181. doi:10.1016/j.ejcb.2005.09.004.
71. Geiger B, Spatz JP, Bershadsky AD. Environmental sensing through focal adhesions. *Nat Rev Mol Cell Biol.* 2009;10(1):21-33. doi:10.1038/nrm2593.
72. Dugina V, Fontao L, Chaponnier C, Vasiliev J, Gabbiani G. Focal adhesion features during myofibroblastic differentiation are controlled by intracellular and extracellular factors. *J Cell Sci.* 2001;114:3285-3296.
73. Desmoulière A, Badid C, Bochaton-Piallat ML, Gabbiani G. Apoptosis during wound healing, fibrocontractive diseases and vascular wall injury. *Int J Biochem Cell Biol.* 1997;29(1):19-30. doi:10.1016/S1357-2725(96)00117-3.
74. Desmoulière a, Geinoz A, Gabbiani F, Gabbiani G. Transforming growth factor-beta 1 induces α -smooth muscle actin expression in granulation tissue myofibroblasts and in quiescent and growing cultured fibroblasts. *J Cell Biol.* 1993;122(1):103-111. doi:10.1083/jcb.122.1.103.

75. TGF- β 1 Stimulates Expression of Keratinocyte Integrins During Re-Epithelialization of Cutaneous Wounds.pdf.
76. Montesano R, Orci L. Transforming growth factor β stimulates collagen-matrix contraction by fibroblasts: implications for wound healing. *Proc Natl Acad Sci U S A*. 1988;85(13):4894-4897. doi:10.1073/pnas.85.13.4894.
77. Wozniak MA, Modzelewska K, Kwong L, Keely PJ. Focal adhesion regulation of cell behavior. *Biochim Biophys Acta - Mol Cell Res*. 2004;1692(2-3):103-119. doi:10.1016/j.bbamcr.2004.04.007.
78. Pipes GCT, Creemers EE, Olson EN. regulators of cell growth , migration , and myogenesis The myocardin family of transcriptional coactivators : versatile regulators of cell growth , migration , and myogenesis. 2006;(214):1545-1556. doi:10.1101/gad.1428006.
79. Wang DZ, Chang PS, Wang Z, et al. Activation of cardiac gene expression by myocardin, a transcriptional cofactor for serum response factor. *Cell*. 2001;105(7):851-862. doi:10.1016/S0092-8674(01)00404-4.
80. Kuwahara K, Barrientos T, Pipes GCT, Li S, Olson EN. Muscle-Specific Signaling Mechanism That Links Actin Dynamics to Serum Response Factor Muscle-Specific Signaling Mechanism That Links Actin Dynamics to Serum Response Factor †. 2005;25(8):3173-3181. doi:10.1128/MCB.25.8.3173.
81. Sun Q, Chen G, Streb JW, et al. Defining the mammalian CArGome. *Genome Res*. 2006;16(2):197-207. doi:10.1101/gr.4108706.
82. Velasquez LS, Sutherland LB, Liu Z, Grinnell F, Kamm KE, Schneider JW. Activation of MRTF-A – dependent gene expression with a small molecule promotes myofibroblast

- differentiation and wound healing. 2013. doi:10.1073/pnas.1316764110/-
/DCSupplemental.www.pnas.org/cgi/doi/10.1073/pnas.1316764110.
83. Volk SW, Wang Y, Mauldin EA, Liechty KW, Adams SL. Diminished type III collagen promotes myofibroblast differentiation and increases scar deposition in cutaneous wound healing. *Cells Tissues Organs*. 2011;194(1):25-37. doi:10.1159/000322399.
84. Kwartler CS, Zhou P, Kuang S-Q, Duan X-Y, Gong L, Milewicz DM. Vascular Smooth Muscle Cell Isolation and Culture from Mouse Aorta. *Bio-Protocol*. 2016;6(23):1-15. doi:10.21769/BioProtoc.2045.
85. Yassin R, Shefcyk J, White JR, et al. Effects of chemotactic factors and other agents on the amounts of actin and a 65,000-mol-wt protein associated with the cytoskeleton of rabbit and human neutrophils. *J Cell Biol*. 1985;101(1):182-188. doi:10.1083/jcb.101.1.182.
86. Hackam D, Ford H. Cellular, biochemical, and clinical aspects of wound healing. *Surg Infect (Larchmt)*. 2002;3:s23. doi:10.1089/sur.2002.3.s1.
87. Pakyari M, Farrokhi A, Maharlooei MK, Ghahary A. Critical Role of Transforming Growth Factor Beta in Different Phases of Wound Healing. *Adv Wound Care*. 2013;2(5):215-224. doi:10.1089/wound.2012.0406.
88. Barrientos S, Stojadinovic O, Golinko MS, Brem H, Tomic-Canic M. Growth factors and cytokines in wound healing. *Wound Repair Regen*. 2008;16(5):585-601. doi:10.1111/j.1524-475X.2008.00410.x.
89. Li Y, Takeshita K, Liu PY, et al. Smooth muscle notch1 mediates neointimal formation after vascular injury. *Circulation*. 2009;119(20):2686-2692. doi:10.1161/CIRCULATIONAHA.108.790485.

90. Schäfer K, Konstantinides S, Riedel C, et al. Different mechanisms of increased luminal stenosis after arterial injury in mice deficient for urokinase- or tissue-type plasminogen activator. *Circulation*. 2002;106(14):1847-1852. doi:10.1161/01.CIR.0000031162.80988.2B.
91. Morissette R, Schoenhoff F, Xu Z, et al. Transforming growth factor-beta and inflammation in vascular (type IV) Ehlers-Danlos syndrome. *CircCardiovascGenet*. 7(1):80-88.
92. DORDONI PL, VENTURA M DELLA, STEFANELLI A, et al. Effect of ketorolac, ketoprofen and nefopam on platelet function. *Anaesthesia*. 1994;49(12):1046-1049. doi:10.1111/j.1365-2044.1994.tb04352.x.
93. Rothschild BM. Comparative antiplatelet activity of COX1 NSAIDS versus aspirin, encompassing regimen simplification and gastroprotection: A call for a controlled study. *Reumatismo*. 2004;56(2):89-93.
94. Catella-Lawson F, Reilly MP, Kapoor SC, et al. Cyclooxygenase inhibitors and the antiplatelet effects of aspirin. *N Engl J Med*. 2001;345(25):1809-1817. doi:10.1056/NEJMoa003199.
95. Kim KS, Fraser JF, Grupke S, Cook AM. Management of antiplatelet therapy in patients undergoing neuroendovascular procedures. *J Neurosurg*. 2017:1-16. doi:10.3171/2017.5.JNS162307.
96. Pierot L, Cognard C, Anxionnat R, Ricolfi F. Ruptured intracranial aneurysms: factors affecting the rate and outcome of endovascular treatment complications in a series of 782 patients (CLARITY study). *Radiology*. 2010;256(3):916-923. doi:10.1148/radiol.10092209.
97. Sibbing D, Byrne RA, Bernlochner I, Kastrati A. High platelet reactivity and clinical outcome - fact and fiction. *Thromb Haemost*. 2011;106(2):191-202. doi:10.1160/TH11-01-0040.
98. Fusco MR, Harrigan MR. Cerebrovascular dissections - A review part I: Spontaneous dissections. *Neurosurgery*. 2011;68(1):242-257. doi:10.1227/NEU.0b013e3182012323.

99. Duchesneau P, Besla R, Derouet MF, et al. Partial Restoration of CFTR Function in *cftr*-Null Mice following Targeted Cell Replacement Therapy. *Mol Ther*. 2017;25(3):654-665. doi:10.1016/j.ymthe.2016.11.018.
100. Schwarze U, Schievink WI, Petty E, et al. Haploinsufficiency for one COL3A1 allele of type III procollagen results in a phenotype similar to the vascular form of Ehlers-Danlos syndrome, Ehlers-Danlos syndrome type IV. *Am J Hum Genet*. 2001;69(5):989-1001. doi:10.1086/324123.
101. Hori K, Sen A, Artavanis-Tsakonas S. Notch signaling at a glance. *J Cell Sci*. 2013;126(10):2135-2140. doi:10.1242/jcs.127308.
102. Zhang X, Goncalves R, Mosser DM. The Isolation and Characterization of Murine Macrophages. *Curr Protoc Immunol / Ed by John E Coligan .[et al]*. 2008;CHAPTER(November):Unit-14. doi:10.1002/0471142735.im1401s83.The.
103. Quan TE, Bucala R. Culture and analysis of circulating fibrocytes. *Methods Mol Med*. 2007;135:423-434. doi:1-59745-401-X:423 [pii].
104. Mount NM, Ward SJ, Kefalas P, Hyllner J. Cell-based therapy technology classifications and translational challenges. *Philos Trans R Soc B Biol Sci*. 2015;370(1680):20150017. doi:10.1098/rstb.2015.0017.

Vita

Ping Zhou was born in Hefei, Anhui, China on June 26, 1986 to Chaoyin Zhou and Yiyun Xiang. After graduating from Anhui Medical University, Anhui in 2009, she attended Graduate School of Fudan University in Shanghai, China and earned her M.S from the Program in Genetics. She subsequently attended the University of Texas M.D Anderson Cancer Center/UTHealth GSBS at Houston in August, 2012.